RICE UNIVERSITY

The Effects of ER Morphology on Synaptic Structure and Function in *Drosophila melanogaster*

by

James Brian Summerville

A THESIS SUBMITTED
IN PARTIAL FULFILLMENT OF THE
REQUIREMENTS FOR THE DEGREE

DOCTOR OF PHILOSOPHY

APPROVED, THESIS COMMITTEE

Michael Stern, *Advisor*
Professor of BioSciences

Mary C. Farach-Carson, *Chair*
Ralph and Dorothy Looney Professor
Vice Provost for Translational BioSciences

Michael C. Gustin
Professor of BioSciences

Caleb T. Kemere
Assistant Professor of Electrical
and Computer Engineering

Daniel S. Wagner
Associate Professor of BioSciences

HOUSTON, TEXAS
MAY 2016

ABSTRACT

The Effects of ER Morphology on Synaptic Structure and Function in *Drosophila melanogaster*

by

James Brian Summerville

Hereditary Spastic Paraplegias (HSPs) comprise a diverse set of genetic diseases caused by mutations in any of up to 70 genes, denoted *SPG1* to *SPG72*. Age-dependent corticospinal axon degeneration, accompanied by spasticity and weakening of the lower limbs, represents the most prominent HSP clinical feature. Two genes implicated in HSPs encode proteins that regulate ER morphology. Atlastin (responsible for *SPG3A*), encodes an ER membrane GTPase responsible for the fusion of juxtaposed ER membranes, and Reticulon 2 (responsible for *SPG12*), inserts into the ER membrane, induces membrane curvature, and thus promotes ER tube formation. Here we describe the effects of altered atlastin (*atl)* and reticulon (*Rtnl1)* on ER structure, evoked neurotransmitter release, synaptic bouton formation (arborization), and locomotor behavior in Drosophila. Using a novel fluorescent ER marker, we show that the ER within wildtype motor nerve terminals forms an elaborate network of tubules that resembles a “basket”, but this network is fragmented and diffuse in larvae lacking *atl*. Additionally, we find that loss of *atl* or *Rtnl1* decreases evoked transmitter release from motor neurons and increases motor neuron arborization. We also find that *atl* acts cell autonomously in the motor neuron to affect

transmitter release, whereas *Rtnl1* acts in all three cell types (neuron, muscle, and peripheral glia) of the tripartite synapse to control transmitter release. Similarly to other HSP genes, *atl* inhibits bone morphogenetic protein (BMP) signaling, and loss of *atl* causes age-dependent locomotor deficits in adults. These results demonstrate a critical role for the ER in neuronal function and identify mechanistic links between ER morphology, neuronal structure and function, BMP signaling, and adult behavior. These studies provide novel insights into the mechanisms underlying the neurological deficits in these HSPs.

Acknowledgements

I wish to first and foremost thank my advisor Dr. Michael Stern. I will always be incredibly grateful for the wisdom, patience, and guidance he imparted during my stay at Rice University. It was truly a pleasure to have worked in his lab. I would also like to thank Dr. James McNew, with whom we have worked extensively, for all his contributions and dedication to our collaborative efforts.

I am very thankful for my committee of Dr. Cindy Farach-Carson, Dr. Michael Gustin, Dr. Daniel Wagner, and Dr. Caleb Kemere. They provided me with the understanding, direction, insight, and kindness necessary for completion of this work.

Dr. Joseph Faust and Dr. Curtis Lin are genuine friends and were integral members of our research team who taught me many of the finer points of scientific investigation. I am also grateful to Dr. Cassidy Johnson, Dr. Magda Walkiewicz, and Dr. Avani Verma for their friendship and assistance within the lab.

Lastly I wish to thank my parents James and Kathleen, my brother Kevin, and my extended family and friends for their support. This endeavor would not have been possible without their continuous encouragement and love.

Figure Index

I.) Synaptic Function, Calcium Gradients, & ER Morphology

II.) The effects of ER morphology on synaptic structure and function in *Drosophila melanogaster*

Abbreviations

ANOVA:	analysis of variance
arm:	armadillo
atl:	atlastin
ATP:	adenosine triphosphate
BiP:	binding protein
BMP:	bone morphogenetic protein
BMPR:	bone morphogenetic protein receptor
CAMKII:	calcium/calmodulin-dependent kinase II
CICR:	Ca^{2+}-induced Ca^{2+} release
CRAC:	Ca^{2+} release-activated Ca^{2+}
da:	daughterless
Dad:	Daughters against decapentaplegic
DAG:	diacylglycerol
DmGluRA:	Drosophila metabotropic glutamate receptor A
DN:	dominant negative
DP1:	deleted in polyposis
eag:	ether a go-go
EJP:	excitatory junctional potential
elav:	embryonic lethal abnormal vision
ER:	endoplasmic reticulum
FAK:	focal adhesion kinase
Gal4:	galactose-responsive transcription factor

GAP:	GTPase activating protein
gbb:	glass bottom boat
Gli:	Gliotactin
GTP:	guanosine triphosphate
HC-TEM:	high contrast transmission electron microscope
HEPES:	2-(4-(2-Hydroxyethyl)piperazin-1-yl)ethanesulfonic acid
ine:	inebriated
IP3:	inositol 1,4,5-trisphosphate
LOH:	loss of heterozygosity
Mad:	Mothers against decapentaplegic
Mef2:	Myocyte enhancer factor 2
mEJP:	mini excitatory junctional potential
MMP:	matrix metallopeptidase
mV:	millivolts
NCX:	Na^{+}/Ca^{2+} exchanger
NF1:	Neurofibromin 1
NGF:	nerve growth factor
NMJ:	neuromuscular junction
nSyb:	neuronal synaptobrevin
PDPK1:	3-phosphoinositide dependent protein kinase 1
PI3K:	phosphatidylinositol-4,5-bisphosphate 3-kinase
PIP2:	phosphatidylinositol 4,5-bisphosphate
PIP3:	phosphatidylinositol 3,4,5-trisphosphate

pMad: phosphorylated Mothers against decapentaplegic

PMCA: plasma membrane Ca^{2+} ATPase

push: pushover

put: punt

REEP1: receptor expression enhancer protein 1

RHD: reticulon homology domain

RNAi: RNA interference

ROI: region of interest

Rtnl1: Reticulon-like1

sax: saxophone

sfGFP: superfolder green fluorescent protein

SERCA: sarco/endoplasmic reticulum calcium ATPase

SPG[X]: spastic paraplegia gene [X]

SOCE: store-operated Ca^{2+} entry

STIM1: stromal interaction molecule 1

TGF-β: transforming growth factor β

tkv: thickveins

TMD: transmembrane domain

UAS: upstream activating sequence

VEGF: vascular endothelial growth factor

VGCC: voltage-gated Ca^{2+} channel

wit: wishful thinking

wt: wildtype

I). Synaptic Function, Calcium Gradients, & ER Morphology

1: Background

1.1: Action potential induction & propagation

Cellular communication and adaptation requires cells to first sense their surrounding environment and respond in an appropriate manner. These responses can include, among other actions, gene expression, cellular motility, the repositioning of organelles during mitosis, and the secretion of signaling peptides. The last example includes the release of neurotransmitter from the axon terminal of nerve cells when signaling to other neurons or myocytes. Neurons are specialized cells which consist of three main components: the signal receiving dendrites, the cell body or soma, and the axon which transmits the outgoing signal to other cells. The reception, processing, and transmission of information within neurons occur in the form of transient changes in the electrochemical gradient that exists across the plasmalemma. This polarity is primarily established by K^+ leak channels which allow K^+ ions to efflux out of the cell, creating a charge potential across the plasma membrane where the inside of the neuron is approximately -70 mV in relation to the extracellular space. The Na^+/K^+ ATPase pump also helps to maintain this gradient by pumping 3 Na^+ ions out of the cell for every two K^+ ions pumped into the cell. The plasma membrane is relatively although not entirely impermeable to inorganic ions. As a result, neurons, using specialized pores known as voltage-gated ion channels, are capable of regulating where and when ions cross the plasma membrane.

Ligand gated Na^+ channels within the dendrites and along the soma are activated by excitatory neurotransmitter released from presynaptic cells. These channels open to allow Na^+ to enter the neuron, increasing the potential of the area immediately surrounding the channels. This influx of positive charge spreads outward from the localized area around the channels as like charges repel each other. Temporal and spatial summation of these currents can accumulate positive charge at the action potential initiation region known as the axon hillock. Voltage-gated Na^+ channels at the axon hillock possess a cytosolic voltage sensing domain that detects the localized intracellular charge. It should be noted that voltage-gated ion channels open in a stochastic manner, meaning that as a channel encounters its threshold voltage, the channel has an increased probability of opening. For voltage-gated Na+ channels, if the threshold voltage of approximately -55 mV is reached, there is a high probability that these channels will open and initiate an action potential. As the first voltage-gated Na^+ channels at the axon hillock open, Na^+ enters and the localized membrane potential increases from roughly -55 mV to +50 mV. The inside of the cell at this region is now positive in comparison to the extracellular space. This increased voltage catalyzes the inactivation of the previously opened voltage-gated Na^+ channels. This inactivated state differs from the initial closed conformation and occurs when a region of the channel blocks the pore. In this conformation no amount of positive current will open the channel. A drop in membrane potential must be applied to first close the channel before it can be opened again. This necessary decrease in voltage is accomplished via voltage-gated K^+ channels

which have a high probability of opening at the threshold voltage of +50 mV. The opening of these channels results in K^+ flowing down its concentration gradient and out of the cell. With the voltage-gated Na^+ channels inactivated, this efflux of K^+ repolarizes the plasma membrane. At this point the K^+ channels inactivate, and the membrane potential returns to its resting state. The resulting localized depolarization is subsequently detected by other immediately adjacent voltage-gated Na^+ channels. These voltage-gated Na^+ and K^+ channels are present along the length of the axon but not in a contiguous arrangement. In vertebrates, many axons possess regions which are devoid of voltage-gated ion channels and are instead concentrically wrapped by specialized glia, known as oligodendrocytes in the central nervous system and Schwann cells in the peripheral nervous system, in a process called myelination. Alternatively, oligodendrocytes and Schwann cells may not differentiate to form myelin sheaths but rather ensheath smaller nerve fibers, such as C nerve fibers, into what are known as Remak bundles (Taveggia et al., 2005). This occurs when a single glial cell associates with and ensheaths several axons instead of myelinating a single nerve. However, where myelin is present, it enables higher conduction velocity by sequestering voltage-gated ion channels to sections of the axon known as the nodes of Ranvier and restricting areas of the neuronal plasmalemma from exposure to the extracellular fluid. Myelin insulates axons by wrapping them and effectively increasing the amount of membrane present, which decreases the capacitance and increases the resistance between the extracellular and intracellular spaces. Increasing the distance between these ionic fluids thus decreases the attraction between their

net opposing charges. The nodes of Ranvier are densely packed with voltage-gated Na^+ channels. This results in Na^+ ions flowing into the axon only at these designated locations. Thus, the increased resistance, reduced capacitance, and restricted points of ion exchange allow for action potentials to travel via saltatory conduction to axon terminals. The end goal of action potentials is to catalyze a calcium (Ca^{2+}) influx into the cytosol at the axon terminal which facilitates neurotransmitter release. However, before neurons can use employ this Ca^{2+} influx, they must first establish a Ca^{2+} electrochemical gradient. The generation of this Ca^{2+} gradient and the directed distribution, handling, and utilization of Ca^{2+} in cells is further discussed below.

1.2: Calcium electrochemical gradients

1.2.1: Plasmalemmal calcium pumps & channels

Calcium affects a number of cellular signaling pathways, including the release of neurotransmitter at the axon terminal. Therefore, cells exert a great deal of time and effort in maintaining a Ca^{2+} gradient across the plasmalemma. The average cytosolic [Ca^{2+}] of a cell at rest is approximately 100 nM while the extracellular space has a [Ca^{2+}] of approximately 2 mM (Clapham, 2007). Some of this potential is maintained using energy consumption to load Ca^{2+} into the extracellular space to establish the Ca^{2+} electrochemical gradient. This is done in part via the plasma membrane Ca^{2+} ATPase (PMCA) pump which hydrolyzes one ATP molecule to pump one Ca^{2+} ion out of the cell (Clapham, 2007). The Na^+/Ca^{2+} exchanger (NCX) also uses energy, in the form of an electrochemical

gradient, to allow 3 Na^+ ions to travel down their gradient into the cell for the exchange of one Ca^{2+} ion against its gradient out of the cell (Carafoli et al., 2001). Unlike PMCA, NCX is reversible because it is subject to the polarity of the membrane and the fluctuations of the Na^+ and Ca^{2+} gradients (Carafoli et al., 2001). Although reversible in its flow, the majority of the time NCX is extruding Ca^{2+} for the uptake of Na^+ since the [Na^+] of the extracellular space, like that of Ca^{2+}, is much greater than the cytosolic [Na^+]. However, while PMCA has a higher affinity for Ca^{2+}, NCX has a higher capacity, capable of transporting approximately 2,500 to 5,000 Ca^{2+} ions per second (Carafoli et al., 2001).

1.2.2: The Sarco/Endoplasmic Reticulum Calcium ATPase (SERCA) pump

In addition to maintaining a Ca^{2+} gradient across the plasmalemma, cells also preserve a Ca^{2+} potential across the ER membrane. The ER acts as an internal Ca^{2+} store that allows cells to rapidly increase their cytosolic [Ca^{2+}] for signaling. Accumulation of Ca^{2+} in the ER is accomplished through ATP expenditure via the Sarco/Endoplasmic Reticulum Ca^{2+} ATPase (SERCA) pump. SERCA is a P-type ATPase in that the terminal phosphate it hydrolyzes is used to phosphorylate one of its own aspartate residues, which allows for a conformational change that pushes Ca^{2+} across the membrane and into the ER lumen. Twice as efficient as PMCA, SERCA pushes two Ca^{2+} ions into the ER lumen for the hydrolysis of one ATP nucleotide.

1.2.3: Store-Operated Ca^{2+} Entry (SOCE): STIM1 & Orai

The ER must replenish its Ca^{2+} stores after Ca^{2+} release has occurred. One way the ER does this is through a process called store-operated Ca^{2+} entry (SOCE). This process involves an interaction between the ER membrane stromal interaction molecule (STIM1) and the plasmalemma Ca^{2+} release-activated Ca^{2+} (CRAC) channel forming protein Orai (Várnai et al., 2009). STIM1 possesses an EF hand motif near its N-terminus which binds Ca^{2+}, allowing STIM1 to act as an ER lumen Ca^{2+} sensor. In a resting state, STIM1 is evenly distributed throughout the ER membrane (Liou et al., 2005). Upon ER Ca^{2+} store release, bound Ca^{2+} dissociates from the EF hand motif, causing STIM1 to aggregate in regions of the ER membrane adjacent to the plasmalemma (Liou et al., 2005; Xu et al., 2006). Once there, STIM1 oligomers facilitate CRAC channel formation within the plasmalemma via their cytosolic Orai1-activating region (Yang et al., 2012). Under resting conditions, Orai is evenly distributed along the plasmalemma as dimers but becomes a tetramer that forms the CRAC channel following STIM1 induced activation (Penna et al., 2008). Influxing Ca^{2+} enters the cytosol and is immediately transferred to the ER lumen via SERCA pumps that have been recruited to high [Ca^{2+}] microdomains near CRAC channel openings (Jousset et al., 2007; Manjarrés et al., 2010). This allows cells to rapidly refill their ER Ca^{2+} stores without disrupting the cytosolic [Ca^{2+}].

1.3: Use of the Ca^{2+} electrochemical gradient for neurotransmitter release

1.3.1: Voltage-gated Ca^{2+} channels: specialized Ca^{2+} influx in excitable cells

Excitable cells have need of specialized Ca^{2+} channels to allow for rapid, transient cytosolic Ca^{2+} increases necessary for events such as neurotransmitter vesicle release in neurons and excitation-contraction coupling in muscles. The voltage-gated Ca^{2+} channels (VGCC) are heteromultimeric calcium pores which respond to depolarization of the membrane. These channels are comprised of 5 subunits (α_1, α_2, β, δ, and γ). The α_1 subunit is the largest protein of these components and contains 4 homologous regions, with each region consisting of 6 transmembrane domains that form the Ca^{2+} channel within the membrane (Gurkoff et al., 2013). This subunit also contains the voltage-sensory and gating mechanisms which allow the channel to open and close depending upon the voltage encountered (Gurkoff et al., 2013). There are several subtypes of VGCCs which include the L, N, P/Q, R, and T-type channels. All except the T-type channel are classified as high voltage activation channels in that they open at a higher depolarization, between -40 to -10 mV, in comparison to the lower voltage activation T-type channel that opens at roughly -70 to -60 mV (Yamakage & Namiki, 2002). N-type channels play a major role in Ca^{2+} influx in presynaptic neurons of the mammalian nervous system while P/Q type channels are found primarily in presynapses within the central nervous system (Catterall & Few, 2008), and L-type channels are predominantly located in skeletal muscle, smooth muscle, endocrine tissue, and the brain (Dunlap et al., 1995).

Drosophila contains two genes which encode for voltage-gated Ca^{2+} channels, *cacophony/DmCα1A* and *DmCα1D* (Peng & Wu, 2007). *DmCα1D* encodes an L-type channel.α1 subunit and is expressed postsynaptically (Lee et al., 2013). *Cacophony* encodes for an α1 subunit that is similar to those found in vertebrate N, P/Q, and R-type channels (Peng & Wu, 2007) and is localized in presynaptic neurons at active zones where neurotransmitter vesicles are released into the synaptic cleft (Kawasaki et al., 2004). Voltage-gated ion channels in general pass an ionic current across the membrane at approximately 10^6-10^8 ions per second (Tombola et al., 2006). VGCCs are the fastest Ca^{2+} channels, passing approximately 10^6 Ca^{2+} ions per second down a 20,000:1 gradient (Clapham, 2007). VGCCs are inactivated through both voltage-dependent inactivation (VDI) and Ca^{2+}-dependent inactivation (CDI) (Cens et al., 2005). CDI relies on calmodulin, which is a second messenger activated by binding Ca^{2+}.

1.3.2: ER Ca^{2+} release channels: The ryanodine receptor & the IP3 receptor

Cells can release Ca^{2+} from the ER into the cytosolic space using several different channels. Ryanodine receptors (RyRs) are Ca^{2+} channels present within the ER membrane in both neurons and muscles. RyRs release Ca^{2+} from the ER in response to different stimuli depending on the isoform of the protein and the cell it inhabits. The name of the receptor is derived from its high affinity for the plant alkaloid ryanodine, which locks the receptor in an open position, causing

constant contractility (Fleischer, 2008). In mammalian skeletal muscle, RyRs form a direct protein-protein interaction with VGCCs, specifically the L-type Ca^{2+} channels, in the plasmalemma (Zalk et al., 2007). Upon activation of the L-type Ca^{2+} channel, a conformational change takes place which opens the RyRs and allows Ca^{2+} to exit the ER (Zalk et al., 2007). In cardiac muscle, RyRs open upon an initial influx of Ca^{2+} into the cytosol from the extracellular space via L-type VGCCs (Zalk et al., 2007). This phenomenon is known as Ca^{2+}-induced Ca^{2+} release (CICR). In neurons, both the direct protein-protein interaction between L-type VGCCs and RyRs (Mouton et al., 2001; Lanner et al., 2010) and CICR (Llano et al., 1994; Verkhratsky & Shmigol, 1996; Berridge, 1998; Mothet et al., 1998; Lanner et al., 2010) have been shown to activate RyRs for ER Ca^{2+} release.

Another Ca^{2+} release channel located within the ER membrane is the inositol 1,4,5-trisphosphate receptor (IP3R). Upon activation via G-protein coupled receptors, Phospholipase C cleaves the plasma membrane bound phospholipid phosphatidylinositol 4,5-bisphosphate (PIP2) into diacylglycerol (DAG) and inositol 1,4,5-trisphosphate (IP3). DAG remains bound to the plasmalemma while IP3, a soluble second messenger, binds to and opens the IP3R within the ER membrane. Release of ER Ca^{2+} via IP3R has been implicated in release of gonadotropin in rats (Tse et al., 1997). IP3R activation and subsequent RyR activation has also been shown to release neurotransmitter in *Xenopus* nerve-muscle co-cultures (He et al., 2000).

1.4: Atlastin & morphology of the endoplasmic reticulum

1.4.1: Atlastins are GTPases responsible for fusing juxtaposed ER membranes

One protein responsible for the arrangement and structural integrity of the ER is atlastin (Atl) (Orso et al., 2009). Atlastin is a Dynamin-like membrane bound GTPase necessary for homotypic fusion of the ER membrane (Orso et al., 2009). Humans possess three atlastin proteins, Atlastin-1, Atlastin-2, and Atlastin-3, with Atl-1 being highly expressed in the central nervous system while Atl-2 and Atl-3 are largely localized to peripheral tissues (Rismanchi et al., 2008). All atlastins possess 5 distinct regions. The first three of these domains, the N-terminal GTPase domain, linker domain, and the 3 α-helix bundle, are cytosolic. These are followed by two transmembrane domains and lastly a cytosolic C-terminal tail. The first and largest domain is the cytosolic N-terminal GTPase, which consists of a single beta sheet surrounded by 6 alpha helices (Bian et al., 2011). The binding of GTP causes a conformational change that allows the 3 helix bundles of apposing atlastins to associate and dimerize the two proteins (Pendin et al., 2011). This means that atlastin proteins will dimerize even in the presence of GTPγS, a nonhydrolyzable form of GTP; although full membrane fusion is dependent upon GTP hydrolysis (Pendin et al., 2011). Anchoring atlastin to the ER membrane are two transmembrane domains (TMDs) which form a hairpin structure (Bian et al., 2011). Lastly, the C-terminal tail of atlastin consists of an amphipathic α-helix. Parallel insertion of the hydrophobic face of the C-terminal tail along the length of the membrane reorganizes acyl chains and

thins the ER lipid bilayer to facilitate membrane fusion (Faust et al., 2015). Consistent with their function, atlastins localize primarily within smooth ER tubules where they facilitate the formation of three way junctions.

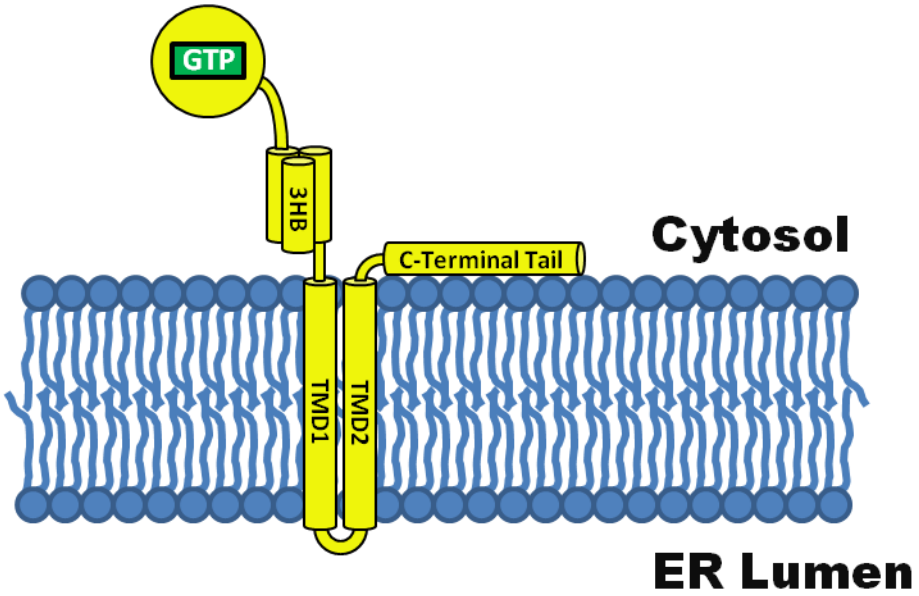

Figure 1: Atlastin is an integral ER protein responsible for homotypic membrane fusion. Atlastin domains include a cytosolic N-terminal GTPase, 3 helix bundle, two transmembrane domains, and a cytosolic, amphipathic C-terminal tail.

1.4.2: Mutations in *SPG3A* cause Hereditary Spastic Paraplegia

Mutations of the *SPG3A* gene, which encodes Atlastin-1 in humans, are implicated in the onset of Hereditary Spastic Paraplegia (HSP) (Reid et al., 2003). *SPG3A* mutations are responsible for approximately 10% of autosomal dominant HSP diagnoses, including the characteristic symptoms of increasing weakness and spasticity of the lower limbs (Reid et al., 2003). HSP mutations have been documented in all regions of the atlastin protein, with the majority of *SPG3A* mutations occurring within the GTPase domain or the 3 helix bundle (Namekawa et al., 2007; Smith et al., 2009). These mutations disrupt atlastin's

ability to hydrolyze GTP and/or dimerize, inhibiting membrane fusion. Another mutation which causes HSP is R495W, located within the second TMD (Scarano et al., 2005). Finally, mutations affecting the atlastin C-terminal tail also inhibit fusion and cause HSP (Moss et al., 2011). Atlastin's TMDs are necessary for inclusion of the protein into the ER membrane as well as association with other ER membrane proteins. Atlastin binds the AAA ATPase microtubule severing protein spastin (Evans et al., 2006; Sanderson et al., 2006) and through its TMDs also forms a complex with spastin and the ER shaping protein REEP1 (Park et al., 2011). Spastin exists in two forms, the larger 64 kDa M1 isoform and the 60 kDa M87 isoform (Park et al., 2011). Only the larger M1 form of spastin binds atlastin via its N-terminal ER intramembrane hairpin domain. All three forms of human atlastin have also been shown to interact with Protrudin, another ER shaping protein (Chang et al., 2013).

1.4.3: Atlastin homologs in Drosophila

Drosophila possesses a single gene for atlastin (*atl*) which yields a 61 kDa protein of 541 amino acids (Moss et al., 2011). The atl^{1} mutation contains a P-element insertion which deletes the first intron of the *atl* gene, yielding no protein product (Lee et al., 2008). Atl^{1} flies are small compared to wildtype larvae, possess locomotory dysfunction, are sterile (Lee et al., 2008), and exhibit a fragmented ER membrane, whereas *atl* overexpression constitutes an expanded ER (Orso et al., 2009). Another *atl* mutant was generated by imprecisely excising the atl^{1} P-element. The resulting atl^{2} mutant is missing exons 3 and 4, both of

which are present in two alternative transcripts of Atlastin (Lee et al., 2009). *Atl*^{2} flies are also sterile, are smaller than wildtype flies, and have locomotory problems but are viable up to the pupal stage (Lee et al., 2009). Therefore this mutant allows for analysis of the larval neuromuscular junction (NMJ), the site of neuron-muscle interaction, in the absence of Atlastin. It is this *atl*^{2} mutant which was utilized in all our experiments.

1.5: Reticulon & morphology of the endoplasmic reticulum

1.5.1: Reticulon is a membrane protein that helps shape ER tubules

Another family of proteins responsible for shaping the ER membrane is the reticulons (Voeltz et al., 2006). Reticulons are found primarily in tubular ER structures and are mostly absent from the ER's sheet-like areas of the membrane (Voeltz et al., 2006). They share a conserved hairpin loop of approximately 200 amino acids termed the reticulon homology domain (RHD) (Oertle & Schwab, 2003). This domain possesses two short hairpin transmembrane domains (TMDs) of roughly 33 amino acids each, separated by a soluble region and flanked by N-terminal and C-terminal soluble regions (Zurek et al., 2011). Insertion of reticulons into the ER membrane occurs co-translationally and is dependent upon the length of the first TMD (He et al., 2007). These TMDs are too long to traverse the membrane only once but also too short to fully span the membrane twice (Zurek et al., 2011). Interestingly, the length of these hairpin TMDs is responsible for the proper partitioning and oligomerization of reticulons almost exclusively within the ER tubules (Zurek et

al., 2011). Additionally, the hairpin TMDs cause curvature of the ER membrane to form the tubules they occupy and also immobilize reticulons to keep them from migrating to other areas of the ER, such as the nuclear envelope and adjacent sheet structures (Zurek et al., 2011). Reticulons may curve the ER during tubule formation by partially inserting into the membrane and creating a “wedge” that inhabits a larger portion of the outer layer than it does of the inner layer (Hu et al., 2008; Montenegro et al., 2012).

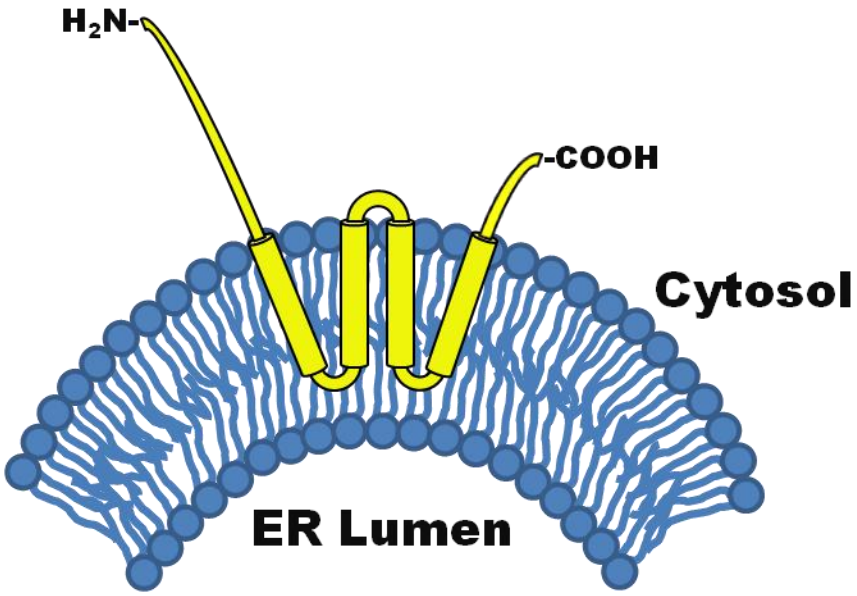

Figure 2: Reticulons aid in curving the ER membrane. Reticulons possess two hairpin domains, which occupy more of the outer membrane leaflet than the inner leaflet, forming a “wedge” that induces positive curvature of the ER membrane.

Reticulons have been shown to oligomerize with other ER shaping proteins such as the mammalian Dp1 and its yeast ortholog Yop1p (Shibata et al., 2008). Moreover, reticulon overexpression can result in abnormally elongated ER tubules which exhibit a smaller diameter, minimal branching, and the displacement of luminal ER proteins (Hu et al., 2008). Reticulon overexpression

can also maintain ER tubule structure in the presence of depolymerized microtubules, which normally results in retraction of ER tubules and an upregulation of disorganized sheet-like ER (Shibata et al., 2008). They are also known to bind and inhibit BACE1, a protease responsible for cleaving the Alzheimer's disease related amyloid precursor protein (He et al., 2007).

1.5.2: Reticulon homologs in Drosophila

Drosophila carries two reticulons, termed Reticulon-like1 (*Rtnl1*) and Reticulon-like 2 (*Rtnl2*) (O'Sullivan et al., 2012). *Rtnl1* is widely expressed while *Rtnl2* expression is confined to the testes and fat body (O'Sullivan et al., 2012). Knockdown of *Rtnl1* produces several observable phenotypes in flies. For instance, ubiquitous knockdown of *Rtnl1* results in reorganization of the ER structure that triples the amount of sheet-like ER (O'Sullivan et al., 2012). Additionally, *Rtnl1* knockdown engenders an age-dependent loss of locomotor activity and initiates an ER stress response, as indicated by upregulating the ER stress response reporter Xbp1 (O'Sullivan et al., 2012). In concordance with reticulons belonging to the family of HSP genes, flies with widespread *Rtnl1* inhibition also experience structural defects in distal segments of their motor axons; however, the proximal regions of these same axons remain free from abnormalities (O'Sullivan et al., 2012). Deletion of *Rtnl1* (*Rtnl1*^{1}) was achieved via the imprecise excision of a P-element insertion located 3 kb upstream of the RHD exons (Wakefield & Tear, 2006). This excision removed all RHD exons (Wakefield & Tear, 2006). These observations suggest that Atl and Rtnl1 have

opposing effects on ER morphology and that flies possessing both *atl* and *Rtnl1* mutations simultaneously (*Rtnl1*^{1}*; atl*^{2} mutants) may possess an ER that resembles a wildtype ER more closely than that of a fly possessing only a single mutation in either *atl* or *Rtnl1*.

1.6: Drosophila genetics

Drosophila larvae provide an excellent model with which to study both nervous system function and disease. It is an experimentally tractable yet applicable model that is easily accessible and possesses approximately ten million times fewer neurons than the less tractable human system (Neuser et al., 2005). Roughly 75% of human genes known to cause neuropathies have orthologs within Drosophila (Reiter et al., 2001; Marsh & Thompson, 2004).

1.7: The Drosophila Gal4/UAS system

The Gal4-UAS system enables tissue specific transgene expression in Drosophila. *Gal4* encodes a transcription factor that selectively activates a promoter known as the upstream activating sequence (UAS) (Duffy, 2002). Target transgenes downstream of the UAS promoter are transcribed according to synthesis of the Gal4 protein (Brand & Perrimon, 1993). Therefore, expression of the UAS-possessing transgene can be manipulated on a tissue-specific level by crossing it with a *Gal4* driver that is expressed in a particular tissue (Figure 3).

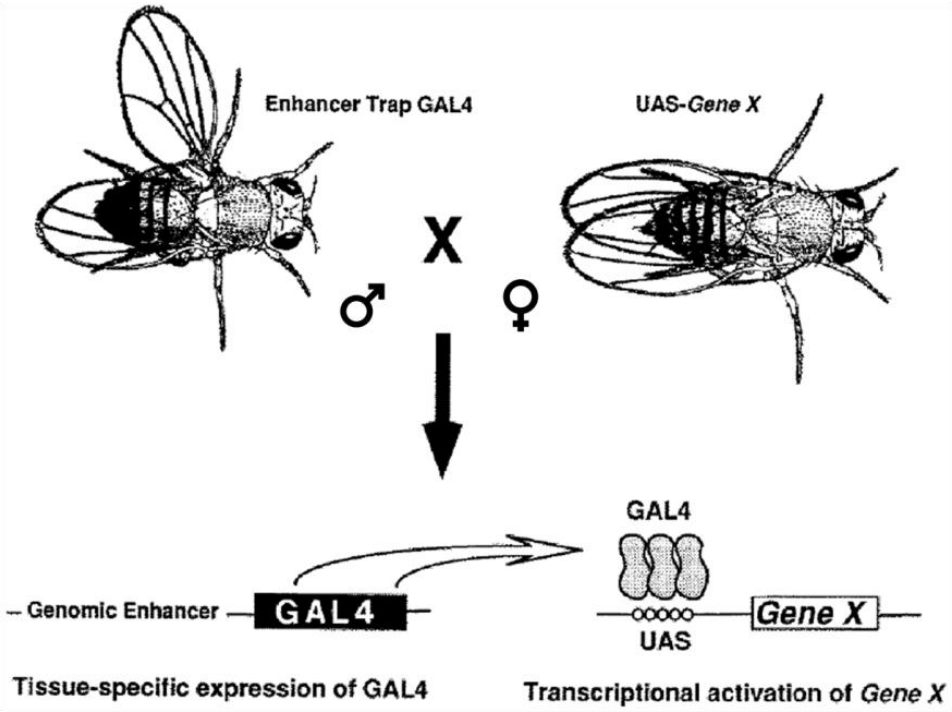

Figure 3: The Drosophila Gal4-UAS system. Tissue-specific expression of *Gal4* by a chosen promoter (referred to as a driver) causes subsequent tissue-specific *Gene X* expression. Shorthand notation for *Gene X* expression according to driver specificity is written as *Driver>Gene X* (Adapted from Brand & Perrimon et al., 1993).

1.8: Retrograde signaling at the neuromuscular junction

Retrograde signaling, whereby muscles communicate reciprocally with their motor neurons, is essential for many processes such as synaptic connectivity, axonal preservation, and microtubule stability of presynaptic target neurons. This signaling takes place via bone morphogenetic proteins (BMPs), which belong to the TGF-β family of secretory proteins (McCabe et al., 2003). Activated BMP receptors exist as heterotetramers of two Type I and two Type II serine/threonine kinase receptors (Miyazono et al., 2010). One particular Type II receptor known as wishful thinking (wit) in Drosophila is capable of binding BMP

ligands in the absence of the Type I receptors (known as saxophone (sax) and thick veins (tkv) in Drosophila), but signaling is dependent upon the presence of both receptors (Liu et al., 1995). The other Type II receptor, known as punt (put), also binds BMP ligands but does so only in the presence of Type I receptors (Letsou et al., 1995). Upon ligand binding, Type II receptors phosphorylate Type I receptors which in turn phosphorylate receptor-regulated Smads (R-Smads) (Miyazono et al., 2010). R-Smads (Mad in Drosophila) then bind to Co-Smads (Medea in Drosophila) to enter the nucleus for transcriptional regulation of target genes (Miyazono et al., 2010).

In addition to the inhibitory Smad, known as Dad in Drosophila, there are a variety of proteins that regulate BMP pathway activity. For instance, deletion of Drosophila endocytotic regulatory proteins such as endophilin, dap160, and nervous wreck exhibit increased pMad signaling in presynaptic terminals at the NMJ (O'Connor-Giles et al., 2008). Interestingly, pMad found at the synapse may not migrate to the neuronal soma to enter the nucleus. Instead, it has been suggested that nuclear pMad is accumulated when activated BMP receptors travel via a signaling endosome on dynein motors to the cell body to phosphorylate a different population of Mad than that found at the axon terminal (Smith et al., 2012). Additionally, mammalian HSP related Non-Imprinted in Prader-Willi/Angelman Syndrome 1 (NIPA1) is implicated in downregulating BMP signaling by interacting with the BMP Type II Receptor (BMPRII) and targeting it to endosomes for degradation (Tsang et al., 2009). Spartin and spastin also inhibit BMP signaling (Tsang et al., 2009) which subsequently regulates

microtubule stability and neuronal survivability (Nahm et al., 2013). HSP related atlastin has also been shown to bind BMPRII in rat brains as well as HEK239-T cells, where overexpression of *atl* HSP mutants prevented BMPRII from reaching the cell surface (Zhao & Hedera, 2013). However, the absence or overexpression of wt *atl* in these cells does not affect BMPRII plasmalemma localization, demonstrating that *atl* is not required in these cells to properly traffic BMPRII (Zhao & Hedera, 2013). Atlastin also negatively regulates BMP signaling in zebrafish, and zebrafish embryos with decreased levels of atlastin also display thin and abbreviated spinal motor neurons that possess ectopic branch points and abnormalities in axon pathfinding, showing direct correlation between BMP inhibition and HSP neuronal phenotypes (Fassier et al., 2010). The Drosophila HSP related orthologue for spichthyin, *SPG20*, also negatively affects BMP signaling (Wang et al., 2007). These data suggest that Drosophila atlastin may also inhibit BMP signaling.

II.) The effects of ER morphology on synaptic structure and function in *Drosophila melanogaster*

2: Introduction

The function of intracellular organelles is tightly coordinated with location within the cytoplasm. The Endoplasmic Reticulum (ER) is an interconnected network of narrow tubes and flattened cisternae or sheets (Hu et al., 2011; Shibata et al., 2009; Shibata et al., 2006; Terasaki et al., 2013; Westrate et al., 2015). In most cells, the ER is the most abundant subcellular organelle and extends elaborate processes throughout the cytoplasm. The ER membrane is formed into its tubular architecture by the action of structural proteins within the Reticulon/REEP/DP1 family (English and Voeltz, 2013; Hu et al., 2008; Shibata et al., 2009; Voeltz et al., 2006; Yang and Strittmatter, 2007). The members of this diverse family of proteins share a common protein motif called the Reticulon Homology Domain (RHD). The hydrophobic ~200 amino acid RHD likely forms a helical hairpin structure that intercalates four hydrophobic helical segments into the outer leaflet of the ER membrane to induce curvature and maintain a tubular shape (Voeltz et al., 2006; Zurek et al., 2011). Many members of the Reticulon/REEP/DP1 family also contain an extended N-terminal segment ranging from a few hundred to a thousand amino acids that likely provides additional functionality (Di Sano et al., 2012). The nature of most of these secondary functions remains to be revealed.

The large ER network also maintains luminal and membrane continuity throughout the cytoplasm. This interconnected nature of the ER network is required for ER function and is maintained by the ER membrane fusion GTPase

atlastin (*atl*) (Orso et al., 2009), which is a member of the fusion dynamin related protein family (fusion DRP) (McNew et al., 2013; Moss et al., 2011; Pendin et al., 2011).

The ER is closely associated with and functionally connected to the plasma membrane (PM). This connection is often associated with the management of calcium (Ca^{2+}) stores in the ER lumen. The ER protein STIM1 diffuses through the ER membrane to find binding partners in the plasma membrane including the Orai channel (Jozsef et al., 2014; Soboloff et al., 2012). This set of protein-protein associations works to restore ER calcium through the Store Operated Ca^{2+} channels system. ER-PM contact sites are also generated by the association of ER integral Extended-synaptotagmins (E-Syt) with phospholipids in the plasma membrane (Fernandez-Busnadiego et al., 2015; Giordano et al., 2013; Schauder et al., 2014) as well as proteins like junctophillins in certain cell types (Helle et al., 2013; Stefan et al., 2013).

Most recently, the ER has been found stably associated with endosomal structures (Raiborg et al., 2015a; Rowland et al., 2014). In this circumstance, the specific proteins on each surface that interact remain to be precisely defined, but the consequence of the interaction is functional segregation of certain cargoes within the endosome that permits regulated sorting into membrane subdomains prior to an ER-directed membrane fission event (Raiborg et al., 2015a; Raiborg et al., 2015b; Rowland et al., 2014).

ER structure appears to be critically important for cell function since human pathology results when components that control this structure are

compromised by mutation. The Hereditary Spastic Paraplegias (HSPs) are a group of related genetic disorders caused by mutations in any of more than 70 genes, named *SPG1* to *SPG72* (Lo Giudice et al., 2014; Noreau et al., 2014). Lower limb weakness and spasticity represent two prominent clinical features of these diseases, which occur as a consequence of dysfunction or degeneration of the upper motor neurons (Blackstone et al., 2010). The observation that *atl* and *Reticulon 2* are HSP genes responsible for *SPG3A* and *SPG12,* respectively, implicates ER morphology in the neuronal dysfunction that causes HSPs.

The properties of three additional HSP genes, *spartin* (*SPG20*), *spastin* (*SPG4*), and *NIPA1/spichthyin* (*SPG6*), implicate receptor trafficking through the endocytic system in HSP neuronal dysfunction. For example, loss of *spartin* attenuates both ligand-stimulated EGF receptor uptake (Bakowska et al., 2007) as well as depolarization-stimulated FM1-43 uptake (Nahm et al., 2013), whereas loss of *spastin* increases endosome tubule number and alters transferrin receptor sorting (Allison et al., 2013). NIPA1 is also located in endosomes and promotes the endocytosis of receptors for bone morphogenetic protein (BMP) (Tsang et al., 2009).

Phenotypic analysis of mutations in the HSP orthologs of model systems has provided additional clues to the cellular function of these proteins. In Drosophila, loss of *spastin*, *spartin* and *spichthyin* confers a similar but not identical set of phenotypes including stabilized microtubules, increased synaptic bouton number and decreased evoked transmitter release at the larval neuromuscular junction (NMJ), age-dependent locomotor deficits, and increased

BMP signaling at the larval NMJ (Nahm et al., 2013; Ozdowski et al., 2011; Sherwood et al., 2004; Wang et al., 2007). These shared phenotypes might reflect disruption of a common pathway in endocytic receptor trafficking in these mutants. Some of these phenotypes, such as stabilized microtubules, age-dependent locomotor deficits, and increased synaptic bouton number, are also observed in flies lacking atlastin (Lee et al., 2009; Lee et al., 2008).

Here we extend this phenotypic analysis of altered atlastin (*atl)* and Reticulon-like1 (*Rtnl1)* activities in Drosophila. We show that the ER in motor nerve terminals from wildtype larvae forms a network of tubules that resembles a "basket", but is diffuse in larvae lacking *atl*. We find that neuronal RNAi knockdown of either *atl* or *Rtnl1* increases arborization at the larval neuromuscular junction and decreases evoked transmitter release from larval motor nerve terminals, and that elevated bath [Ca^{2+}] fully rescues these transmitter release phenotypes. We also show that *atl* is required only in motor neurons to affect transmitter release, whereas *Rtnl1* is required additionally in the target muscle and peripheral glia. Finally we show that loss of *atl* increases BMP signaling in larval motor neurons and causes age-dependent locomotor deficits in adults. Thus, loss of *atl* and *Rtnl1* confers phenotypes similar but not identical to each other as well as to mutants defective in *spartin, spastin* and *spichthyin*. Our results demonstrate specific mechanistic links between ER morphology and several aspects of neuronal anatomy and function.

3: Materials and Methods

3.1: Drosophila stocks and media

The following lines were obtained from the Bloomington Drosophila Stock Center at Indiana University: *w*^{1118} (#3605), *arm-Gal4* (#1560), *elav-Gal4* (#458), *elav-Gal4; UAS-Dcr-2* (#25750), *nSyb-Gal4* (#51635), *OK371-Gal4* (#26160), *Mef2-Gal4* (#27390), *UAS-Dcr-2* (#24650), *UAS-Dcr-2* (#24651), and *UAS-myr::tdTomato* (#32221). The *da G32* (#108252) Gal4 driver line was provided by the Drosophila Genetic Resource Center. *UAS-Rtnl1*^{RNAi} (#7866) was obtained from the Vienna Drosophila Resource Center. *OK6-Gal4* (Aberle et al., 2002) was provided by Dr. Hermann Aberle (Heinrich Heine University, Düsseldorf, Germany). *D42-Gal4* (Yeh et al., 1995) was provided by Dr. Thomas Schwarz (Children's Hospital Boston, F. M. Kirby Neurobiology Center, Boston, Massachusetts). *Gli-Gal4* (Sepp and Auld, 1999) was provided by Dr. Vanessa Auld (The University of British Columbia, Department of Zoology, Vancouver, British Columbia, Canada). *UAS-atl*$^{+}$, *UAS-atl*^{K51A}, and *UAS-atl*^{RNAi} were described in (Orso et al., 2009). *atl*^{2} and *Rtnl1*^{1} were described in (Lee et al., 2009) and (Wakefield and Tear, 2006) respectively. *UAS-Rtnl1*$^{+}$ was provided by Andrea Daga (Eugenio Medea Scientific Institute, Conegliano, Italy).

All fly stocks were maintained on cornmeal/agar media (6% w/v dextrose, 6.8% w/v cornmeal, 1.2% w/v yeast, 0.72% w/v agar, 2% w/v methyl 4-hydroxybenzoate) at room temperature (~23ºC) or 25ºC.

3.2: Plasmid construction

pJM952 (pAc5/BiP-sfGFP-HDEL): Superfolder GFP (sfGFP) in pEGFP-N1 (Aronson et al., 2011) was provided by Erik Snapp (Albert Einstein College of Medicine, Department of Anatomy & Structural Biology, Bronx, New York). The BiP signal sequence (MKLCILLAVVAFVGLSLG-RS) was fused to sfGFP with a C-terminal ER retention signal (-HDEL) in pAc5.1/V5-His A (Invitrogen).

pJM1033 (*UAS-BiP-sfGFP-HDEL*): pUASTattB (Bischof et al., 2007) was provided by Konrad Basler (University of Zürich: Institute of Molecular Life Sciences, Zürich, Switzerland). The BiP-sfGFP-HDEL cassette from pJM952 was moved to pUASTattB.

pJM1072 (UAS-tdTomato-dSec61β): tdTomato was fused to Drosophila Sec61β (Drosophila Genomics Resource Center cDNA clone #RE18615) in a 20X-UAS-IVS vector derived from pJFRC7 (Addgene #26220).

3.3: Drosophila stock construction

pJM1033 and pJM1072 were injected into attP2 and VK37 embryos by Genetivision (Houston, TX). Injected flies were backcrossed twice to w^{1118} flies and stocks carrying insertions on chromosome two (VK37) and three (attP2) were established.

3.4: Live larval imaging

Wandering 3rd instar larvae, reared at 25ºC, were dissected in HL6 buffer (Macleod et al., 2002) with 0 mM $CaCl_2$ and 7 mM monosodium glutamate on 35

mm petri dish lids completely filled with Sylgard 184 (Electron Microscopy Sciences). Minutien pins (0.1mm diameter, Fine Science Tools), bent to 90º and trimmed, were used to secure the larvae to the Sylgard. Round 25 mm coverslips (#1 thickness) were cut in half with a diamond knife and securely attached to the Sylgard on either side of the dissected larvae to form a channel. Square 22 mm coverslips (#1.5 thickness) were placed over the larvae and secured to the bottom coverslips with nail polish. Larvae were imaged on a Zeiss LSM 710 inverted confocal microscope using a Plan-Apochromat 63x (1.40 NA) oil immersion objective. GFP was excited with a 488 nm argon laser and emitted light between 493 and 522 nm was collected. tdTomato was excited with a 543 nm Helium Neon laser and emitted light between 552 and 691 nm was collected. Images were adjusted for brightness and contrast in ImageJ. Regions of interest (ROIs) were manually drawn around boutons in ImageJ. Pixel intensities within each ROI were extracted and processed with a custom python script. For each ROI, pixel intensities were scaled by dividing each value by the mean pixel intensity. These data were binned into 50 equally spaced bins ranging from 0 to 8 to generate a frequency histogram. The median and mode of pixel intensities were calculated for each image and graphed with Kaleidagraph.

3.5: Fixed larval imaging

Wandering 3rd instar larvae, reared at 25ºC, were dissected in HL6 buffer (Macleod et al., 2002) with 0 mM $CaCl_2$ and 7 mM monosodium glutamate on Sylgard plates. Larvae were fixed with 4% v/v formaldehyde in HL6 buffer for 5

minutes, washed with HL6, and mounted in Vectashield (Vector Labs). Slides were imaged as described for live larvae.

3.6: S2 cell imaging

pJM952 was transfected into S2R+ cells (Drosophila Genomics Resource Center) using Fugene HD (Promega) as per manufacturer's protocols. Cells were adhered to Concanavalin A-coated glass-bottom dishes (Mat-tek) overnight. Fixed cells were exposed to 4% v/v formaldehyde in HL3 for 5 minutes and washed with PBS. Cells were imaged on a Nikon A1-Rsi laser scanning confocal microscope using a CFI Plan Apo VC 60x (1.4 NA) oil immersion objective. GFP was excited with a 488 nm argon laser and emitted light between 500 and 550 nm was collected.

3.7: Electrophysiology

Flies were raised on food as described above. For electrophysiology experiments, ten mating pairs on average were allowed to mate and lay embryos in half pint bottles for 3-4 days. Wandering third instar larvae from these matings were either dissected in HL3 media (70 mM NaCl, 5 mM KCl, 20 mM $MgCl_2$, 10 mM $NaHCO_3$, 5 mM Trehalose, 115 mM Sucrose, 5 mM HEPES, pH of 7.2) for data collected at a bath [Ca^{2+}] of 0.4 mM, 0.6 mM, 1.0 mM, and 1.5 mM, or HL3.1 media (70 mM NaCl, 5 mM KCl, 4 mM $MgCl_2$, 10 mM $NaHCO_3$, 5 mM Trehalose, 115 mM Sucrose, 5 mM HEPES, pH of 7.2) for data collected at a bath [Ca^{2+}] of 0.1 mM. Nerves were cut just posterior to the ventral nerve cord. A single nerve

was then isolated and stimulated at a 5 mV intensity using a suction electrode. Recordings were taken from muscle 6 of segment A6 with a recording electrode filled with 3 M KCl and having a resistance between 10-40 MΩ. Glass filaments used for suction electrodes (B120-90-10) and recording electrodes (BF120-94-10) were from World Precision Instruments. Recording electrodes were pulled by a Model P-87 Flaming/Brown Micropipette Puller from Sutter Instruments Company. Stimulus duration was set to at least 1.5 times the threshold required to elicit an evoked response to ensure both axons innervating muscles 6 and 7 were fully stimulated. Evoked response traces for all larvae were recorded for a minimum of 20 s. Quiescent traces of 60 s were recorded for mEJP frequency and amplitude analysis. EJP and mEJP analysis was accomplished using the Synaptosoft Mini Analysis Program. Frequency and amplitude of mEJPs were analyzed using the "non-stop analysis" function. For this analysis, mEJP amplitude threshold was set at 0.7 mV with a LoPass Butterworth filter and a cut off frequency of 200 Hz. EJP amplitude was determined by manually selecting the peaks, which corresponded to the first 20 stimulations within a trace. Failures occurring during the first 20 stimulations of a trace were denoted as zeroes and contributed toward average EJP data. No threshold minimum was employed for EJPs. Corrected quantal content was calculated using the formula $m = v/v_1(1-v/V_o)^{-1}$, where v = EJP amplitude, v_1 = mEJP amplitude, and V_o = resting potential - 15 mV (Martin, 1955).

3.8: Phospho-Mad quantitation

Wandering 3rd instar larvae, reared at room temperature, were dissected in S2 media (Invitrogen) and fixed immediately with 4% v/v formaldehyde (in S2 media) for 15 min. Fixed larvae were washed with PBS-T (PBS + 0.1% v/v Triton X-100) and transferred to a Sylgard-coated 24 well plate. Larvae were incubated with Phospho-Smad1/5 (Ser463/465) rabbit mAb (Cell Signaling, 41D10, 1:50 in PBS-T) overnight at 4ºC with gentle orbital shaking, washed with PBS-T, incubated with goat anti-rabbit IgG Alexa 488 conjugated antibody (1:1000 in PBS-T) for 90 minutes at room temperature, washed with PBS, and mounted in vectashield. For each experiment, at least three w^{1118} larvae were included, and all larvae were exposed to the same dilution of antibody. For each genotype, ventral ganglia from at least eight larvae from two independent experiments were analyzed. Larvae were imaged as described for live larvae. ROIs were manually drawn around motor neuron nuclei in the ventral nerve cord using ImageJ. For each ROI, mean pixel intensity was divided by area. ROIs were summed and averaged for each larva and normalized to the w^{1118} internal control.

3.9: Arborization

Flies were reared at 25°C on standard cornmeal media. Wandering 3rd instar larvae were dissected in HL3, fixed in 4% v/v formaldehyde (in HL3), and washed with PBS-T. Larval pelts were placed in sylgard-coated 24 well plates and exposed to goat anti-HRP Alexa 488 primary antibodies (1:500) overnight at 4ºC with gentle orbital shaking, washed in PBS, and mounted in vectashield. Boutons

at muscles 6 and 7 in segment A3 were imaged as described for live larvae. Boutons were counted manually in ImageJ.

3.10: Climb tests

Crosses were made with ten mating pairs in half pint bottles and placed at 25°C. Progeny were collected 2 days after the first sign of eclosion, aging all flies between 0-2 days post eclosion. Males were anesthetized and placed into vials in groups of 10-12 flies and aged at 25°C. Adult male flies were separated into individual empty vials, tapped to the bottom of the vial, and timed to see how long it took them to climb 6 vertical centimeters. Each fly experienced three time trials with at least 5 minutes of rest between each trial. If a fly failed to cross the 6 cm mark in 60 seconds, the time was recorded as 60 s. The minimum time for each fly was then compiled and averaged as the time for that day, with each bar representing a minimum of ten flies.

3.11: Velocity tests

Flies were reared on standard cornmeal media at 25ºC. 0-2 day old flies were anesthetized with carbon dioxide and groups of 6-10 males were aged until 3, 10, 15, 25, and 30 days (+/- 1 day). Flies were transferred, without anesthesia, into vials with approximately 10 mL of 1% w/v agar and allowed to rest for 10 min. Flies were placed in a chamber made of white, translucent Plexiglas with a digital video camera focused on the vial. Two mirrors placed behind the vial at 40 degree angles produce two reflections visible in the video. Vials were banged to

knock flies to the agar surface and videos of the climbing behavior were captured. Three trials of 30 s each were recorded in succession for each group. Average velocity for each vial was measured using the iFly system (Jahn et al., 2011; Kohlhoff et al., 2011).

3.12: Statistics

3.12.1: Statistics for BiP-sfGFP-HDEL signal intensity distribution

Pixel intensity frequency histograms in Figure 6 are the averages taken from regions of interest around boutons for control (Ciii) and *atl*^{2} (Civ). Dashed boxes in Ci and Cii represent the ROIs used for the pixel intensity frequency histograms for wildtype (Ciii) and *atl*^{2} (Civ). The mode and median of these pixel intensity frequency histograms are averaged in (D). Each scattergram data point is the average of a single larva. Bars and error bars represent genotype averages and standard errors, respectively. P-values shown represent an unpaired Students t-test performed with KaleidaGraph.

3.12.2: Statistics for electrophysiology

For Figures 8E, 8F, 8H, 9, 10, and 11, each scattergram data point is the average of the first 20 EJP responses (both successes and failures) recorded for a single larva. Bars and error bars represent genotype averages and standard errors, respectively. For Figures 8F, 8H, 9, 10, and 11, p-values represent unpaired Students t-tests performed with KaleidaGraph. For Figure 8E, p-values represent a one-way ANOVA using a Fisher's LSD post hoc test performed with

KaleidaGraph. For Figure 8G, data points are the averages of at least 6 individual animals. Each average for these animals is the average of the first 20 EJP responses (both successes and failures) recorded for a single larva. Data are expressed as corrected quantal content using the formula $m = v/v_1(1-v/V_o)^{-1}$, where v = EJP amplitude, v_1 = mEJP amplitude, and V_o = resting potential - 15 mV (Martin, 1955).

3.12.3: Statistics for BMP signal intensity

Using ImageJ, ROIs were manually drawn around each motor neuron nucleus within the optical slice which was most intense for that nucleus. For each ROI, mean pixel intensity was divided by area. ROIs were summed and averaged for each larva and normalized to the w^{1118} internal control. Each scattergram data point is the average nuclear signal intensity per area for a single larva. Bars and error bars represent genotype averages and standard errors, respectively. P-values represent unpaired Students t-test performed with KaleidaGraph.

3.12.4: Statistics for arborization

Each scattergram data point is the average number of boutons for a single larva. Averages for each larva are determined by counting boutons in segments A3 over muscles 6/7 on both the left and right side of the larva. Bars and error bars represent genotype averages and standard errors, respectively. P-values represent unpaired Students t-tests performed with KaleidaGraph

3.12.5: Statistics for adult locomotor assays

For Figure 14A, each scattergram data point is the average of three separate time trials for a single male fly. In turn, the average for each trial is the time it takes a fly to climb a vertical distance of 6 cm. Flies that were unable to climb 6 cm within 60 seconds were assigned a value of 60. Bars and error bars represent genotype averages and standard errors, respectively.

For Figure 14B, each scattergram data point is the average of three separate time trials for a group of 6-10 male flies. In turn, the average for each trial is the mean velocity for that group of flies for a duration of 30 s subsequent to bang stimuli. Bars and error bars represent genotype averages and standard errors, respectively.

4: Results

4.1: Chemical fixation disrupts ER morphology in Drosophila motor neurons, muscles, and S2 cells

Direct imaging of ER morphology within Drosophila larval tissues has been performed on muscle and neuronal cell bodies within the ventral nerve cord (VNC) (Lee et al., 2009; Orso et al., 2009) as well as nerve terminals (Wong et al., 2014). These studies, primarily on fixed tissue, suggested that ER signal in the nerve terminal was low relative to other tissues. We hypothesized that this low abundance signal could be a consequence of poor expression or difficulties in trafficking of the marker. To circumvent these potential problems we developed improved reagents for *in vivo* imaging of the ER. First, we generated an ER

luminal maker with improved protein folding characteristics by utilizing mutant Green Fluorescent Protein (GFP) that has been optimized for proper folding in the ER lumen. This protein, termed Superfolder GFP (sfGFP) (Aronson et al., 2011), traffics to the ER via a signal sequence derived from the resident chaperone BiP and is retained by the addition of the HDEL ER retention signal (BiP-sfGFP-HDEL). Next, we similarly constructed a transgenic fly line expressing an ER membrane marker containing the ER membrane protein sec61β linked to tandem dimer Tomato (tdTomato) as a fluorescent marker. The expression of both of these transgenes is driven by the *Gal4 UAS*. In Figure 4, we show the ER labeled by BiP-sfGFP-HDEL expressed in the motor neuron (Figure 4A), the neuromuscular junction (NMJ) (Figure 4B), larval body wall muscle (Figure 4C), and cultured S2 cells (Figure 4D).

Previous results have suggested that organelle structure *in vivo* is labile to fixation (Johnson et al., 2015), and therefore a more accurate depiction of ER structure and dynamics might require imaging in live cells. To determine if ER structures in Drosophila larvae or S2 cells were similarly labile to fixation, we compared ER structure in live cells with the fixed tissue described above. We found that very mild fixation (4% v/v formaldehyde for 5 minutes with no permeabilization) significantly altered ER structure in all tissues that were examined (Figure 4). Overall, the network of ER tubules appeared to fragment into discrete foci or punctae. Uniformly labeled tubules seen in live imaging converted to a “beads on a string” morphology consistent with ruptured tubules. ER tubules extend via association with microtubule-dependent motors in cell

culture (Upadhyaya & Sheetz, 2004) and can be remodeled by the elongating (+) ends of microtubules via protein-protein interaction (Grigoriev et al., 2008). Perhaps the ER tubules are maintained under stress by association with the underlying cytoskeletal network and chemical fixation disrupts this mechanical tension. Regardless of the mechanism, these observations reveal the disruptive effect of tissue fixation on the ER *in vivo*. For this reason, all subsequent ER imaging exhibited here was performed on live cells.

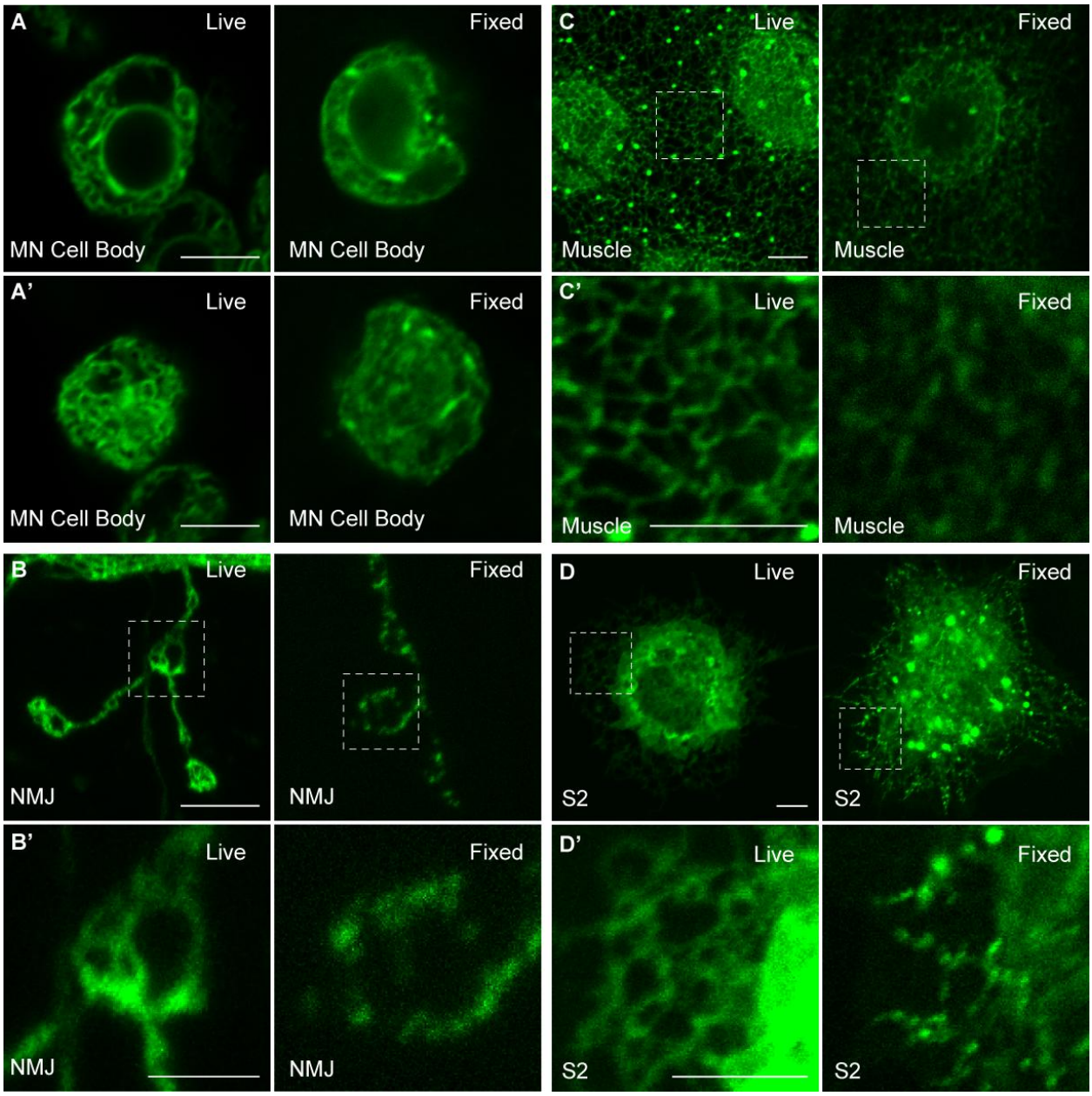

Figure 4: Chemical fixation disrupts the ER network in motor neurons, muscles, and S2 cells. Representative confocal slices through the center **(A)** and periphery **(A')** of live and fixed wt motor neuron cell bodies in the ventral nerve cord. **(B)** ER in wildtype larval boutons under live and fixed conditions. **(B')** Magnification of boxed regions in **B**. **(C)** ER in wildtype muscle 6 from segment A3 under live and fixed conditions. **(C')** Magnification of boxed regions in **C**. **(D)** ER in S2 cells under live and fixed conditions. **(D')** Magnification of boxed regions in **D**. Chemical fixation was achieved via 5 minute exposure to 4% v/v paraformaldehyde. ER was imaged using BiP-sfGFP-HDEL. Scale bar = 5 µm, except **B'** which is 2 µm.

4.2: BiP-sfGFP-HDEL marks the ER

We investigated ER anatomy in larval motor nerve terminals in more detail. To orient the BiP-sfGFP-HDEL signal with the plasma membrane, we co-expressed BiP-sfGFP-HDEL with the plasma membrane marker myr::tdTomato. We found that BiP-sfGFP-HDEL was located immediately adjacent to the myr::tdTomato signal (Figure 5A-5C), indicating that the ER baskets in motor nerve terminals directly underlie the plasma membrane. We also co-expressed BiP-sfGFP-HDEL along with the ER membrane marker tdTomato-Sec61β. As expected, these two markers showed extensive overlap (Figure 5E-5F), thus validating both transgenes as ER markers.

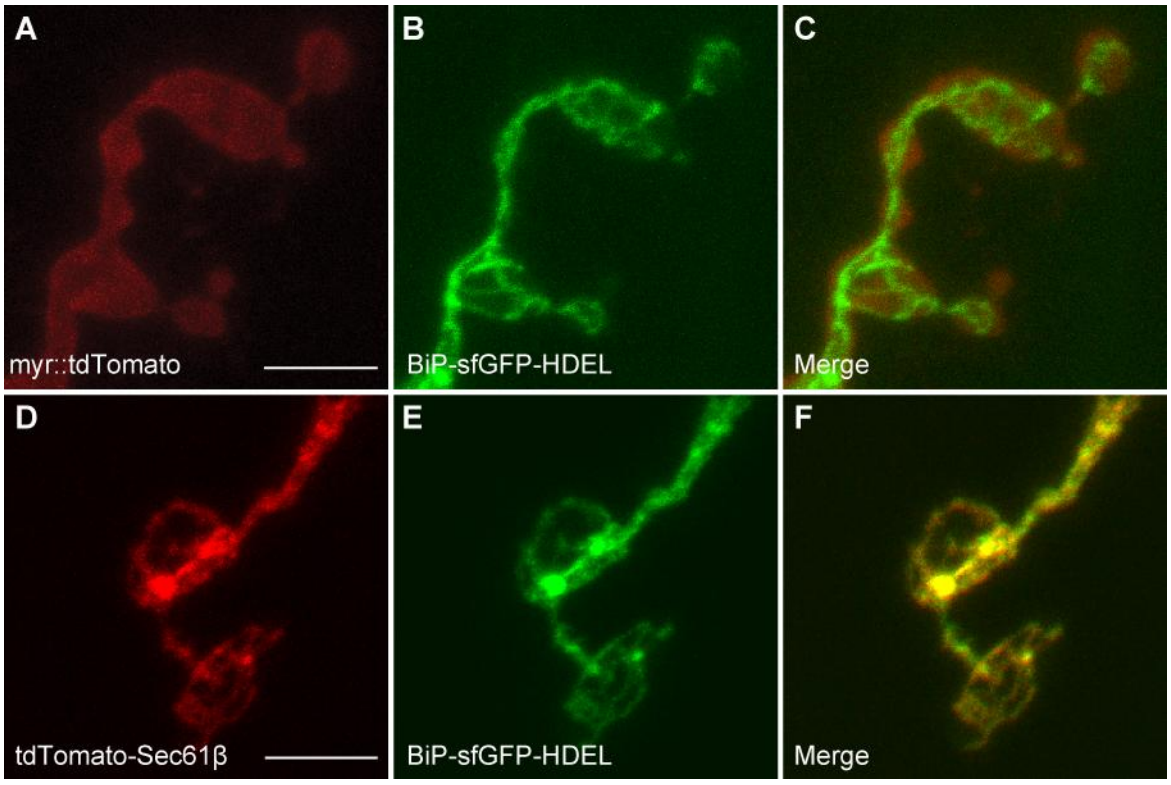

Figure 5: The ER lumen marker BiP-sfGFP-HDEL colocalizes with the ER membrane marker tdTomato-Sec61β. Third instar larval motor nerve terminals from segment A2 muscle 4. **(A-C)** Representative confocal Z-projections showing the plasma membrane marker myr-tdTomato **(A)**, the ER marker BiP-sfGFP-HDEL **(B)**, and the merged signals **(C)**. **(D-F)** Z-projections showing the ER membrane marker tdTomato-Sec61β **(D)**, the ER lumen marker BiP-sfGFP-HDEL **(E)**, and the merged signals **(F)**. All transgene were driven by motor neuron driver *OK371-Gal4*. Scale bar = 5 µm.

4.3: The *atl*^{2} null mutation alters ER structure in motor axons and presynaptic boutons

The *atl* gene encodes an ER fusion GTPase (Orso et al., 2009), and thus we anticipated that by preventing ER fusion, the *atl*^{2} null mutation would confer ER fragmentation as has been shown in fixed tissue by electron microscopy. To test this prediction, we used BiP-sfGFP-HDEL to compare ER morphology in motor neuron cell bodies, motor axon initial segments, and motor nerve terminals

in control and *atl*^{2} animals (Figure 6A). We found little effect on ER morphology in cell bodies (Figure 6Bi vs. Figure 6Bii), but in axon initial segments, we found that the ER crossbridges found in wildtype were almost completely eliminated in *atl*^{2}, and that the long straight ER tubules observed in wildtype became wavy in *atl*^{2} (Figure 6Biii and 6Biv). In motor nerve terminals, we found that *atl*^{2} eliminated the basket structures and caused a diffuse ER signal, which we attribute to ER fragmentation (Figure 6Ci and Figure 6Cii).

To quantitate the effects of *atl*^{2} on ER morphology in nerve terminals, we reasoned that the BiP-sfGFP-HDEL signal in *atl*^{2} larvae would be uniformly distributed across the synapse and thus a frequency histogram for the pixel intensities within each terminal would exhibit a Gaussian distribution, centered around the mean pixel intensity for the nerve terminal. The Gaussian distribution of pixel intensities is due to the center of the three dimensional bouton being thicker than the edges and thus containing a greater number of pixels than the edges within the z-projection. In contrast, we anticipated that pixel intensities in wildtype nerve terminals would comprise a small number of bright pixels indicating the tubules and a larger number of dark pixels indicating voids between tubules. Thus, we predicted that a frequency histogram for the pixel intensities from wildtype would be positively skewed. To test this prediction, we compared frequency histograms of pixel intensities, normalized to mean intensity, between wildtype and *atl*^{2}. We found, as predicted, a strong positive skew in wildtype (Figure 6Ciii) but a more Gaussian distribution in *atl*^{2} (Figure 6Civ). We confirmed these skews by comparing modes and medians for these

histograms with the mean. For *atl*^{2}, the mode and median were very close to the mean, consistent with a Gaussian distribution, whereas for wildtype, both the mode and median were significantly decreased, consistent with a positive skew (Figure 6D). In addition, we compared line scans across nerve terminals in *atl*^{2} and wildtype. Whereas wildtype line scans showed multiple peaks, corresponding to tubules within the baskets, the line scan from *atl*^{2} nerve terminals were uniform, consistent with a diffuse ER signal (Figure 6Cv and Figure 6Cvi).

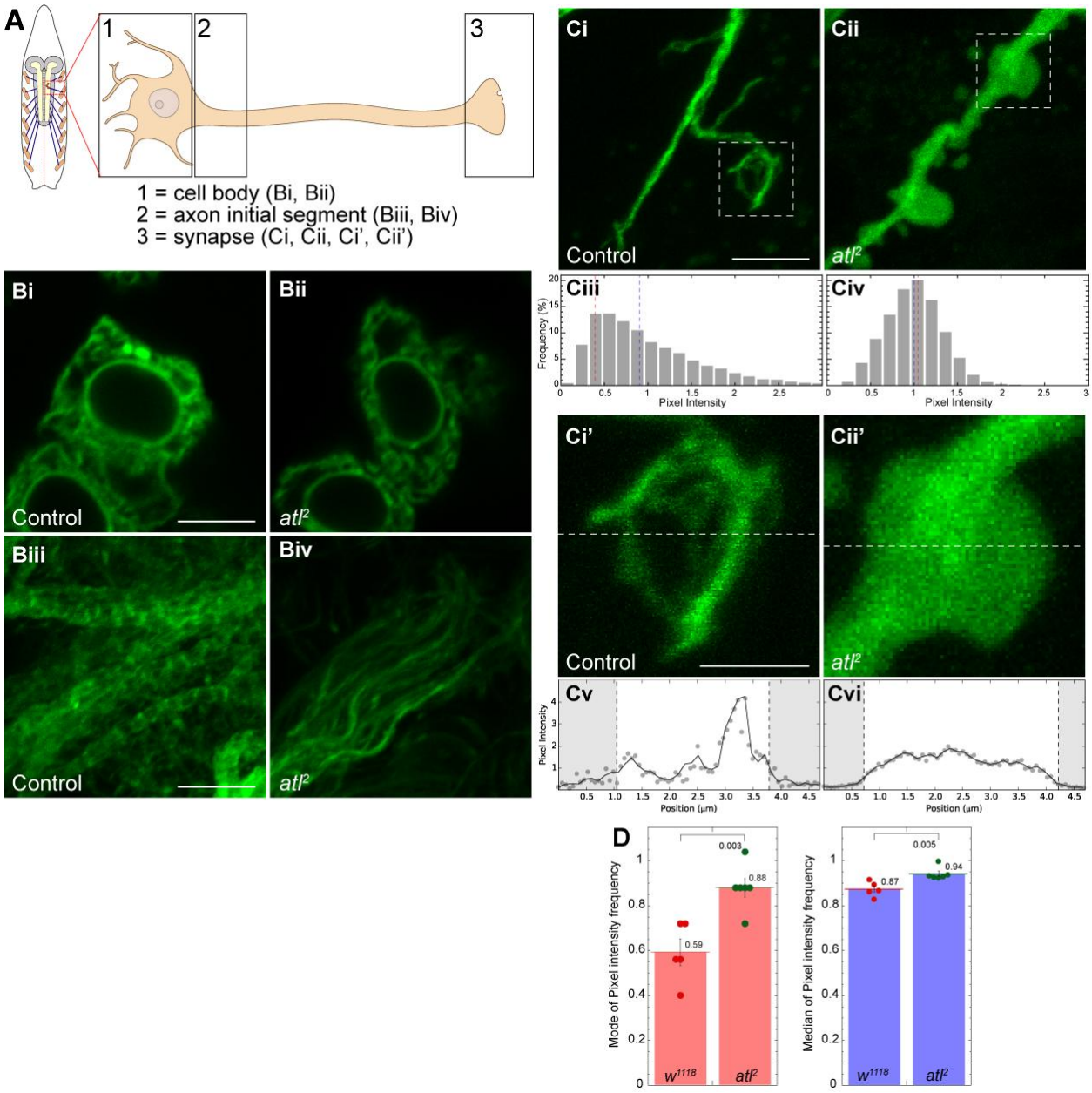

Figure 6: Loss of *atl* disrupts the tubular ER network in motor axons and motor nerve terminals of third instar larvae. (**A**) Schematic of the regions of the motor neuron from which images were collected. **(B)** Representative central confocal slices of motor neuron cell bodies in control [*OK371>BiP-sfGFP-HDEL*] **(Bi)** and *atl*^{2} [*atl*^{2}*, OK371>BiP-sfGFP-HDEL*] **(Bii)** larvae. Z-projections of motor axons within the ventral nerve cord in control **(Biii)** and *atl*^{2} **(Biv)** larvae. **(C)** Z-projections of neuromuscular junctions from muscle 4 at segment A6 in wildtype **(Ci)** and *atl*^{2} **(Cii)** larvae. Average frequency histograms of pixel intensities taken from regions of interest around boutons for control (**Ciii)** and *atl*^{2} **(Civ)**. Boxed regions in **Ci** and **Cii** are expanded in **(Ci')** and

(Cii'), respectively. Dashed lines in **Ci'** and **Cii'** represent the positions used for the line scans of pixel intensities for wildtype **(Cv)** and *atl*^{2} **(Cvi)**. **(D)** Mode and median of pixel intensity frequency histograms are shown for five control and six *atl*^{2} images. Error bars represent the standard error of the mean. Scale bar = 5 µm, except for **Ci'** and **Cii'** which is 2 µm. P-values shown represent an unpaired Students t-test performed with KaleidaGraph.

4.4: Neuron-specific atl inhibition alters ER structure

To confirm that these effects of ER morphology were caused by the *atl*^{2} mutation itself rather than a genetic background polymorphism, we determined if the ER fragmentation that we observed in *atl*^{2} could be recapitulated by targeted *atl* knockdown in neurons. Thus we expressed both an *atl RNAi* transgene as well as the dominant-negative *atl*^{K51A} allele (Orso et al., 2009) in neurons and found a similar decrease in ER tubule crossbridges in axon initial segments (Figure 7D-F) and a similar diffuse ER signal at the motor nerve terminals (Figure 7G-I). Taken together, these results demonstrate that proper ER structure in motor neurons requires atlastin activity.

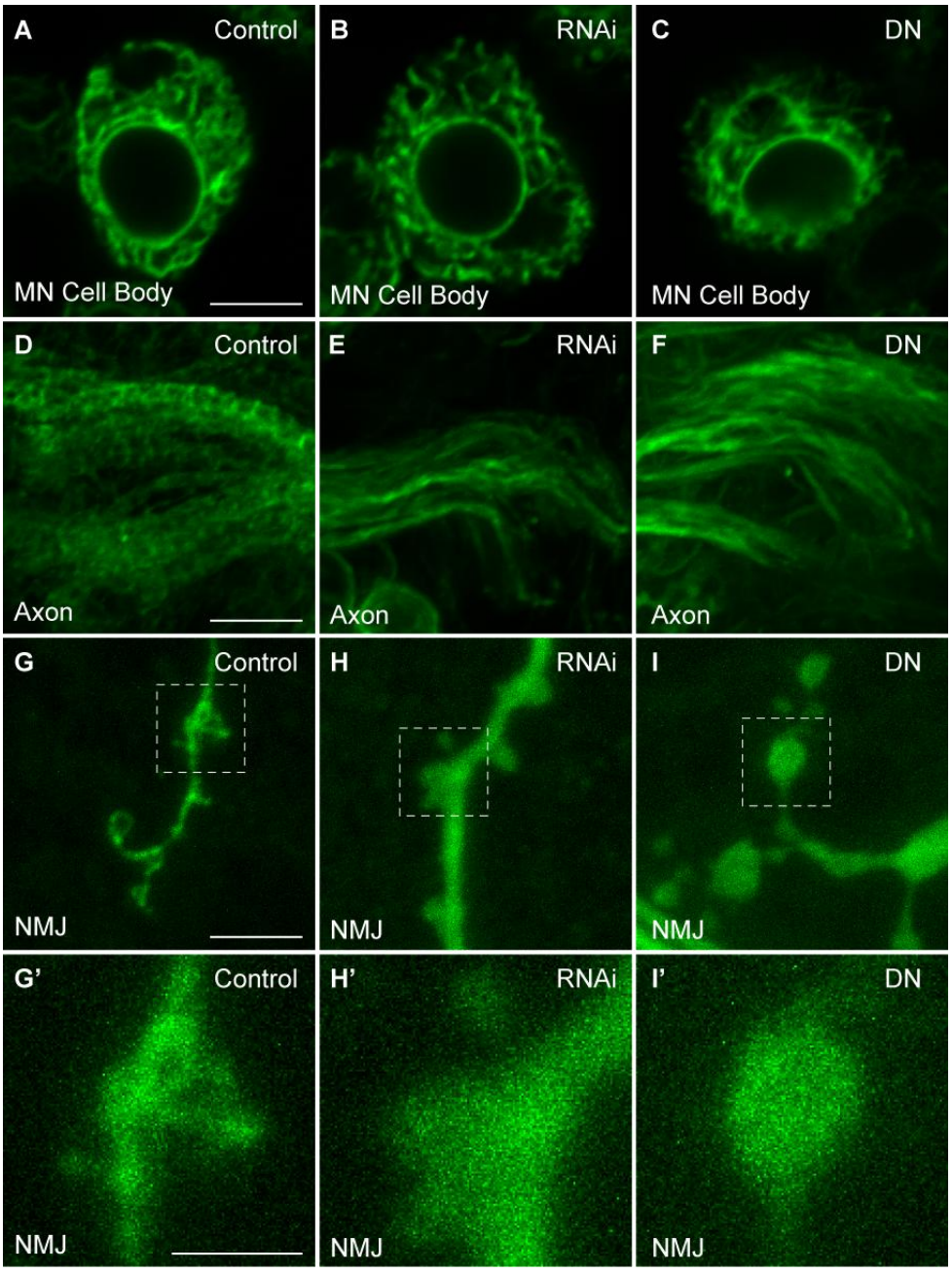

Figure 7: Expression of *UAS-atl^{RNAi}* or *UAS-atl^{K51A}* disrupts the tubular ER network in motor axons and presynaptic boutons. **(A-C)** ER in motor neuron cell bodies for control [*nSyb>BiP-sfGFP-HDEL*] **(A)**, RNAi [*nSyb>BiP-sfGFP-HDEL, atl^{RNAi}*] **(B)**, and dominant negative [*nSyb>BiP-sfGFP-HDEL, atl^{K51A}*] **(C)**. **(D-F)** ER in motor axons for control **(D)**, RNAi **(E)**, and dominant negative *atl^{K51A}* **(F)**. **(G-I)** ER in presynaptic boutons for control **(G)**, RNAi **(H)**, and DN **(I)**. **(G'-I')** Magnification of boxed regions for wt **(G')**, RNAi **(H')**, and dominant negative *atl^{K51A}* **(I')**. Scale bar = 5 µm, except for **G'**, **H'**, and **I'** which is 2 µm.

4.5: Impaired evoked transmitter release in *atl*^{2} and *Rtnl1*^{1} null mutants

Altered levels of several HSP proteins, including Spartin and Spastin, alter transmitter release from Drosophila motor nerve terminals. We tested the possibility that *atl*^{2} and *Rtnl1*^{1} might similarly affect transmitter release. We used the larval neuromuscular preparation (Jan and Jan, 1976; Stewart et al., 1994) to measure synaptic transmission and found that each mutation indeed decreased evoked transmitter release, using the consequent muscle depolarization termed excitatory junctional potential (EJP) as a readout. Figure 8A and 8B compare averaged EJPs in wildtype vs. *atl*^{2}, respectively, at the 4 indicated different bath [Ca^{2+}]. At a bath [Ca^{2+}] of 0.6 mM, both *atl*^{2} and *Rtnl1*^{1} decrease transmitter release almost two-fold (Figure 8C).

To confirm that these transmitter release phenotypes were caused by loss of *atl* and *Rtnl1*, we determined if expression of *UAS-atl*$^{+}$ and *UAS-Rtnl1*$^{+}$ transgenes would be sufficient to restore wildtype transmitter release to *atl*^{2} and *Rtnl1*^{1}. We found that the *atl*^{2} transmitter release phenotype was fully rescued by expression *UAS-atl*$^{+}$ driven by the weak, ubiquitous *Gal4* driver *arm-Gal4* (Figure 5D). In contrast, the *Rtnl1*^{1} transmitter release phenotype was rescued only partially by *arm-Gal4*-driven *UAS-Rtnl1*$^{+}$; this partial rescue most likely reflected weak expression of the *Rtnl1*$^{+}$ transgene because as shown below, driving *UAS-Rtnl1*$^{+}$ expression with the stronger *da-Gal4* driver elicited complete rescue (Figure 11B).

Previous reports indicated that nerve terminal ER is capable of controlling transmitter release by influencing cytoplasmic [Ca^{2+}]. In particular, inhibition of

the Ryanodine Receptor (RyR) attenuates the cytoplasmic [Ca^{2+}] increase due to evoked single or short trains of action potentials (Emptage et al., 2001; Liang et al., 2002; Llano et al., 2000). Because both Atl and Rtnl1 alter ER morphology, and as shown above, decreased levels of Atl perturbs ER structure in nerve terminals, we wondered if the decreased evoked transmitter release in *atl*^{2} and *Rtnl1*^{1} might reflect attenuation of the increased cytoplasmic [Ca^{2+}] caused by nerve stimulation. If so, then we predicted that this decreased transmitter release would be rescued by elevated bath [Ca^{2+}], at which Ca^{2+} is less limiting for transmitter release (Wong et al., 2014). For both *atl*^{2} and *Rtnl1*^{1} we found that as we increased bath [Ca^{2+}], transmitter release became progressively similar to wildtype (Figure 8E, which shows quantal content, corrected for nonlinear summation and normalized to wildtype). Elevated bath [Ca^{2+}] completely rescued the *Rtnl1*^{1} transmitter release phenotype, but rescued the *atl*^{2} phenotype only partially. In addition, we found that RNAi-mediated knockdown of either *atl* or *Rtnl1* in neurons similarly failed to decrease transmitter release at elevated bath [Ca^{2+}] (Figure 8F; efficacy of the *atl* and *Rtnl1* RNAis is demonstrated in experiments described below). The suppression of the *atl* and *Rtnl1* transmitter release phenotypes by elevated bath [Ca^{2+}] is consistent with the possibility that deficits in the rise of intracellular [Ca^{2+}] might underlie the impaired transmitter release observed in these genotypes. It is not known why elevated bath [Ca^{2+}] rescues the *atl RNAi* knockdown phenotype completely, but *atl*^{2} only partially. However, it is possible that *atl* acts in non-neuronal tissues to affect transmitter release at elevated bath [Ca^{2+}], or that general anatomical deficits of *atl*^{2} (for

example, dwarf body size and developmental delays) that are not recapitulated by the RNAi knockdown, might contribute to these differences.

It has been previously observed that atlastin and reticulon confer opposite effects on ER morphology. In particular, whereas *atl*^{2} fragments the ER (Orso et al., 2009), *Rtnl1* knockdown by RNAi (O'Sullivan et al., 2012) converts ER tubes into sheets. These effects are consistent with the known biochemical roles of atlastin and reticulon as ER fusion protein and ER curvature-generating protein, respectively. We found a mutual suppression of the evoked transmitter release phenotype in the *Rtnl*^{1}*; atl*^{2} double mutant (Figure 8C and Figure 8E), which supports the possibility that atlastin and reticulon have antagonistic effects on ER morphology.

We examined synapse architecture in *atl*^{2} and *Rtnl1*^{1} mutants by performing immunocytochemistry with antibodies directed at the presynaptic active zone protein Bruchpilot and the postsynaptic neurotransmitter receptor GluRII. We found no obvious structural or organizational defects in the number or size of active zones or in the pattern of GluRII immunoreactivity (data not shown). Thus at a low resolution level, neither Atl nor Rtnl1 appear to play a role in organizing synaptic structure.

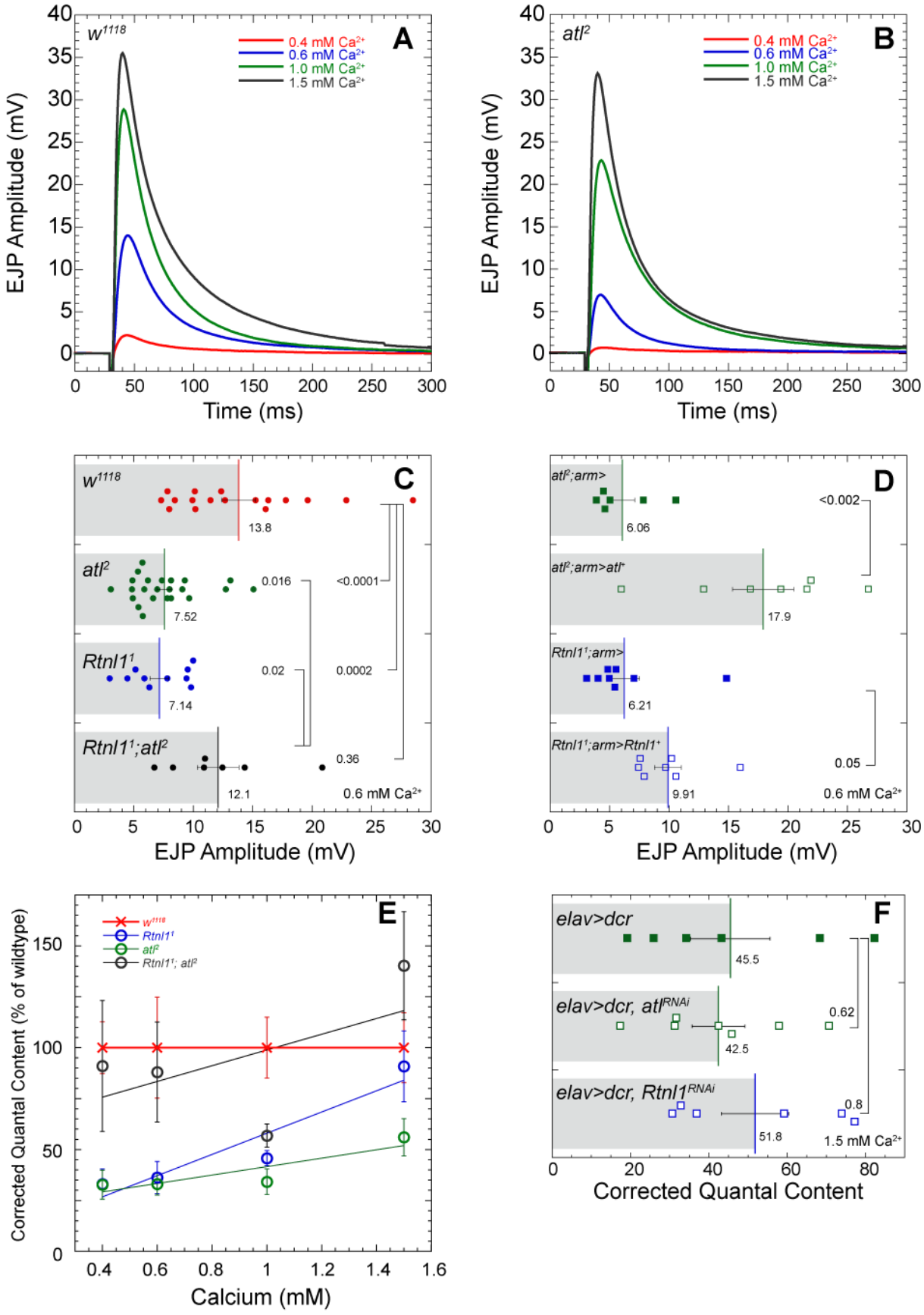
A
w1118
0.4 mM Ca2+
0.6 mM Ca2+
1.0 mM Ca2+
1.5 mM Ca2+
EJP Amplitude (mV)
Time (ms)
B
atl2
C
w1118
13.8
atl2
7.52
0.016
<0.0001
Rtnl11
7.14
0.02
0.0002
Rtnl11;atl2
12.1
0.36
0.6 mM Ca2+
EJP Amplitude (mV)
D
atl2;arm>
6.06
<0.002
atl2;arm>atl+
17.9
Rtnl11;arm>
6.21
Rtnl11;arm>Rtnl1+
9.91
0.05
E
w1118
Rtnl11
atl2
Rtnl11; atl2
Corrected Quantal Content (% of wildtype)
Calcium (mM)
F
elav>dcr
45.5
elav>dcr, atlRNAi
42.5
0.62
elav>dcr, Rtnl1RNAi
51.8
0.8
1.5 mM Ca2+
Corrected Quantal Content

Figure 8: *atl*^{2} and *Rtnl1*^{1} decrease evoked neurotransmitter release. Average EJP traces for *w*^{1118} **(A)** and *atl*^{2} **(B)** larvae at 0.4, 0.6, 1.0, and 1.5 mM Ca^{2+}. In ascending [Ca^{2+}], for *w*^{1118} n = 7, 17, 7, and 7 and for *atl*^{2} n = 7, 23, 7, and 7. **(C)** Average EJP amplitude for *w*^{1118}, *atl*^{2}, *Rtnl1*^{1}, and *Rtnl1*^{1}*; atl*^{2}. P-values shown represent a one-way ANOVA using a Fisher's LSD post hoc test performed with KaleidaGraph. **(D)** Average EJP amplitude for *atl*^{2}*; arm>UAS-atl*$^{+}$, *Rtnl1*^{1}*; arm>UAS-Rtnl1*$^{+}$, and their respective controls using the ubiquitous *arm-Gal4* driver. P-values shown represent an unpaired Students t-test performed with KaleidaGraph. Recordings for **C** and **D** were performed at 0.6 mM Ca^{2+}. **(E)** Average corrected quantal content for *w*^{1118}, *Rtnl1*^{1}, *atl*^{2}, and *Rtnl1*^{1}*; atl*^{2}. In ascending [Ca^{2+}], *w*^{1118} n = 7, 17, 7, and 7; *atl*^{2} n = 7, 23, 7, and 7; *Rtnl1*^{1} n = 7, 10, 7, and 7; *Rtnl1*^{1}*; atl*^{2} n = 7, 7, 7, and 7. **(F)** Average corrected quantal content for *elav>dcr*, *elav>dcr, atl*^{RNAi}, *and elav>dcr, Rtnl1*^{RNAi} at 1.5 mM [Ca^{2+}]. P-values shown represent an unpaired Students t-test performed with KaleidaGraph. Recordings were performed in HL3 from muscle 6 in segment A6. For **C-E**, bars and error bars represent averages and standard errors, respectively. Each scattergram data point is the average of the first 20 EJP responses (successes and failures) recorded for each larva.

4.6: *atl* acts in the motor neuron to control transmitter release

Next we wished to identify the tissues in which Atl and Rtnl1 are required to control neurotransmitter release. Because *atl*^{2} and *Rtnl1*^{1} exhibited the greatest deficit in neurotransmitter release at the lowest bath [Ca^{2+}] (Figure 8), we performed the next set of measurements at the low bath [Ca^{2+}] of 0.1 mM, in a solution (HL3.1) conducive for low [Ca^{2+}] recordings.

Transgenic rescue for *atl* is problematic because Drosophila will not tolerate even moderate levels of *atlastin* overexpression. No wandering third instar larvae are produced when our fly line carrying *UAS-atl*$^{+}$ (Orso et al., 2009) is crossed with flies bearing the moderate, ubiquitous *da-Gal4* or pan-neuronal *elav-Gal4* drivers, even at 18°C (data not shown). In addition, driving *UAS-atl*$^{+}$

with the motor neuron *D42* driver causes retention of the CD8-GFP marker within the cell body ER and prevents CD8-GFP transport to nerve terminals (Orso et al., 2009). Therefore we used tissue specific RNAi-mediated knockdown and expression of the dominant-negative *UAS-atl*^{K51A} to identify the tissue(s) in which *atl* is required for normal transmitter release. *UAS-Dicer (Dcr)* was also included in larvae involving RNAi to improve efficiency of RNAi knockdown.

We first observed that inhibiting atlastin function by driving *atl RNAi* expression with the motor neuron driver *D42-Gal4* (Figure 9A, left, green diamonds) or the pan-neuronal driver *elav-Gal4* (Figure 9A, left, green squares) significantly decreased EJP amplitude. Similarly, inhibiting *atl* by expressing the dominant-negative *atl*^{K51A} with either *D42* (Figure 9A, left, green inverted triangles) or the pan-neuronal driver *nSyb-Gal4* (Figure 9A, left, green triangles) also significantly decreased EJP amplitude. These results indicate that *atl* activity is required in the motor neuron for wildtype evoked transmitter release.

We used two additional pieces of data to confirm that the decrease in EJP amplitude represented decreased transmitter release rather than decreased muscle responsiveness to transmitter. First, we observed that amplitudes of 'mini' EJPs, generated by spontaneous release of individual vesicles of transmitter, were not significantly affected by the *atl* genotype (data not shown). Thus, the *atl* mutant muscle responds normally to released transmitter. Second, we analyzed the frequency of synaptic transmission failures to confirm a presynaptic role for Atl. At the low bath [Ca^{2+}] utilized in Figure 9, the motor neuron responds to nerve stimulation with release of either no transmitter, which is called a failure, or

one or two vesicles of transmitter, which is called a success. The decreased transmitter release in the *atl* knockdown larvae was accompanied by a decreased frequency of successes (Figure 9A, right), indicating that *atl* knockdown decreases transmitter release.

Transmitter release at the Drosophila neuromuscular junction can be affected by the target muscle or the neighboring peripheral glia (Huang and Stern, 2002; Kerr et al., 2014; McCabe et al., 2003; Schmidt et al., 2012). To test a requirement for *atl* in target muscle or peripheral glia, we used RNAi to knock down *atl* in these tissues. No effect on transmitter release or frequency of synaptic failures was detected when atlastin was reduced in muscle (Figure 9B, left, green squares) or glia (Figure 9B, left, green diamonds). These observations suggest that atlastin is required specifically in the motor neuron to regulate transmitter release.

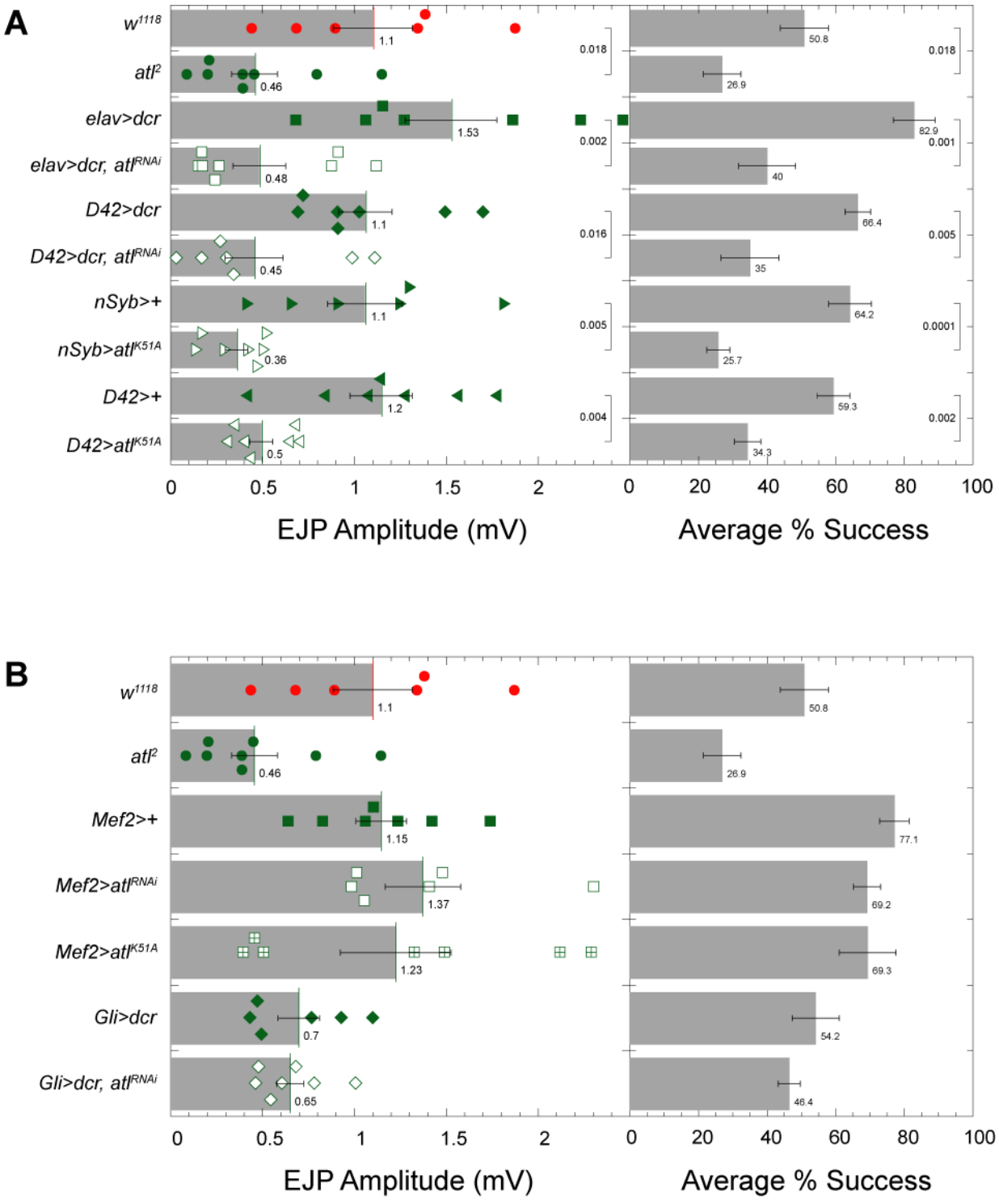

Figure 9: Neuronal expression of *UAS-atl^{RNAi}* and *UAS-atl^{K51A}* decreases evoked neurotransmitter release. **(A)** Average EJP amplitude and corresponding percent success for *wt*, *atl^{2}*, *UAS-atl^{RNAi}* and *UAS-atl^{K51A}*. Drivers include the pan-neuronal *elav-Gal4* and *nSyb-Gal4* and the motor neuronal *D42-Gal4*. **(B)** Average EJP amplitude and

percent success for muscle (*Mef2-Gal4*) and glial (*Gli-Gal4*) expression of *UAS-atl*^{RNAi} and *UAS-atl*^{K51A}. Recordings for **A** and **B** were made in HL3.1 at 0.1 mM Ca^{2+} from muscle 6 in segment A6. Bars and error bars represent averages and standard errors, respectively. Each scattergram data point is the average of the first 20 EJP responses (successes and failures) recorded for each larva. P-values shown represent an unpaired Students t-test performed with KaleidaGraph.

4.7: Overexpression of *atl* in the motor neuron impairs neurotransmitter release

Expression of *UAS-atl*$^{+}$ in Drosophila motor neurons causes excessive fusion and expansion of the nuclear envelope and ER membrane and defects in the secretory pathway in both the neuron cell body and presynaptic terminal (Orso et al., 2009). We used the BiP-sfGFP-HDEL imaging reagent described above to determine if *atl*$^{+}$ overexpression disrupted ER morphology in live cells. We found that *atl*$^{+}$ overexpression caused accumulation of large ER punctae in motor neuron cell bodies and axons (Figure 10A). These punctae appear similar to the punctae found when the plasma membrane marker mCD8-GFP was visualized in *atl*$^{+}$ overexpressing neurons (Orso et al., 2009). To determine if *atl*$^{+}$ overexpression affected transmitter release, we compared EJP amplitudes in *atl*$^{+}$ overexpressing and control larvae at both low (0.1 mM) and high (1.5 mM) bath [Ca^{2+}]. We found that *atl*$^{+}$ overexpression significantly decreased EJP amplitudes and the frequency of synaptic successes at low bath [Ca^{2+}] (Figure 10B) and decreased corrected quantal content at high bath [Ca^{2+}] (Figure 10C). *Rtnl1*$^{+}$ overexpression also decreased transmitter release, but to a lesser extent than

atl^{+}. We conclude that maximum levels of evoked transmitter release require specific levels of both Atl and Rtnl1.

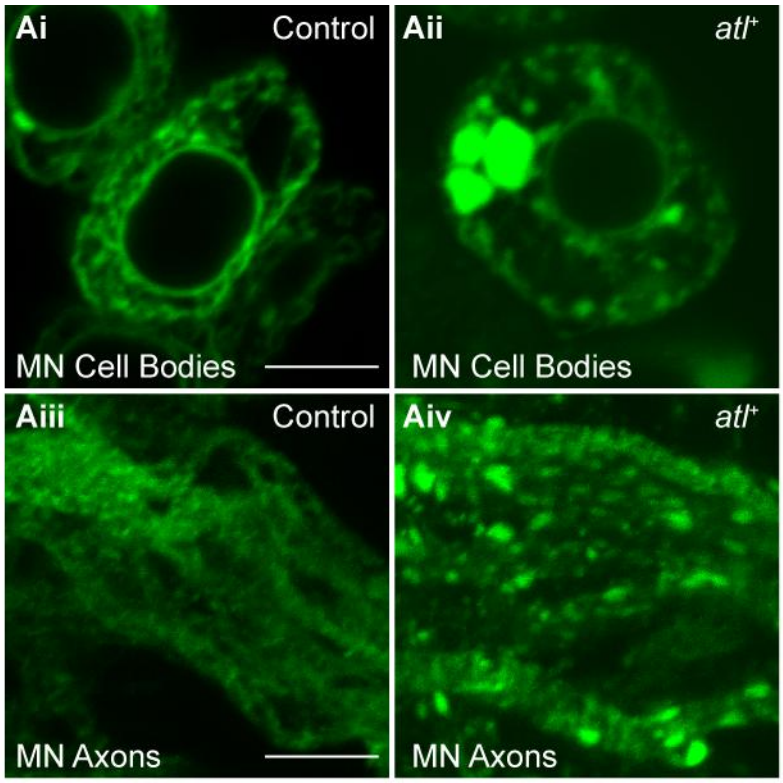
Ai
Control
MN Cell Bodies
Aii
atl+
MN Cell Bodies
Aiii
Control
MN Axons
Aiv
atl+
MN Axons

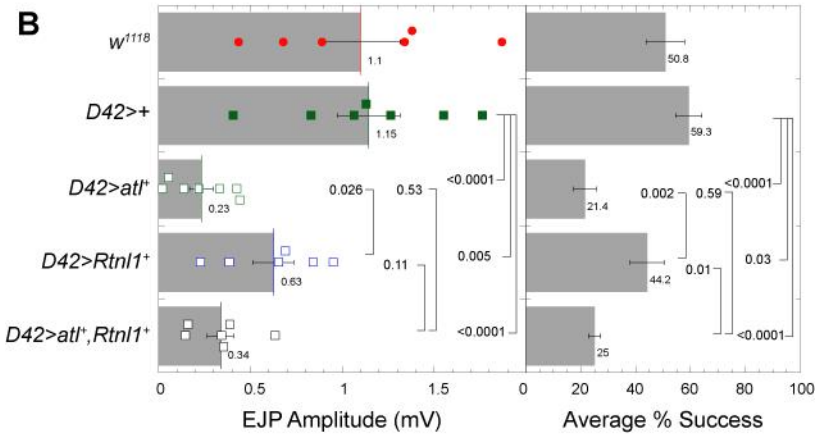
B
w1118
D42>+
D42>atl+
D42>Rtnl1+
D42>atl+,Rtnl1+
1.1
1.15
0.23
0.63
0.34
50.8
59.3
21.4
44.2
25
0.026
0.53
<0.0001
0.11
0.005
<0.0001
0.002
0.59
<0.0001
0.01
0.03
<0.0001
0
0.5
1
1.5
EJP Amplitude (mV)
0
20
40
60
80
100
Average % Success

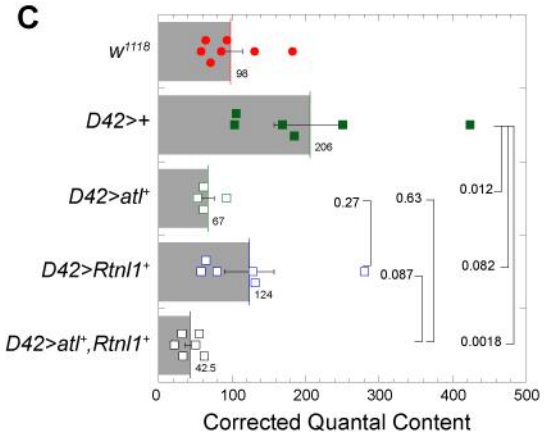
C
w1118
D42>+
D42>atl+
D42>Rtnl1+
D42>atl+,Rtnl1+
98
206
67
124
42.5
0.27
0.63
0.012
0.087
0.082
0.0018
0
100
200
300
400
500
Corrected Quantal Content

Figure 10: Motor neuronal expression of *UAS-atl*$^{+}$ causes aggregation of BiP-sfGFP-HDEL and impairs evoked neurotransmitter release. **(A)** Representative central confocal slices of motor neuron cell bodies in wt **(Ai)** and *atl*$^{+}$ **(B)** Average EJP amplitude and corresponding percent success for motor neuronal expression of *UAS-atl*$^{+}$, *UAS-Rtnl1*$^{+}$, or *UAS-atl*$^{+}$*, Rtnl1*$^{+}$. Recordings were made in HL3.1 at 0.1 mM Ca^{2+} from muscle 6 in segment A6. **(C)** Average corrected quantal content for the indicated genotypes. Recordings were made in HL3 at 1.5 mM Ca^{2+} from muscle 6 in segment A6. For **A** and **B**, bars and error bars for represent averages and standard errors, respectively. Each scattergram data point is the average of the first 20 EJP responses (successes and failures) recorded for each larva. P-values shown represent an unpaired Students t-test performed with KaleidaGraph.

4.8: Rtnl1 regulates transmitter release from multiple tissues at the NMJ

We used both tissue-specific transgenic rescue and RNAi-mediated knockdown to identify the tissue(s) within which *Rtnl1* functions to control transmitter release. First, we found that driving *Rtnl1 RNAi* expression with the pan-neuronal driver *elav-Gal4* (Figure 11A, left, blue squares) significantly decreased both evoked EJP amplitude and percentage of synaptic successes (Figure 11A, right). This result demonstrates that activity of Rtnl1, like atlastin, is required cell-autonomously in the motor neuron to affect transmitter release. To determine if Rtnl1 activity is required in the other cell types of the tripartite synapse, we drove *Rtnl1 RNAi* expression with the muscle driver *Mef2-Gal4* (Figure 11A, left, blue diamonds) and the peripheral glial driver *Gli-Gal4* (Figure 11A, left, blue triangles). Unexpectedly, we found that *Rtnl1* knockdown in these tissues also significantly decreased evoked EJP amplitude and synaptic success rate (Figure 11A, right). Thus, Rtnl1 activity is required in all three cell types of the tripartite synapse for proper evoked transmitter release.

We next determined if Rtnl1 activity in these three cell types was sufficient for proper evoked transmitter release. First we verified effectiveness of the *Rtnl1*$^{+}$ rescue construct by determining that ubiquitous expression of the *Rtnl1*$^{+}$ transgene, driven by the *da-Gal4* driver, was sufficient to rescue both evoked EJP amplitude (Figure 11B, left) and frequency of synaptic successes of *Rtnl1*^{1} (Figure 11B, right). As expected from the RNAi results described above, expression of *Rtnl1*$^{+}$ driven pan-neuronally, in the motor neuron alone, the muscle alone, or both the motor neuron and muscle, was not sufficient to rescue the EJP amplitude or synaptic success phenotypes of *Rtnl1*^{1} (Figure 11B and not shown). However, simultaneous expression of *Rtnl1*$^{+}$ in the motor neuron, muscle, and peripheral glia was sufficient to significantly restore wildtype EJP amplitude and synaptic success frequency to *Rtnl1*^{1} (Figure 11B). We conclude that Rtnl1 activity in the motor neuron, target muscle, and neighboring peripheral glia is sufficient as well as necessary to maintain proper synaptic transmission.

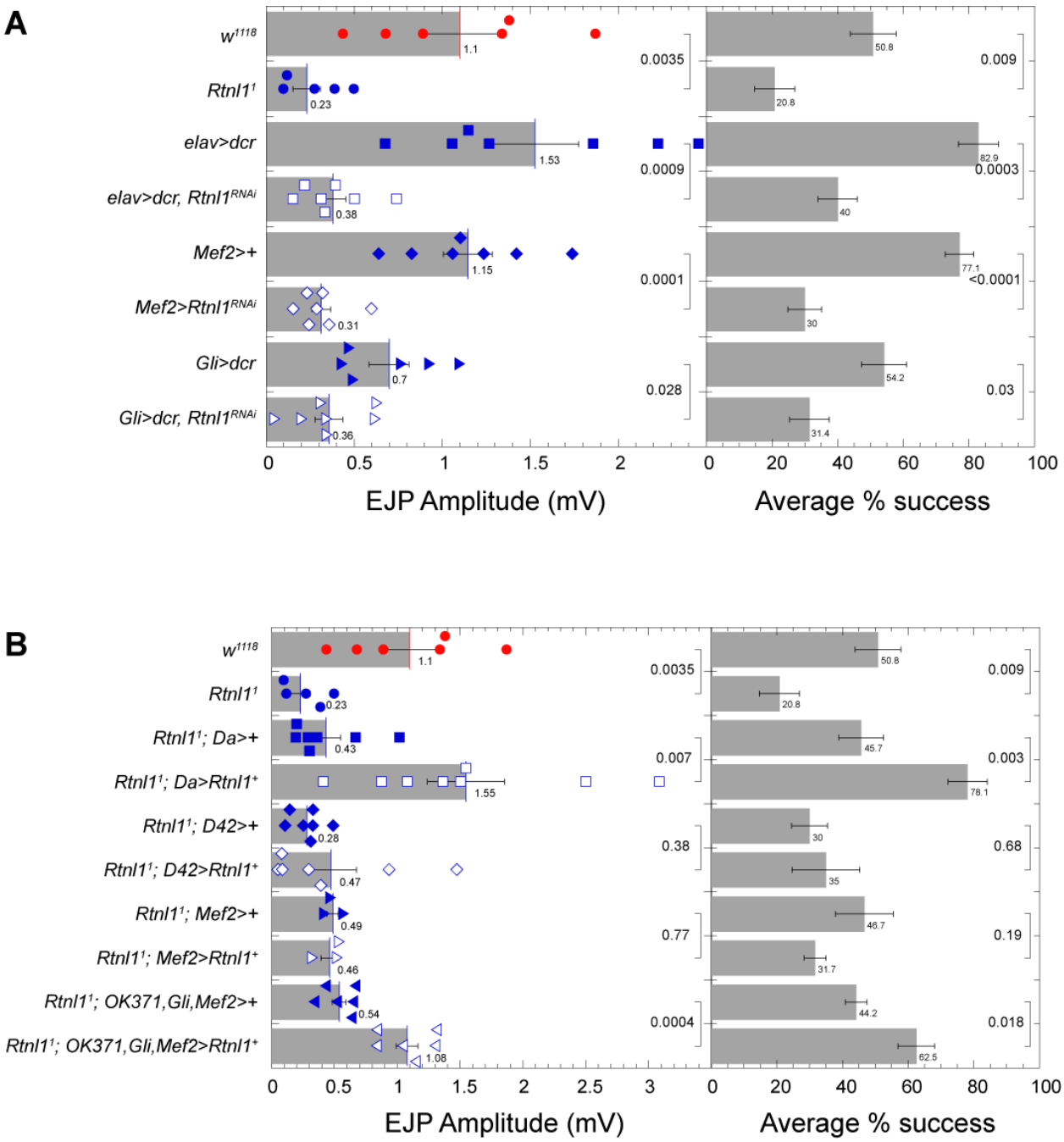

Figure 11: Rtnl1 affects neurotransmitter release from multiple tissues at the NMJ. **(A)** Average EJP amplitude and corresponding percent success for *wt*, *Rtnl1*^{1}, and *UAS-Rtnl1*^{RNAi} expression in neurons, muscles, and glia using *elav-Gal4*, *Mef2-Gal4*, and *Gli-Gal4*, respectively. **(B)** Average EJP amplitude and corresponding percent success for *wt*, *Rtnl1*^{1}, and expression of *UAS-Rtnl1*$^{+}$ in *Rtnl1*^{1} mutants. *UAS-Rtnl1*$^{+}$ was expressed ubiquitously, from motor neurons, and from muscles using *da-Gal4*, *D42-Gal4*, and *Mef2-Gal4*, respectively. *OK371, Mef2, Gli-Gal4* denotes concurrent expression of *UAS-*

Rtnl1^{+} from motor neurons, muscles, and glia. Recordings for **A** and **B** were made in HL3.1 at 0.1 mM Ca^{2+} from muscle 6 in segment A6. Bars and error bars represent averages and standard errors, respectively. Each scattergram data point is the average of the first 20 EJP responses (successes and failures) recorded for each larva. P-values shown represent an unpaired Students t-test performed with KaleidaGraph.

4.9: *atl*^{2} increases BMP signaling in larval motor neurons

BMPs (Bone Morphogenetic Proteins) are a family of secreted ligands that control a wide variety of organismal functions. Following binding to membrane receptors, BMPs trigger the phosphorylation and activation of the Mad transcription factor (Miyazono et al., 2010), which is assayed with antibodies specific to the active pMad. In addition to developmental functions, Drosophila BMP ligands released from muscle, peripheral glia, or the motor neuron itself regulate transmitter release and synaptic growth in the motor neurons (Fuentes-Medel et al., 2012; McCabe et al., 2003). Many HSP proteins, including Drosophila Spichthyin and Spartin, mammalian Spastin, and Zebrafish Atlastin, inhibit BMP signaling (Fassier et al., 2010; Nahm et al., 2013; Wang et al., 2007). To determine if Atl might similarly inhibit BMP signaling, we measured nuclear pMad within motor neuron nuclei of *atl*^{2} third instar larvae. We observed a significant increase in nuclear pMad in *atl*^{2}, which was rescued either by weak, ubiquitous (Figure 12C, green squares) or motor neuron-specific expression of *atl*$^{+}$ (Figure 12C, green diamonds). Thus, Atl behaves similarly to other HSP proteins as an inhibitor of BMP signaling.

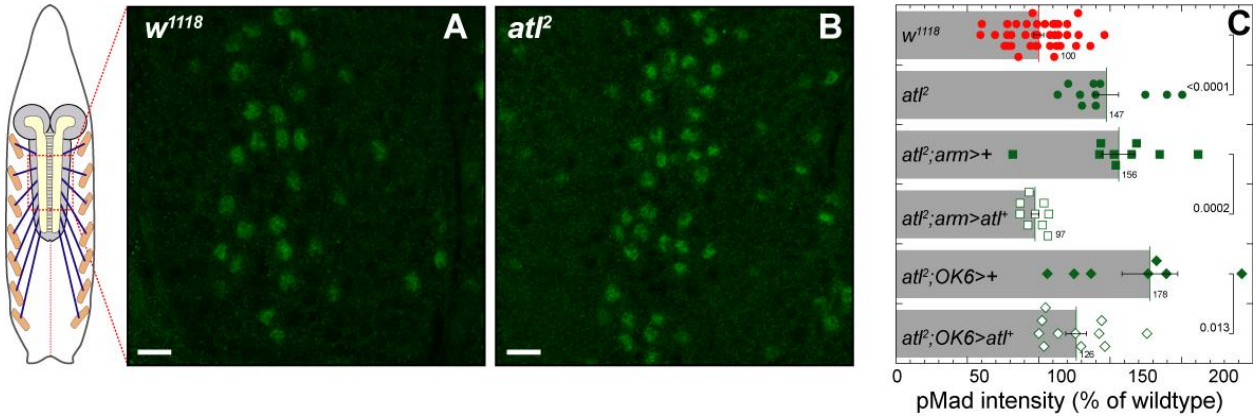

Figure 12: *atl*^{2} increases BMP signaling in motor neurons. Representative confocal images of *w*^{1118} **(A)** and *atl*^{2} **(B)** motor neuron nuclei from 3rd instar larvae labeled with anti-pMad antibody. Scale bar = 10 µm. **(C)** PMad levels for *w*^{1118}, *atl*^{2}, *atl*^{2}*; arm>+, atl*^{2}*; arm>atl*$^{+}$, *atl*^{2}*; OK6>+,* and *atl*^{2}*; OK6>atl*$^{+}$ in motor neuron nuclei. Bars and error bars represent averages and standard errors, respectively. Each scattergram data point is the average nuclear signal intensity per area for a single larva. P-values shown represent an unpaired Students t-test performed with KaleidaGraph.

4.10: Neuronal loss of *atl* and *Rtnl1* causes axon terminal overgrowth

Mutations in several Drosophila HSP orthologues, such as *spichthyin*, *spartin,* and *spastin*, increase axon terminal growth and synaptic bouton number at the third instar larval NMJ. In addition, Lee et al. (2009) reported that bouton number was increased in *atl*^{2} as well, and that this increase was rescued by muscle but not neuronal *atl*$^{+}$ expression. Effects of Rtnl1 activity on bouton number to our knowledge have not been reported. We investigated the roles of neuronal *atl* and *Rtnl1* on axon terminal growth by using RNAi to knock down *atl* and *Rtnl1* pan-neuronally. We found that knock down of either *atl* or *Rtnl1* significantly increased synaptic bouton number, and that this increase was suppressed when both genes were knocked down simultaneously (Figure 13).

These results suggest that Atl and Rtnl1 are required within the motor neuron to restrain axon outgrowth. Our results appear to conflict with those reported by Lee et al. (2009) described above, but note that the *atl* genotypes in the two experiments were not identical. For example, the peripheral glia, which play a key role in regulating synaptic function at the NMJ, were atl^{2} in Lee et al. (2009), but atl^{+} in Figure 13. Given that we found that *atl* knockdown in peripheral glia increases synaptic bouton number (not shown), this could account for the differences in our results.

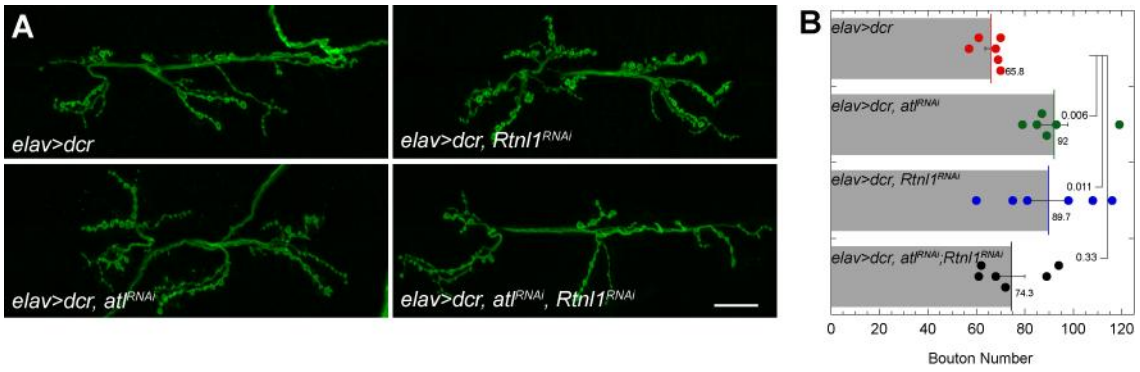

Figure 13: Neuronal knockdown of *atl* and *Rtnl1* increases motor nerve terminal arborization. **(A)** Z-projections of neuromuscular junctions from muscles 6/7 at segment A3. **(B)** Bars and error bars represent averages and standard errors, respectively. Each scattergram data point is the average bouton number for a single larva. P-values shown represent an unpaired Students t-test performed with KaleidaGraph.

4.11: Neuronal knockdown of *atl* causes age-dependent locomotor deficits

HSP patients share a characteristic increase in spasticity and weakening of the lower extremities with age. Drosophila mutant for any of several HSP orthologues similarly display behavioral deficits. These mutants include the atl^{1} hypomorphic mutant, the *spartin* null mutant, and *Rtnl1 RNAi* knockdowns (Lee

et al., 2008; Nahm et al., 2013; Sherwood et al., 2004). To determine if pan-neuronal *atl* inhibition generated locomotor deficits, we constructed *elav>Dcr, atl*^{RNAi} males and used two assays to assess locomotor behavior. First we measured the time required for *elav>Dcr, atl*^{RNAi} flies to climb a 6 cm distance and observed an age-dependent increase (Figure 14A). Second we used the iFly tracking system (Kohlhoff et al., 2011) to measure walking velocity and found an age-dependent decrease in *elav>Dcr, atl*^{RNAi} adult males (Figure 14B). In contrast, the *elav>Dcr* control males exhibited little or no decrease in locomotor activity with either assay upon aging. These results suggest that inhibition of neuronal *atl* causes aberrant locomotion that progressively worsens with age.

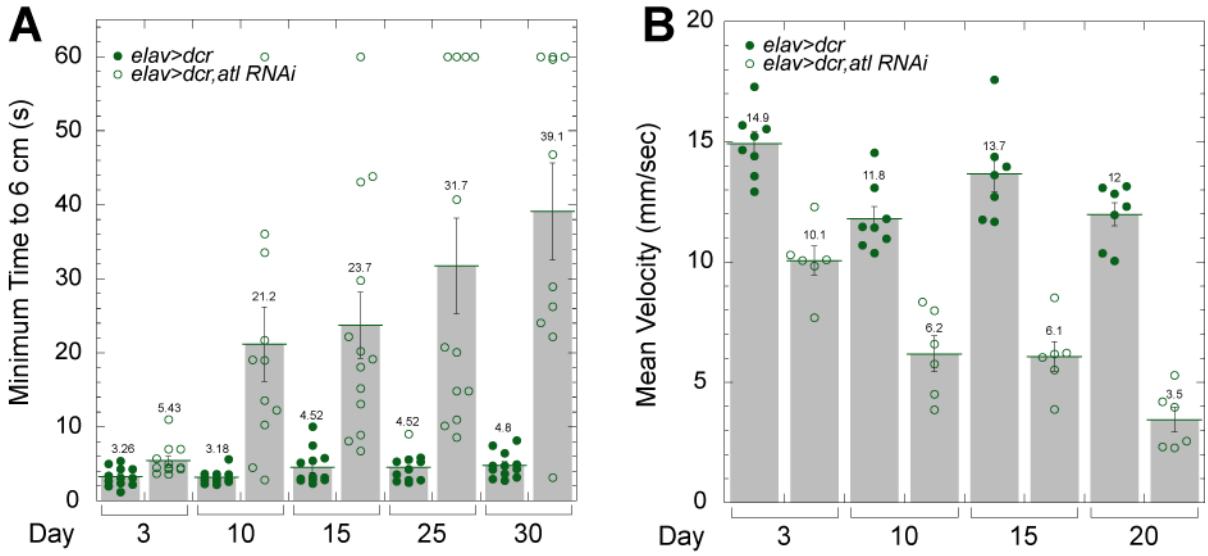

Figure 14: Neuronal expression of *UAS-atl*^{RNAi} impairs locomotion in an age dependent manner. **(A)** Average time for adult males to climb a vertical distance of 6 cm. Flies that were unable to climb 6 cm within 60 seconds were assigned a value of 60. **(B)** Mean velocity of adult males subsequent to bang stimuli. Means +/- SEMs are indicated.

5: Discussion

5.1: The role of ER morphology in nervous system function and anatomy

Mutations in two genes that affect ER morphology, *atlastin (atl)* and *reticulon 2* (*Rtn2*), cause two forms of Hereditary Spastic Paraplegia (HSP), which result in progressive limb weakness, spasticity, and degeneration of the longest motor axons (Blackstone et al., 2010). These observations suggest that altered ER morphology is causal for motor axon dysfunction, but the mechanisms underlying these dysfunctions are unclear. Here we use Drosophila to evaluate the nervous system deficits caused by altered *atl* and *Rtnl1* activity. Using a novel fluorescent ER imaging reagent, we show that the ER in wildtype motor nerve terminals is present as a network of tubules, termed “baskets”, underlying the plasma membrane, and that these baskets are eliminated in larvae lacking or overexpressing *atl*. We also show that loss of either *atl* or *Rtnl1* increases arborization and decreases evoked transmitter release and that evoked release is restored to normal by elevated bath Ca^{2+}. Finally we show that *atl* loss increases signaling through the bone morphogenetic protein (BMP) pathway and causes age-dependent decline in adult locomotion. This set of phenotypes is also exhibited by Drosophila mutant for the HSP orthologues of *spartin, spastin* and *spichthyin*, as well as for *spinster* and *nervous wreck*, which encode regulators of receptor trafficking through endosomes (Nahm et al., 2013; O'Connor-Giles et al., 2008; Ozdowski et al., 2011; Sherwood et al., 2004; Sweeney and Davis, 2002; Wang et al., 2007). The possible involvement of the ER in this receptor trafficking will be discussed.

5.2: Effects of *atl* loss or overexpression on ER morphology in motor neurons

We made two adjustments to improve visualization of the ER. First, we introduced into flies a transgene that encoded an ER-localized superfolder GFP, which was optimized for efficient folding in the ER. Second, based on previous results indicating that the ER is labile to fixation, we imaged ER in live tissues. Lability of organelles to fixation is not unprecedented as the lysosomal tubule network within Drosophila muscles also succumbs to deterioration upon chemical fixation (Johnson et al., 2015). Using these approaches, we showed that the ER is present within the axon initial segments of motor neurons as a polygonal structure with numerous crossbridges (three-way junctions), and in motor nerve terminals as a network of tubules that we term “baskets” that underlie the plasma membrane. We also showed that these structures are disrupted by either loss of or overexpression of *atl*. In particular, *atl* overexpression causes the aberrant appearance of large punctae in motor neuron cell bodies or axon initial segments. In contrast, *atl* loss decreases the number of crossbridges in the axon initial segment, leading to excessively long tubules. A similar appearance was noted previously (Hu et al., 2009; Orso et al., 2009) and attributed to deficits in fusion of orthogonal ER membranes. Loss of *atl* also disrupts nerve terminal baskets and appears to cause ER fragmentation. It is possible that the transition from tubules to baskets as the ER moves from interbouton region to the boutons occurs via ER fragmentation followed by Atl-dependent reassembly. In this view,

loss of *atl* would prevent this reassembly thus causing the fragmented ER that we observe.

5.3: Deficits in evoked transmitter release in larvae lacking *atl* or *Rtnl1* are rescued by elevated bath [Ca^{2+}]

The deficits of evoked transmitter release in both the chromosomal null atl^2 or $Rtnl1^1$ mutants and in pan-neuronal *atl* or *Rtnl1* knockdown larvae were rescued partially or completely by elevated bath [Ca^{2+}]. These results indicate that loss of *atl* or *Rtnl1* decreases evoked transmitter release at low bath [Ca^{2+}] via deficits in evoked increases in cytoplasmic [Ca^{2+}]. Insufficient Ca^{2+} influx could result from attenuated action potentials, which would decrease the opening of voltage-gated Ca^{2+} channels, decreases in number of plasma membrane Ca^{2+} channels, or decreased Ca^{2+} release from the ER. Given the role of atlastin and the reticulons as ER-shaping molecules, effects on ER Ca^{2+} release would be the most direct explanation for this Ca^{2+} phenotype. ER-localized Ca^{2+} release channels such as the IP3 receptor, the ryanodine receptor, and the TRPV1 channel play key roles in evoked neurotransmitter release (Emptage et al., 2001; Liang et al., 2002; Llano et al., 2000; Wong et al., 2014). In addition, dominant-negative mutations in the Drosophila ER-localized Ca^{2+} pump SERCA decrease evoked transmitter release by about 50% (Sanyal et al., 2005), which is consistent with the possibility that ER-derived Ca^{2+} contributes significantly to the Ca^{2+} required to trigger transmitter release.

5.4: Rtnl1 affects evoked neurotransmitter release from multiple tissues

Unlike Atl, which appears to affect evoked transmitter release from neurons alone, Rtnl1 is required in all three tissues of the tripartite synapse (neurons, muscles, and peripheral glia) for proper evoked transmitter release. This finding is consistent with previous data demonstrating that proper synaptic transmission requires intercellular signaling among these three cell types. In particular, loss of activity within the peripheral glia of the kinesin heavy chain gene or the *inebriated*-encoded neurotransmitter transporter alters evoked transmitter release (Huang and Stern, 2002; Schmidt et al., 2012). In addition, the peripheral glia secrete at least two proteins, the TGF-β ligand Maverick and Wnt, which regulate synaptic function (Fuentes-Medel et al., 2012; Kerr et al., 2014). The muscle, in turn, secretes the BMP ligand gbb to regulate both evoked transmitter release and motor neuron arborization (McCabe et al., 2003). It is possible that loss of *Rtnl1* affects transmitter release from glia or muscle by perturbing secretion of these or other regulators.

5.5: Pan-neuronal *atl* knockdown causes progressive adult locomotor deficits during aging

The most prominent clinical symptom in HSP patients is progressive, age-dependent locomotor difficulties. Drosophila mutant for any of several HSP orthologues, including *spartin, spastin, atl*, and *Rtnl1*, as well as *spinster,* exhibit similar age-dependent locomotor deficits or lifespan deficits (Dermaut et al., 2005; Lee et al., 2008; Nahm et al., 2013; O'Sullivan et al., 2012; Orso et al.,

2009; Sweeney and Davis, 2002). Here we show locomotor impairment in adults with neuronal-specific *atl* knockdown. These results indicate a requirement for *atl* in neurons for proper locomotion, but do not rule out critical roles for *atl* in other tissues as well.

5.6: A potential role for the ER in endocytic receptor trafficking

Mutants in Drosophila orthologues of several HSP genes, including *spartin, spastin,* and *spichthyin,* and additional related genes *spinster* and *nervous wreck* share a common set of nervous system phenotypes, including increased arborization and BMP signaling at the larval NMJ, decreased evoked transmitter release and locomotor deficits (Nahm et al., 2013; O'Connor-Giles et al., 2008; Ozdowski et al., 2011; Sherwood et al., 2004; Sweeney and Davis, 2002; Wang et al., 2007) (note that not all phenotypes have been reported for each mutant). The encoded proteins have been localized to various compartments within the endocytic receptor trafficking pathway (Allison et al., 2013; Edwards et al., 2009; O'Connor-Giles et al., 2008; Sweeney and Davis, 2002; Wang et al., 2007). In fact, the increased BMP signaling in several of these mutants has been attributed to trafficking defects of the BMP receptor wishful thinking (abbreviated as “wit”). We have shown that *atl* loss confers these same phenotypes, raising the possibility that *atl* acts in the endocytic receptor trafficking pathway as well. Although the ER is not known to play prominent roles in this pathway, a recent report has demonstrated that the ER is required for endosome fission in COS cells, and in fact, the ER selects the location of fission

(Rowland et al., 2014). In addition, it was found that this process was inhibited by overexpression of *Rtn4a*, which, similarly to *atl* loss, elongates ER tubules and inhibits formation of crossbridges (Rowland et al., 2014). Thus, loss of *atl* could impact the receptor trafficking pathway in Drosophila nerve terminals by similarly preventing endosome fission.

The variety of phenotypes exhibited in common by the mutants described above raises the possibility that certain phenotypes might have causal relationships with others. The subcellular locations suggest that these proteins might directly affect receptor trafficking. If so, then the increased BMP signaling, as a consequence of altered wit trafficking, might be the direct cause of the increased arborization and locomotor deficits. The phenotypes conferred by direct activation of the BMP pathway in neurons are consistent with this possibility (McCabe et al., 2003; Nahm et al., 2013). However, given that decreased BMP signaling, rather than increased BMP signaling, decreases evoked transmitter release, the increased BMP signaling is unlikely to be the cause of the decreased transmitter release. We suggest that trafficking of receptors in addition to wit are altered in the mutants described above, and it is the altered signaling of these additional receptors that is at least partly responsible for the transmitter release phenotype. Drosophila motor nerve terminals express a cholecystokinin-like receptor (CCKLR), a toll-like receptor, a metabotropic glutamate receptor (mGluRA), and likely the insulin receptor (Ballard et al., 2014; Bogdanik et al., 2004; Chen and Ganetzky, 2012; Howlett et al., 2008). Loss of mGluRA increases evoked transmitter release (Bogdanik et

al., 2004; Howlett et al., 2008), raising the possibility that increased mGluRA signaling might decrease transmitter release, which could explain the decreased transmitter release observed in these receptor trafficking mutants.

III.) Proteins Responsible for Neuronal Excitability Homeostasis Affect Perineurial Glial Size in *Drosophila melanogaster*

6: Introduction

Efficient conveyance of sensory and motor signals along the length of axons is essential for proper nervous system functioning. Integral to proper neuronal firing are the many intimately associated glial cells which support, protect, and insulate the neuron (Pfrieger & Barres, 1997). Regulation of glial cell development, known as gliogenesis, has been well documented in many cases (Bonni et al., 1997; Sauvageot & Stiles, 2002; Jones, 2005), and certain mutations, which increase the rate of neuronal firing, are known to enhance glial size (Yager et al., 2001). However, the details of glial cell growth regulation via neuron-glia and glia-glia signaling remain incompletely understood. Elucidation of these mechanisms may generate treatments for the disease neurofibromatosis type 1. This autosomal dominant disease is characterized by the appearance of neurofibromas, which are benign tumors of peripheral nerves consisting of various nerve cell types that may advance to malignancy (Zhu et al., 2002).

6.1: Drosophila Peripheral Nerve Structure

Drosophila peripheral nerves contain axons that are either individually ensheathed or grouped into small bundles by wrapping glia (Stork et al., 2008). Encasing the axons and wrapping glia are the blood-nerve barrier forming peripheral glia, which are analogous to mammalian Schwann cells (Stork et al., 2008). This bundle of axons and peripheral glia are then collectively wrapped by a layer of perineurial glia, and the entire nerve is encased within an extracellular

matrix known as the neural lamella (Stork et al., 2008). Neurons and peripheral glia develop from ectodermal neurogiloblasts (Bernardoni et al., 1999), whereas perineurial glia are derived from the mesodermal cell layer (Edwards et al., 1993).

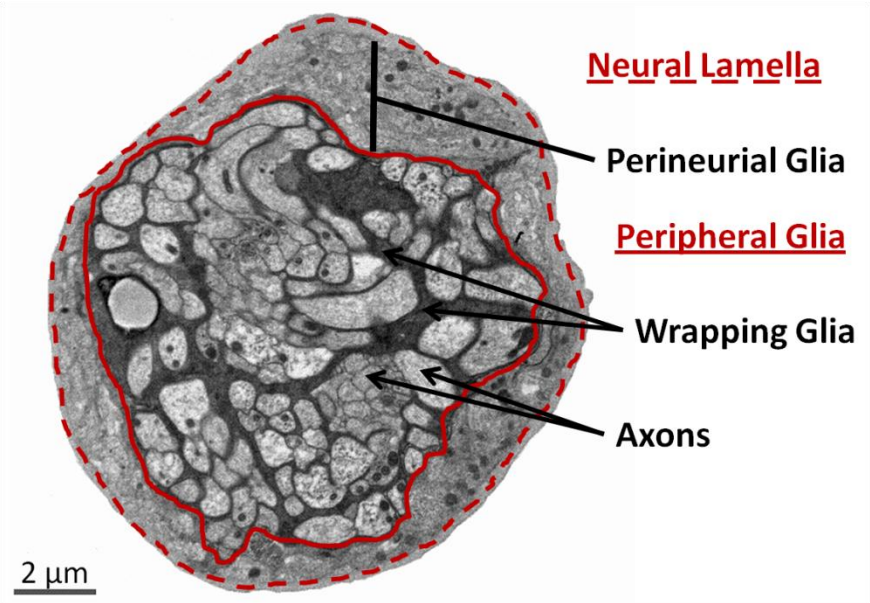

Figure 15: Drosophila peripheral nerve structure. Image obtained by transmission electron microscopy of a *Drosophila* larval peripheral nerve cross-section illustrating positioning of axons, wrapping glia, peripheral glia, and perineurial glia. The peripheral glia and thus the entire axon bundle is outlined in a solid red line while the neural lamella, the extracellular matrix component secreted from the perineurial glia, is outlined in dashed red. It is the area of the perineurial glia that will be measured in all subsequent graphs.

6.2: Drosophila Peripheral Nerves Grow with Increased Neuronal Excitability

It has been demonstrated that perineurial glial overgrowth is induced by mutations that increase neuronal excitability (Yager et al., 2001). Excitability can be described as a cell's tendency to depolarize and subsequently fire an action

potential in response to synaptic input. Perineurial glial overgrowth was also observed in Drosophila larvae in which phosphatidylinositol-4,5-bisphosphate 3-kinase (PI3K) activity within the peripheral glia was increased (Lavery et al., 2007). This raised the possibility that neuronal excitability increases perineurial glial growth by activating PI3K in the peripheral glia.

Glutamate is the excitatory amino acid utilized at the Drosophila neuromuscular junction and may be used to signal between neurons and glia. The Drosophila G-protein coupled metabotropic glutamate receptor (DmGluRA) binds glutamate and activates PI3K within the motor neuron, an important component of neuronal signaling homeostasis (Howlett et al., 2008).

6.3: Neurofibromatosis Causes Tumorigenesis Within Peripheral Nerves

Neurofibromatosis, also known as von Recklinghausen disease, is a dominant genetic disease caused by mutations in the Ras GTPase activating protein (GAP) *NF1* and characterized by the formation of benign tumors, termed neurofibromas, within peripheral nerves (Cichowski and Jacks, 2001; Johannessen et al., 2005). These tumors exhibit cellular heterogeneity and manifest as an amalgam of various cell types including Schwann cells, perineurial cells, fibroblasts, mast cells, and endothelial cells (Riccardi, 2007). This suggests that an intercellular signaling network recruits these cells for tumor formation. Additionally, while a mutation in the *NF1* gene is necessary for the commencement of neurofibroma formation, it is not required in all cell types involved. Loss of heterozygosity (LOH), also known as the two-hit mechanism,

illustrates that mutations in both copies of *NF1* occur in some Schwann cells (*NF1-/-*), whereas other Schwann cells remain heterozygous (*NF1+/-*) (Serra et al., 2000). This demonstrates that two different subpopulations of Schwann cells exist in neurofibromas (Serra et al., 2000). It has been shown in mice that *NF1* nullizygous (*NF1-/-*) Schwann cells are necessary but not sufficient to cause neurofibromatosis (Zhu et al., 2002). Mouse *NF1-/-* Schwann cells secrete signals such as Kit Ligand (KitL) that mobilize and recruit *NF1* haploinsufficient (*NF1+/-*) mast cells, but not *NF1+/+* mast cells, to the site of neurofibroma formation (Zhu et al., 2002). These mast cells, in turn, stimulate angiogenesis and reciprocate proliferative signaling to the Schwann cells in the form of nerve growth factor (NGF) and vascular endothelial growth factor (VEGF) that foster a tumor microenvironment (Yang et al., 2003). Additional intercellular signals involving neuronally expressed neuregulin I (NRG1) in mice (Gomez-Sanchez et al., 2009) and Schwann cell expressed semaphorin 4F (Sema4F) in rats (Parrinello et al., 2008) also may be implicated in neurofibroma formation. Therefore it appears intercellular signaling among cell types is necessary to form neurofibromas. Similarly in the Drosophila peripheral nerve, intercellular signaling from the peripheral glia is responsible for growth of the outer perineurial glial layer (Lavery et al., 2007). Neuronal signaling also may be partly responsible for perineurial glial growth due to the fact that mutations increasing neuronal excitability also increase perineurial glial size (Yager et al., 2001). Therefore, understanding of the Drosophila peripheral nerve structure (Figure 15) and its

signaling pathways together provide a comparably simple model for understanding neurofibroma formation in rodents and humans.

6.4: Peripheral glial Ras, PI3K, & FOXO regulate perineurial glial growth

Signaling among glial cells in Drosophila is important for glial cell migration along axons (Silies, et al., 2007), differentiation required to ultimately ensheath these axons (Franzdóttir et al., 2009), and septate junction formation to insulate axons for proper signal transduction (Bannerjee et al., 2006). Additionally, upregulation of the PI3K pathway exclusively in peripheral glia via expression of a constitutively active Ras isoform, Ras^{V12}, or expression of the constitutively active PI3K-CAAX, causes overgrowth of the perineurial glial layer in Drosophila (Lavery et al., 2007). It has also been shown that *Ras^{V12}* expression causes hyperplastic growth in Drosophila imaginal discs, which are epithelial cells responsible for the generation of most adult structures (Karim & Rubin, 1998).

PI3K phosphorylates phosphatidylinositol 4,5-bisphosphate (PIP_2) to form phosphatidylinositol 3,4,5-trisphosphate (PIP_3). PIP_3 recruits proteins possessing pleckstrin homology domains such as PDPK1 and AKT/PKB to the plasmalemma (Cully et al., 2006; Gray et al. 1999). When both are present at the plasmalemma, PDPK1 phosphorylates and activates AKT (Gray et al. 1999). Once activated, AKT is responsible for the inhibition of a great variety of proteins through phosphorylation. For example, AKT inhibits the forkhead box O (FOXO) transcription factor by phosphorylation and subsequently promoting its

association with 14-3-3 proteins which retains FOXO in the cytoplasm, negating its involvement in the upregulation of pro-apoptotic genes (Downward et al., 2004).

Overexpression of peripheral glial FOXO attenuates perineurial glial growth induced by PI3K activation (Lavery et al., 2007). The fact that FOXO is a downstream target of DmGluRA-PI3K signaling (Howlett et al., 2008) and that its inhibition in peripheral glia favors perineurial glial augmentation suggest that FOXO is a transcriptional repressor for growth factors that allow the peripheral glia to nonautonomously regulate perineurial glial thickness (Lavery et al., 2007).

6.5: DmGluRA may activate PI3K in the peripheral glia

Metabotropic glutamate receptors activate phosphatidylinositol 3-kinase (PI3K) (Hou & Klann, 2004; Gerber et al., 2007; Howlett et al., 2008; Maiese et al., 2008). MGluRs are expressed in glia in rat brains (Petralia et al., 1996) and Schwann cells in frog peripheral nerves (Pinard et al., 2003). If DmGluRA is present within peripheral glia in Drosophila, it may activate PI3K and subsequently inhibit FOXO (Figure 16).

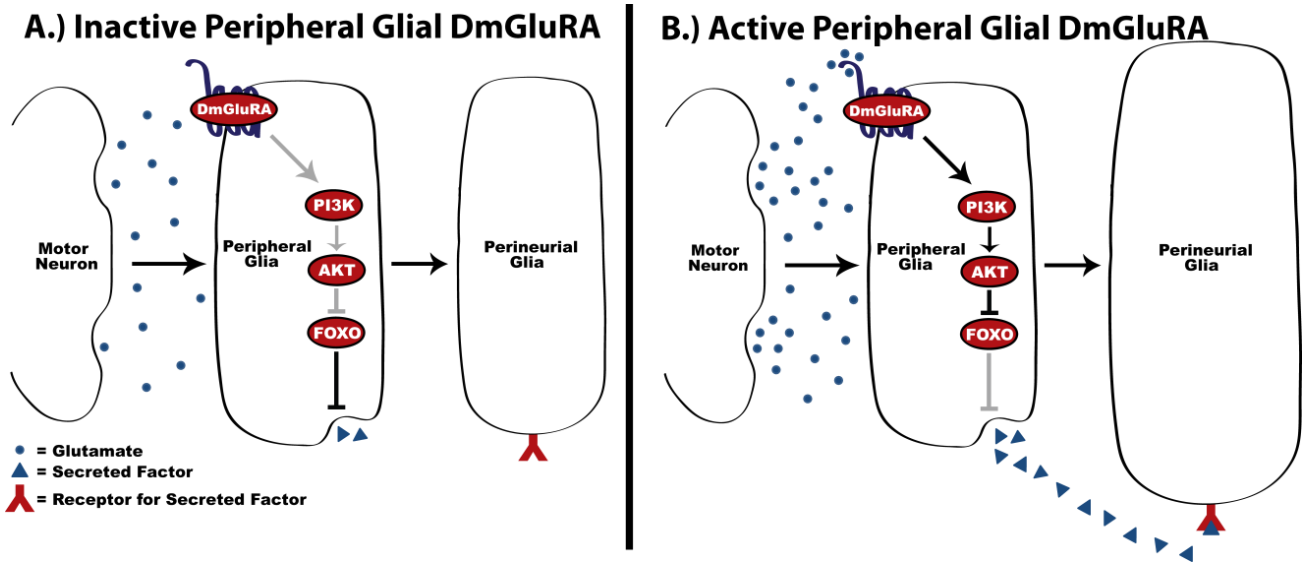

Figure 16: Hypothetical model for peripheral glial DmGluRA facilitation of perineurial glial size increase. DmGluRA, capable of activating PI3K subsequent to binding glutamate, is hypothesized to be present in the peripheral glia and induce perineurial glial growth by inhibiting FOXO activity. (A) Inactive DmGluRA does not activate PI3K, allowing FOXO to negatively regulate a growth factor affecting the perineurial glia. (B) Active DmGluRA activates PI3K, which hinders the inhibition of a hypothesized growth factor by FOXO. Note the increased size of the perineurial glia in (B) compared to that of (A). FOXO overexpression in conjunction with PI3K activation reduces perineurial glial augmentation, suggesting FOXO as a regulator of one or more growth factors influencing perineurial glial size (Permission from Lavery et al., 2007).

6.6: Mutations that increase neuronal excitability also produce perineurial glial overgrowth

NF1 mutations can cause neurofibroma formation. Similarly, specific mutations in Drosophila promote growth of the perineurial glial layer (Yager et al., 2001) (Figure 17). These genes, in addition to the Drosophila *NF1* ortholog, are *pushover/purity of essence* (*push/poe*), *inebriated* (*ine*), and *ether a go-go* (*eag*), which encode a putative E3 ubiquitin ligase, a putative Na^+/Cl^- dependent

neurotransmitter transporter, and a K^+ channel subunit, respectively (Warmke et al., 1991; Soehnge et al., 1996; Tasaki et al., 2005). Specifically, mutations in either *ine* or *eag* alone do not increase perineurial glial growth, and while a mutation in *push* confers a significant increase in perineurial glial size, it is minimal compared to the increase observed in the double mutants eag^1; $push^1$ or ine^1, $push^1$ (Yager et al., 2001). $Push^1$ possesses a nonsense mutation at codon 728 (Yager et al., 2001), and ine^1 produces no mRNA transcript product (Soehnge et al., 1996). The size increase observed in ine^1, $push^1$ and eag^1; $push^1$ suggests that Push works synergistically with both Ine and Eag to determine perineurial glial size. However, the eag^1; ine^1 double mutant does not exhibit a significant increase in perineurial glial size compared to either the single eag^1 or ine^1 mutants, illustrating that Eag and Ine do not share the same synergy (Yager et al., 2001).

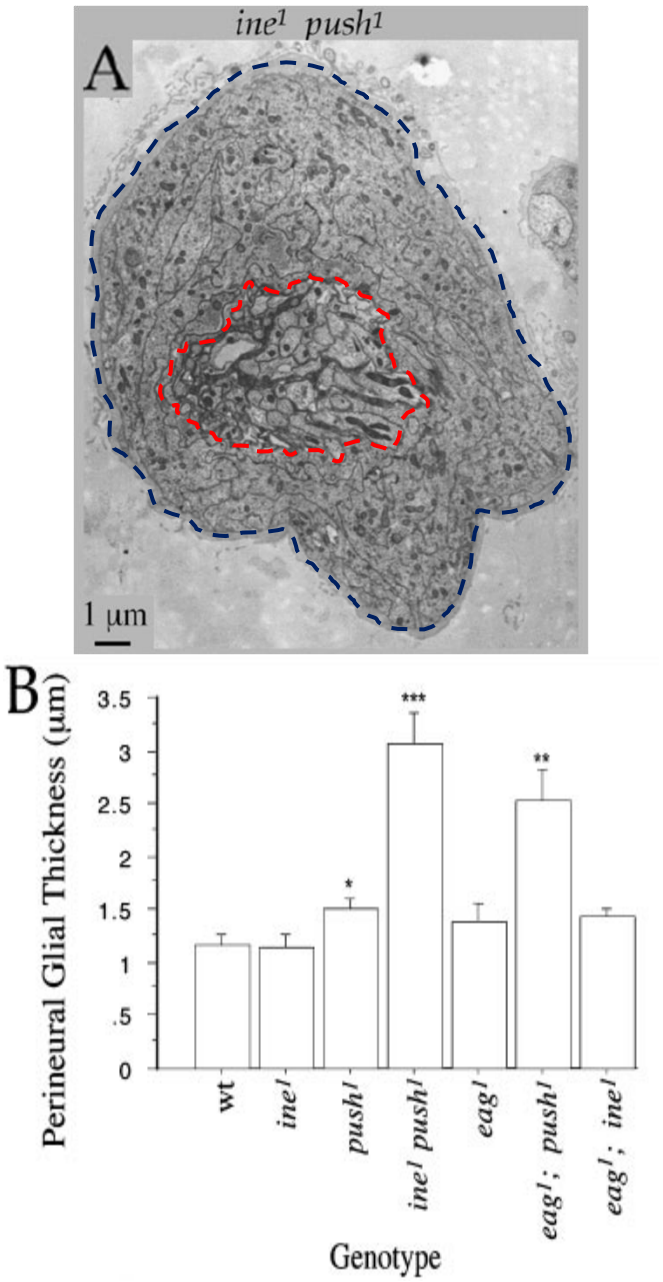

Figure 17: Mutations eliciting neuronal excitability also increase perineurial glial growth. (A) Perineurial glial thickness was measured by dissecting larvae and embedding them in an epoxy mixture and allowing this to harden (Yager et al., 2001). Ultrathin cross-sections (75-125 nm in thickness) then were made and examined under a JEOL or Hitachi (Tokyo) transmission electron microscope (Yager et al., 2001). Thickness of the perineurial glia was calculated by measuring the edge of the nerve to the space containing axons at positions 12, 3, 6, and 9 o'clock and in the intermediate spaces in between these points (Yager et al., 2001). In this figure the measured area

corresponds to the space between the axon bundle, outlined in dashed red, and the neural lamella, outlined in dashed blue. The increase in perineurial thickness within *push* mutants is moderate compared to wildtype flies but is greatly increased in an *ine*^{1}*, push*^{1} double mutant (Yager et al., 2001). (B) *ine*^{1}*, push*^{1} double mutants exhibit a significant thickening of the perineurial glia compared to that of wildtype or single *push*^{1} mutants. Measurements are averages of 4 (n=4) separate nerve cross-sections. Wild type vs. *push*^{1} (*, P = 0.04), *ine*^{1} *push*^{1} vs. *ine*^{1} or *push*^{1} (***, P < 0.0001) (Adapted from Yager et al., 2001).

6.7: *Ine* mutations may activate peripheral glial DmGluRA through a prolonged presence of neurotransmitter

Interestingly, mutations in *eag*, *ine*, and *push* increase neuronal excitability (Ganetzky & Wu, 1983; Stern & Ganetzky, 1992; Richards et al., 1996). Heightened excitability can be described as a neuron's increased probability to depolarize and initiate an action potential in response to synaptic input. Mutations in *eag, ine,* and *push* trigger repetitive firing of action potentials within neurons in response to signal stimulation (Richards et al., 1996). Increased excitability of these neurons translates into higher levels of neurotransmitter release. It is hypothesized that a mutation in *ine* results in the excessive and prolonged presence of neurotransmitter within the space between the motor neuron and peripheral glia, which may augment the perineurial glial layer (Figure 18)

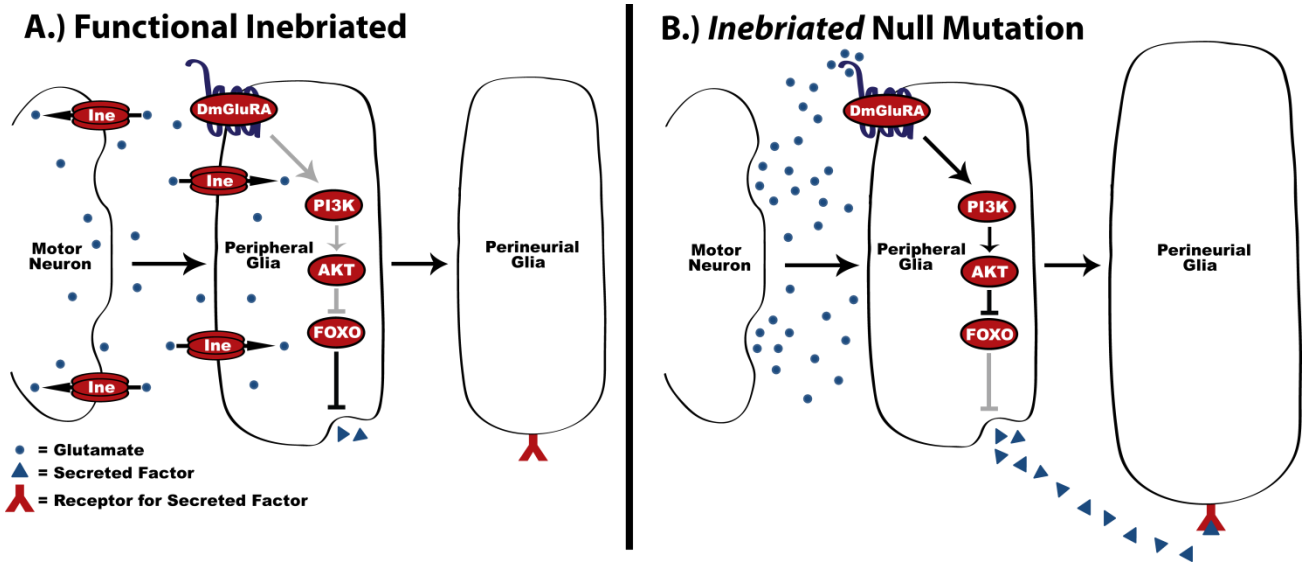

Figure 18: Inebriated is hypothesized to facilitate peripheral glial DmGluRA activation and increase perineurial glial thickness through increased neuronal excitability. It is hypothesized that a mutation in *inebriated* results in the excessive and prolonged presence of neurotransmitter in the synaptic cleft. Excessive neurotransmitter is hypothesized to activate peripheral glial DmGluRA and facilitate release of a growth factor which induces perineurial glial growth.

6.8: *Push* mutations may activate peripheral glial DmGluRA through excessive neurotransmitter release

Interestingly, neuronal excitability conferred by a *push* mutation is similar to excitability observed when inhibiting the neuronal DmGluRA-PI3K pathway (Howlett et al., 2008). This similarity raises the possibility that *push* mutations heighten perineurial glial cell thickness through inhibition of the DmGluRA-PI3K pathway. If so, then inhibiting the neuronal DmGluRA-PI3K pathway also is predicted to elicit increased perineurial glial growth.

DmGluRA activates AKT through PI3K, which is sufficient to attenuate neuronal excitability via inhibition of FOXO (Howlett et al., 2008) (Figure 19).

Thus, inhibition of DmGluRA causes hyperexcitability through FOXO activation whereas overexpression of *FOXO*, even in light of upregulated PI3K levels, is adequate to increase excitability within the neuron (Howlett et al., 2008) (Figure 19). This raises the possibility that Push, like DmGluRA, indirectly inhibits FOXO activity within the motor neuron, and mutations in either *push* or *DmGluRA* allow FOXO upregulation and a subsequent increase in excitability.

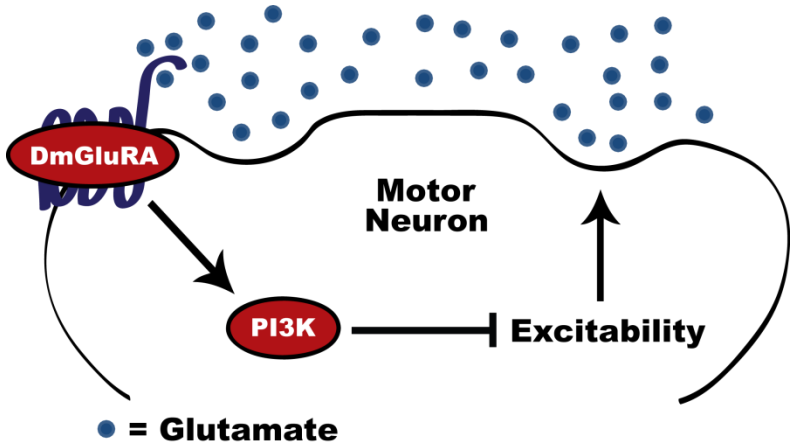

Figure 19: DmGluRA maintains excitability homeostasis within the motor neuron. Presynaptic DmGluRA acts in a negative feedback mechanism to activate PI3K and restrict neuronal excitability. This maintains neurotransmitter release homeostasis (Adapted from Howlett et al., 2008). It is hypothesized that a mutation in *push* (not shown here) inhibits or disrupts this signaling pathway, resulting in a failure to attenuate increased neuronal excitability. This corresponds to increased neurotransmitter release and subsequent perineurial glial growth.

Using neuronal excitability as a starting point, cooperative signaling between the motor neuron and peripheral glia is hypothesized to increase perineurial glial growth. Inhibition of the DmGluRA-PI3K pathway within the neuron, either by directly inhibiting integral components of this pathway or by

mutating *push*, correlates with increased excitability and greater neurotransmitter release. Excess neurotransmitter, which is unable to be properly cleared from the extracellular space due to an *ine* mutation, is hypothesized to be sufficient to activate the proposed DmGluRA receptors in the peripheral glial membrane. DmGluRA-PI3K pathway activation in the peripheral glia then can inhibit FOXO and ultimately increase perineurial glial size (Figure 20).

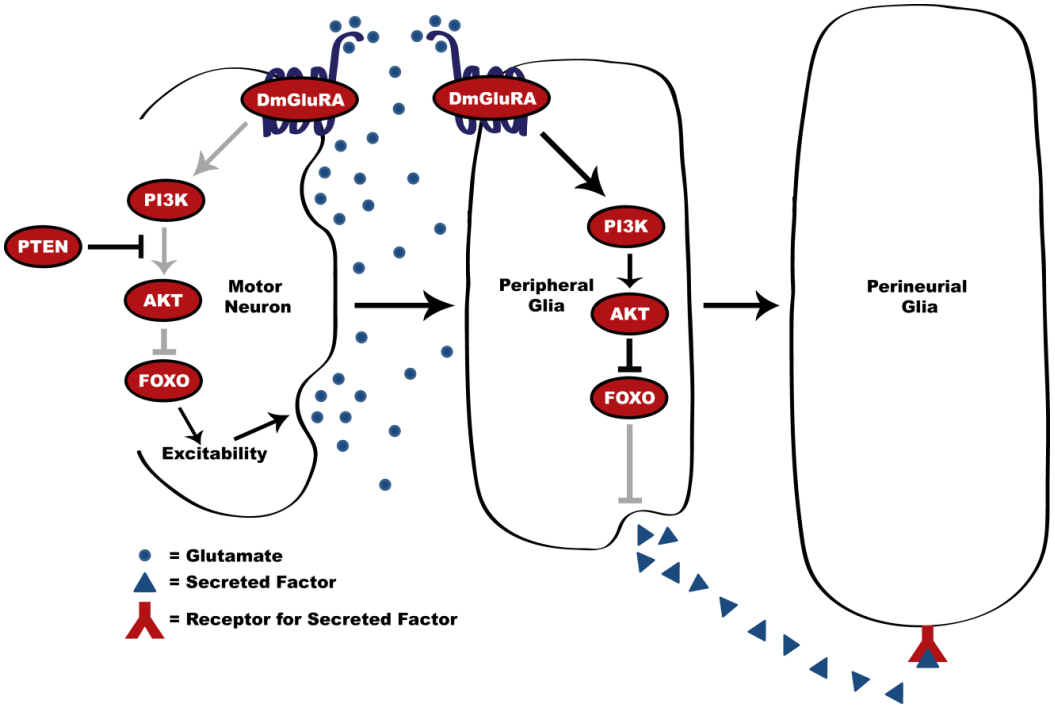

Figure 20: Hypothesized signaling pathway utilizing both the neuron and peripheral glia to stimulate perineurial glial growth. Inhibition of the DmGluRA-PI3K pathway within the motor neuron increases excitability and thus increases neurotransmitter release (Howlett et al., 2008). Additionally, activation of the PI3K-AKT pathway within the peripheral glia increases perineurial glial growth (Lavery et al., 2007). Therefore, it is hypothesized that an increase in neuronal excitability and subsequent increase in neurotransmitter release activates peripheral glial DmGluRA, which then activates the PI3K-AKT pathway. Activation of this DmGluRA-PI3K-AKT pathway is hypothesized to inhibit FOXO, which may be inhibiting transcription of a growth factor that causes perineurial glial growth. It is also hypothesized that peripheral glial DmGluRA-PI3K-AKT pathway activation and subsequent perineurial glial growth are

facilitated by mutations in *push* and *ine* (not shown here) via inhibition of neuronal DmGluRA-PI3K activation and prolonged neurotransmitter presence within the extracellular space, respectively.

7: Materials & Methods

7.1: Drosophila Stocks

D42-Gal4 (Yeh et al., 1995) was provided by Dr. Thomas Schwarz. *Gli-Gal4* (Sepp and Auld, 1999) and *MZ709-Gal4* (Leiserson et al., 2000) were provided by Dr. Vanessa Auld. Flies carrying the *UAS-PI3K*^{DN} (D954A) and *UAS-PI3K-CAAX* transgenes (Leevers et al. 1996) were provided by Sally Leevers (London Research Institute, London, UK). Flies carrying the *UAS-CAMKIIT287A* and *UAS-CAMKIIT287D* transgenes (Griffith et al. 1994; Park et al. 2002), were provided by Leslie C. Griffith (Brandeis University, Waltham, MA). *FAK*^{CG1} mutants and *UAS-FAK*$^{+}$ transgene flies (Grabbe et al. 2004) were provided by Ruth Palmer (Umeå University, Umeå, Sweden). *DmGluRA*^{112b} flies (Bogdanik et al. 2004) were provided by Marie-Laure Parmentier (Unité Propre de Recherche Centre, Montpellier, France). All other fly stocks were provided by the Drosophila Stock Center (Bloomington, IN).

All fly stocks were maintained on cornmeal/agar media (6% w/v dextrose, 6.8% w/v cornmeal, 1.2% w/v yeast, 0.72% w/v agar, 2% w/v methyl 4-hydroxybenzoate) at room temperature (~23ºC).

7.2: Electron Microscopy

Third instar larvae were raised on standard cornmeal media at room temperature (~22°C). Larvae were dissected in S2 media or PBS followed by 3 consecutive exposures to a primary fix (0.1 M cacodylic acid, 2% v/v paraformaldehyde, 2% v/v glutaraldehyde, pH of 7.4) for 15 minutes each. Larvae were then washed 3x for 10 minutes each with 0.1 M cacodylic acid with the last wash on ice. Larvae were then placed in a tube of post fix solution (0.05 M cacodylic acid, 0.0025% v/v OsO_4, 0.415% w/v $Fe(Cn)_6$), wrapped in foil, and placed in ice for 1 hr. Larvae were then washed 3x for 10 minutes each with Milli-Q water while being kept under foil and in ice. The Milli-Q water was discarded and larvae were placed in 2% w/v uranyl acetate at room temperature and covered with foil for 90 minutes. Larvae were then washed 3x for 10 minutes each with Milli-Q water and then taken through an ethanol series via exposure to 30, 50, 70, 95, 100, and 100% v/v EtOH for 10 minutes each under foil. Larvae were then exposed to propylene oxide 2x for 10 minutes each with the tube left open and then exposed to a 50:50 mixture of epoxy (made using PELCO® Eponate 12™ Kit with DMP-30 (#18010)) and propylene oxide for 1 hr with the tube lid open. Individual larvae were then placed in epoxy drops on paraffin wrapped slides and placed at 60°C to cure for at least three days. These cured drops were then placed in PELCO® flat embedding molds (#105), covered in epoxy, and allowed to cure at 60°C for a minimum of three days. After curing, excess epoxy was cut away from blocks using an RMC MTX microtome and glass knives hewn on an LKB KnifeMaker Type 7801B. Each larva was trimmed

with these glass knives to the point where the peripheral nerves immediately exited the tip of the ventral ganglion, and the area around the nerves was then hand trimmed with a utility knife blade. Ultrathin sections were then cut from blocks using an RMC PowerTome MTX and a MicroStar 9151 SU diamond knife. Ultrathin sections were picked up from the diamond knife trough on Ted Pella carbon formvar grids (#01802-F) and stained using 1% w/v uranyl acetate and lead citrate. EM images were collected utilizing a JEOL 1230 High Contrast Transmission Electron Microscope (HC-TEM).

7.3: Statistics for perineurial glial width measurements

Glial width measurements for each nerve cross section were obtained by subtracting the radius of the interior axon bundle from the radius of the total nerve and expressed as µm units. Bars and error bars represent genotype averages and standard errors, respectively. A minimum of 4 larvae were assayed for each genotype, and multiple nerves were assayed for each larva. Number of total nerves assayed for each genotype are indicated for each bar graph.

8: Results

8.1: The double chromosomal mutant *ine^{1}; DmGluRA^{112b}* increases perineurial glial size

I first tested the double mutant *ine^{1}; DmGluRA^{112b}* to see if this led to a comparable size increase in the perineurial glial layer to that of *ine^{1}, push^{1}* (Figure 17). *DmGluRA^{112b}* is a chromosomal null mutation generated by an

imprecise excision of a P element that deletes the start codon and part of the ligand binding domain of DmGluRA (Bogdanik et al., 2004). The double mutant *ine*^{1}*; DmGluRA*^{112b} did not increase the size of the perineurial glial layer to the same extent as *ine*^{1}*, push*^{1}. However, it did significantly increase the size of the perineurial glia in relation to the newly tested control, which is the *DmGluRA*^{112b} mutation in an *ine*$^{+}$ background (Figure 21).

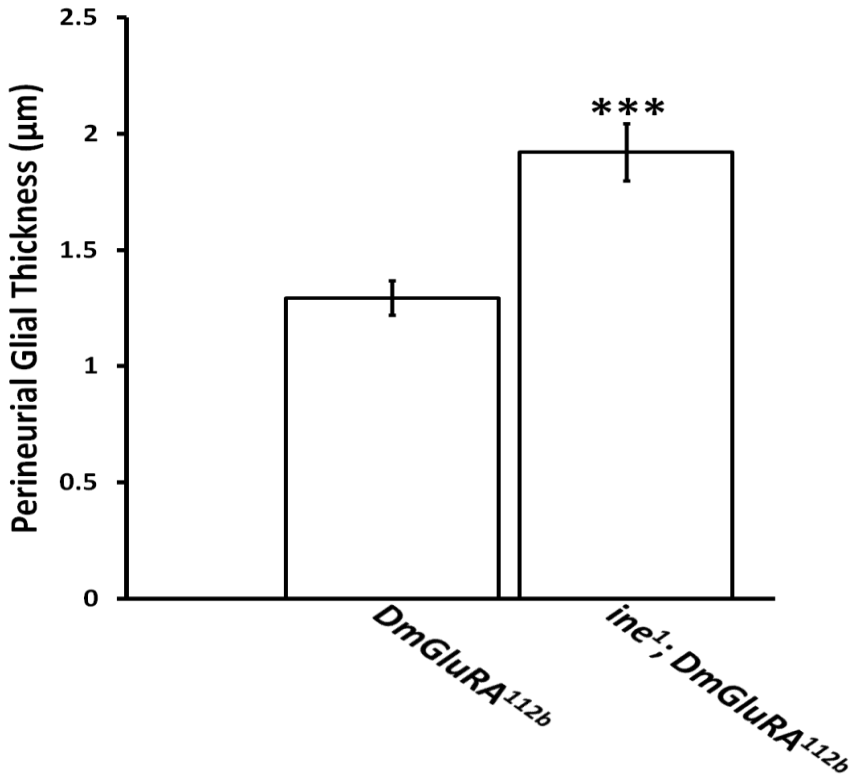

Figure 21: *DmGluRA* deletion significantly increases perineurial glial size. Chromosomal deletion of *DmGluRA* in the absence of Ine significantly increases the size of the perineurial glial layer. This double mutant demonstrates a role for DmGluRA in maintaining proper perineurial glial size. Measurements were obtained by subtracting the radius of the interior axon bundle from the radius of the total nerve. Bars and error bars are representative of averages and standard errors, respectively. Number of larvae assayed for each genotype = 4. Number of nerves measured for each genotype: *DmGluRA*^{112b}, N = 31; *ine*^{1}*; DmGluRA*^{112b}, N = 30. ($P < 0.0001$).

Similar to Push, DmGluRA regulates neuronal excitability (Bogdanik et al., 2004; Howlett et al., 2008). Therefore, we hypothesized it is the absence of DmGluRA that increases perineurial glial size as a consequence of increasing excitability. Additionally, the observation that *ine*^{1}*; DmGluRA*^{112b} is approximately 2 µm in perineurial glial width (Figure 21) while *ine*^{1}*, push*^{1} is approximately 3 µm in perineurial glial width (Figure 17) suggests that DmGluRA is necessary in other cell types, such as the peripheral glia, to facilitate perineurial glial growth or that excitability is not the only phenomenon responsible for causing perineurial glial thickening.

8.2: Motor neuronal PI3K inhibition in *ine*^{1} mutants thickens perineurial glia

The lipid kinase PI3K is a downstream target of DmGluRA activity. Therefore, I determined if inhibiting the lipid kinase PI3K within the neuron would similarly promote growth of the perineurial glia. One way to inhibit PI3K activity is to overexpress the phosphatase *PTEN*, which directly opposes the actions of PI3K by catalyzing PIP_3 to PIP_2. To test this I examined *ine*^{1}*; D42>PTEN*$^{+}$ larvae. With expression of neuronal *PTEN*$^{+}$ in an *ine*^{1} mutant background, I expected to see a size increase similar to that of *ine*^{1}*, push*^{1}. *ine*^{1}*; D42>PTEN*$^{+}$ did elicit a significant increase in perineurial glial thickness, although it was not to the extent of *ine*^{1}*, push*^{1} (Figure 22). Another way to inhibit PI3K is to express a dominant negative form of PI3K, known as PI3K^{DN}. As predicted, *ine*^{1}*; D42>PI3K*^{DN} larvae did possess a significantly increased perineurial glial size compared to the *ine*^{1}*; D42>+* control but still significantly less than *ine*^{1}*; D42>PTEN*$^{+}$ (Figure 22). It is

expected that *ine*^{1}*; D42>PTEN*$^{+}$ would elicit a stronger growth phenotype in the perineurial glia than *ine*^{1}*; D42>PI3K*^{DN} because it is not simply expressed in addition to endogenous PI3K, as is the case for PI3K^{DN}, but directly opposes the actions of endogenous PI3K. Collectively, expression of these transgenes illustrates that both Ine and PI3K must be adversely affected to cause perineurial glial growth because *D42>PTEN*$^{+}$ expression, when Ine is fully functional, does not cause a significant growth phenotype (Figure 22).

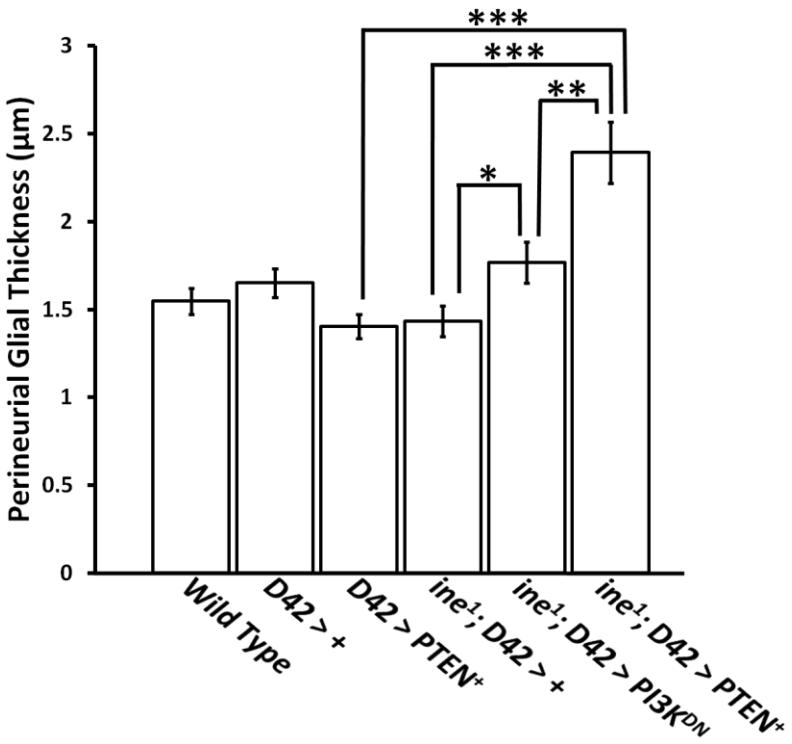

Figure 22: Motor neuronal *PI3K^{DN}* and *PTEN^{+}* expression significantly increases perineurial glial size in *ine^{1}* mutants. Neuronal inhibition of PI3K, either through the use of a dominant negative PI3K or *PTEN^{+}* expression, increases size of the perineurial glial layer but only in the absence of Ine. Measurements were obtained by subtracting the radius of the interior axon bundle from the radius of the total nerve. Bars and error bars are representative of averages and standard errors, respectively. Number of larvae assayed for each genotype = 4. Number of nerves measured for each genotype: *D42*>+, N = 48; *D42>PTEN*, N = 29; *ine^{1}; D42*>+, N = 31; *ine^{1}; D42>PI3K^{DN}*, N = 21; *ine^{1}; D42>PTEN*, N = 26. (*ine^{1}; D42*>+ vs. *ine^{1}; D42>PI3K^{DN}*, P = 0.025; *ine^{1}; D42*>+ vs. *ine^{1}; D42>PTEN*, P < 0.00001; *D42>PTEN* vs. *ine^{1}; D42>PTEN*, P < 0.00001; *ine^{1}; D42>PI3K^{DN}* vs. *ine^{1}; D42>PTEN*, P = 0.0066).

8.3: Motor neuronal expression of *FOXO^{+}* in *ine^{1}* mutants increases perineurial glial size

Similar to expression of *PTEN^{+}*, expression of *FOXO^{+}* also opposes the DmGluRA-PI3K pathway and causes a hyperexcitability phenotype because

PI3K activity downregulates FOXO activity (Howlett et al., 2008). We found that *ine*^{1}*; D42>FOXO*$^{+}$, similar to *ine*^{1}*; D42>PTEN*$^{+}$, exhibited significantly larger perineurial glia than the *ine*^{1}*; D42>*+ control (Figure 23).

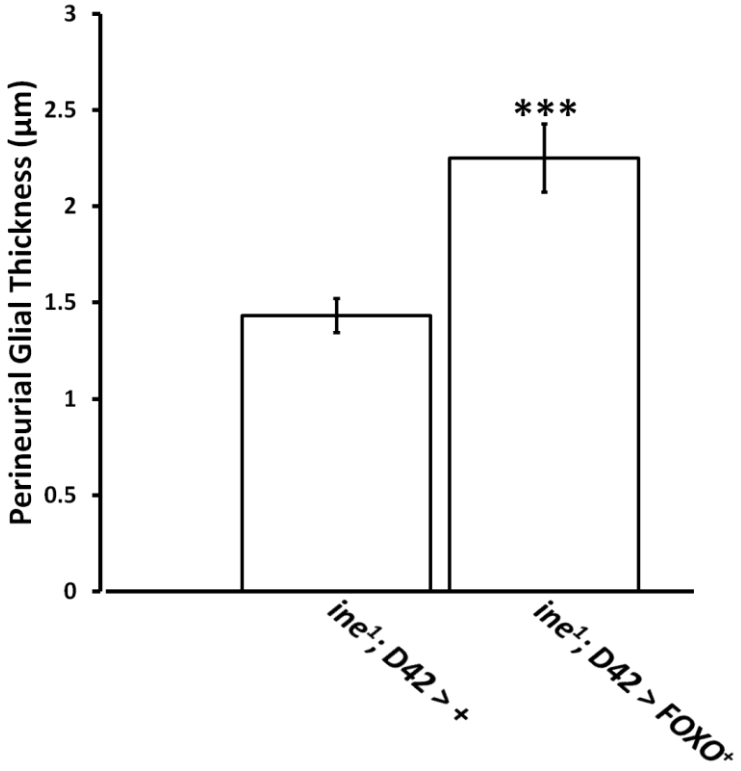

Figure 23: *ine*^{1}*; D42>FOXO*$^{+}$ increases perineurial glial growth. Expression of *FOXO*$^{+}$ significantly increases the size of the perineurial glial layer in the absence of Ine. Measurements were obtained by subtracting the radius of the interior axon bundle from the radius of the total nerve. Bars and error bars are representative of averages and standard errors, respectively. Number of larvae assayed for each genotype = 4. Number of nerves measured for each genotype: *ine*^{1}*; D42>*+, N = 31; *ine*^{1}*; D42>FOXO*$^{+}$, N = 31. (P = 0.00015).

8.4: Motor neuronal inhibition of *push* in *ine*^{1} mutants does not affect perineurial glial growth

Because the *ine*^{1}*, push*^{1} double mutant exhibits such a large increase in the size of the perineurial glial layer (Figure 17) and a *push* mutation is believed to inhibit DmGluRA-PI3K signaling within the neuron, I wished to test if *push* inhibition specifically within the neuron would cause perineurial glial augmentation using *ine*^{1}*; D42>push*^{RNAi}. However, size of the perineurial glia was unaffected (Figure 24). The fact that *ine*^{1}*; D42>push*^{RNAi} does not cause perineurial glial size increase may be due to the fact that *push* mRNA is not being degraded enough by the RNAi transgene.

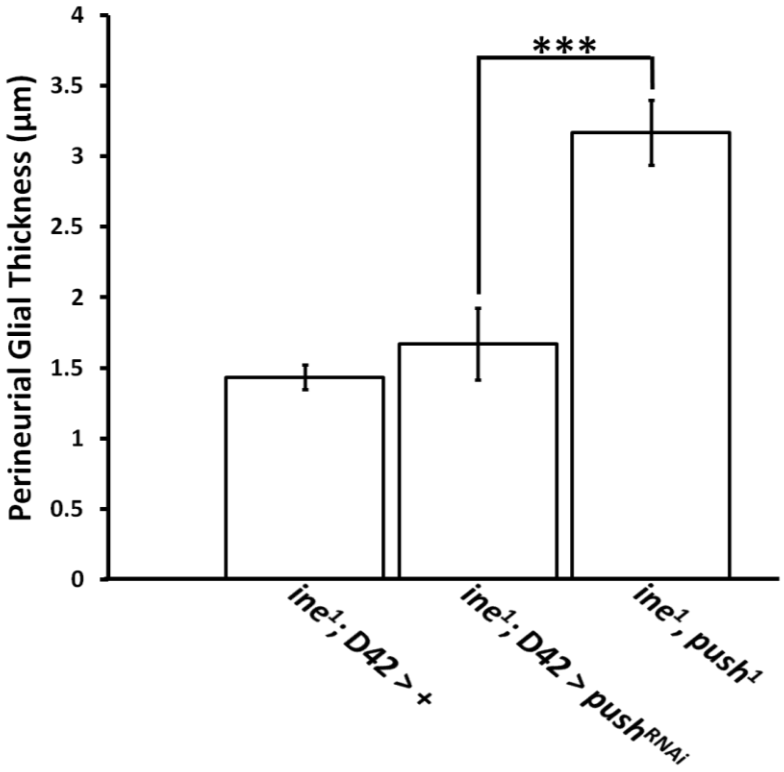

Figure 24: Motor neuronal *push* inhibition in *ine[1]* mutants does not increase perineurial glial size. Measurements were obtained by subtracting the radius of the interior axon bundle from the radius of the total nerve. Bars and error bars are representative of averages and standard errors, respectively. Number of larvae assayed for each genotype = 4. Number of nerves measured for each genotype: *ine[1]; D42*>+, N = 31; *ine[1]; D42>push[RNAi]*, N = 25; *ine[1], push[1]*, N = 16. (*ine[1]; D42>push[RNAi]* vs. *ine[1], push[1]*, P = 0.00022).

8.5: Peripheral glial inhibition of *push* in *ine[1]* mutants increases perineurial glial growth

Next I wanted to test if *push* inhibition specifically within the peripheral glia was capable of eliciting perineurial glial growth. I utilized *ine[1], Gli>push[RNAi]* and observed a significant increase in the size of the perineurial glial layer (Figure 25).

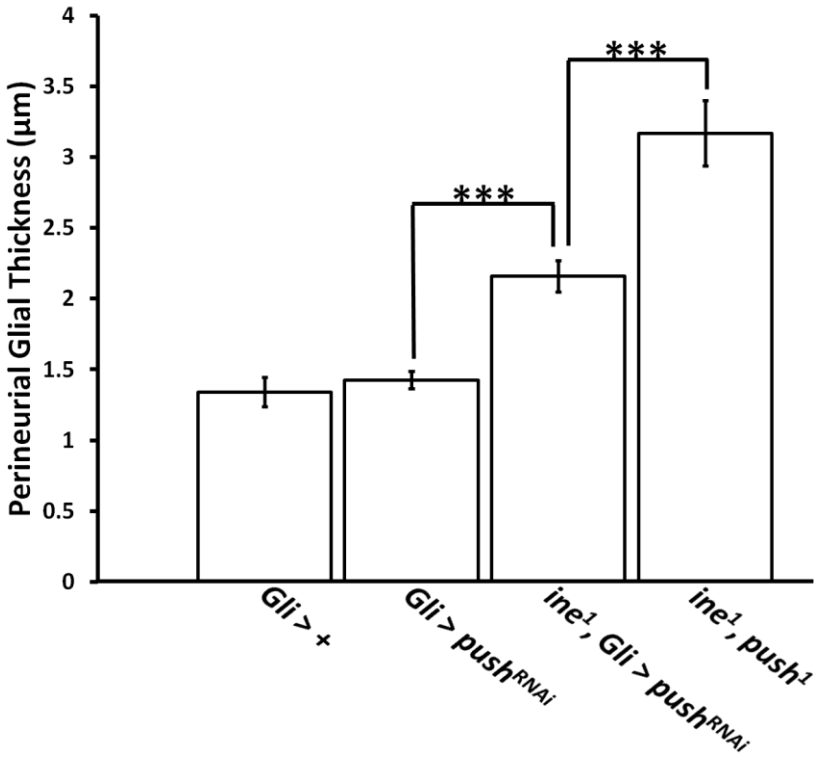

Figure 25: *Gli>push*^{RNAi} increases perineurial glial size but only in *ine*^{1} mutants. A *push* knockdown specifically within the peripheral glia displays a significant increase in perineurial glial growth only when in the absence of Ine, demonstrating that *push* is necessary in the peripheral glia to maintain proper perineurial glial size. Measurements were obtained by subtracting the radius of the interior axon bundle from the radius of the total nerve. Bars and error bars are representative of averages and standard errors, respectively. Number of larvae assayed for each genotype = 4. Number of nerves measured for each genotype: *Gli*>+, N = 25; *Gli>push*^{RNAi}, N = 47; *ine; Gli>push*^{RNAi}, N = 20; *ine*^{1}*, push*^{1}, N = 16. (*Gli*>+ vs. *gli>push*^{RNAi}, P = 0.45; *Gli>push*^{RNAi} vs. *ine*^{1}*; Gli>push*^{RNAi}, P < 0.0001; *ine*^{1}*; Gli>push*^{RNAi} vs. *ine*^{1}*, push*^{1}, P < 0.0001).

This indicates that *push* is required within the peripheral glia to maintain proper perineurial glial size. However, the observation that *ine*^{1}*, Gli>push*^{RNAi} exhibits a perineurial glia approximately 2 µm in width, whereas *ine*^{1}*, push*^{1} exhibits approximately a 3 µm perineurial glial width (Figure 17), suggests that

Push is required in more than just the peripheral glia to maintain proper perineurial glial size. This result also coincides with the size increase observed with *ine^{1}; DmGluRA^{112b}* (Figure 21) in that both *ine^{1}, Gli>push^{RNAi}* and *ine^{1}; DmGluRA^{112b}* translate into perineurial glia of the same size. Also, the fact that *Gli>push^{RNAi}* alone does not cause a size increase in the perineurial glia shows that both Ine and Push must be inhibited within the peripheral glia to elicit such growth.

8.6: Peripheral glial *DmGluRA* inhibition decreases perineurial glial size relative to *ine^{1}, push^{1}* mutants

Understanding that DmGluRA-PI3K pathway inhibition is involved in heightened neuronal excitability and hypothesizing that this inhibition causes a size increase within the perineurial glia, I wished to determine if the DmGluRA-PI3K pathway existed in the peripheral glia and was necessary to facilitate perineurial glial growth. If DmGluRA was localized in peripheral glia and necessary for the *ine^{1}, push^{1}* double chromosomal mutant to elicit such a significant growth of the perineurial glia, then knockdown of *DmGluRA* using the strain *ine^{1}, push^{1}*, *Gli>DmGluRA^{RNAi}* should decrease perineurial glial growth in comparison to that of *ine^{1}, push^{1}*. Indeed, *ine^{1}, push^{1}, Gli>DmGluRA^{RNAi}* does significantly decrease the size of the perineurial glia compared to *ine^{1}, push^{1}* but is still significantly larger compared to the control *Gli*>+ (Figure 26). I also wished to determine if the inhibition of potential downstream targets of DmGluRA within the peripheral glia decreased perineurial glial size in comparison to the *ine^{1},*

push^{1} double mutant. It has been demonstrated that DmGluRA activates PI3K in Drosophila motor neurons (Howlett et al., 2008; Lin et al., 2011). The GTPase Ras is also known to activate PI3K and a constitutively active Ras, *Ras*^{V12}, expressed within the peripheral glia significantly increases perineurial glial thickness (Lavery et al., 2007). Therefore, I assessed the genotype *ine*^{1}*, push*^{1}*, Gli>Ras*^{N17}, where *Ras*^{N17} is a dominant negative form of Ras in which residue 17 is mutated from a serine to an asparagine (Feig & Cooper, 1988). However, I did not observe a decrease in perineurial glial size in comparison to *ine*^{1}*, push*^{1} (Figure 26). This suggests that peripheral glial Ras is not involved in facilitating perineurial glial growth within *ine*^{1}*, push*^{1} mutants. A constitutively active form of PI3K expressed from the peripheral glia also increases perineurial glial size (Lavery et al., 2007). Additionally, increased opposition of endogenous PI3K activity using the genotype *ine*^{1}*, push*^{1}*, Gli>PTEN*$^{+}$ showed no decrease in perineurial glial size when compared to *ine*^{1}*, push*^{1}. (Figure 26).

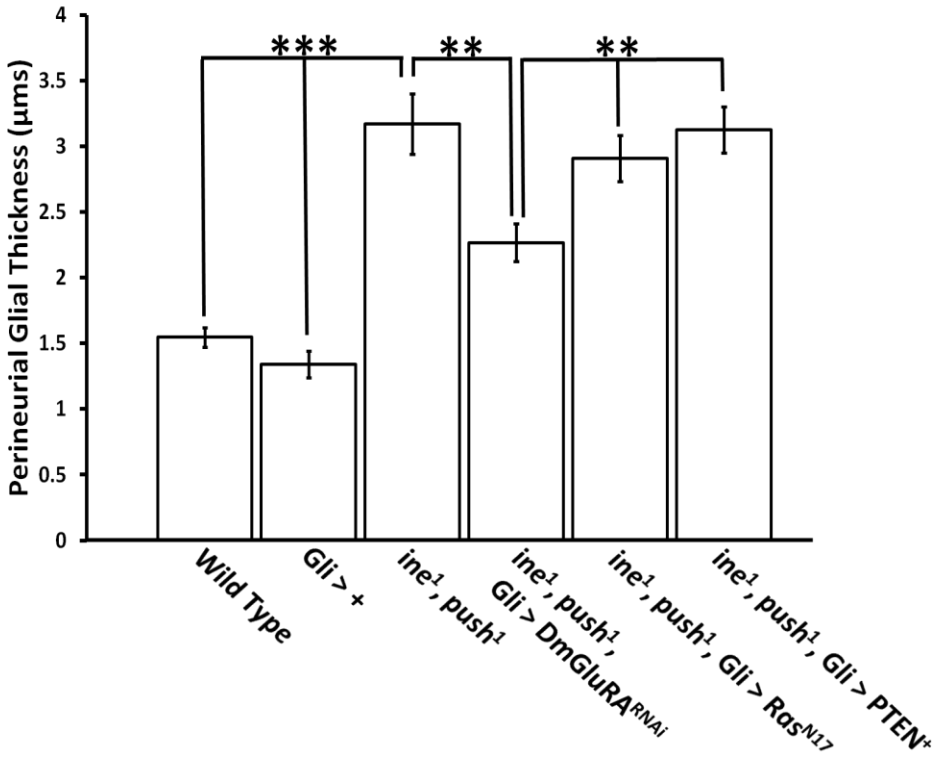

Figure 26: *ine*^{1}, *push*^{1}, *Gli>DmGluRA*^{RNAi} significantly decreases perineurial glial size in comparison to *ine*^{1}, *push*^{1}. This suggests that DmGluRA does not activate the Ras-PI3K pathway within the peripheral glia to elicit perineurial glial growth. Measurements were obtained by subtracting the radius of the interior axon bundle from the radius of the total nerve. Bars and error bars are representative of averages and standard errors, respectively. Number of larvae assayed for each genotype = 4. Number of nerves measured for each genotype: Wild Type, N = 33; *Gli*>+, N = 25; *ine*^{1}, *push*^{1}, N = 16; *ine*^{1}, *push*^{1}, *Gli>DmGluRA*^{RNAi}, N = 33; *ine*^{1}, *push*^{1}, *Gli>Ras*^{N17}, N = 32; *ine*^{1}, *push*^{1}, *Gli>PTEN*, N = 28. (Wild Type vs. *ine*^{1}, *push*^{1}, P < 0.00001; *Gli*>+ vs. *ine*^{1}, *push*^{1}, P < 0.00001; *ine*^{1}, *push*^{1} vs. *ine*^{1}, *push*^{1}, *Gli>DmGluRA*^{RNAi}, P = 0.0013; *ine*^{1}, *push*^{1}, *Gli>DmGluRA*^{RNAi} vs. *ine*^{1}, *push*^{1}, *Gli>Ras*^{N17}, P = 0.0063; *ine*^{1}, *push*^{1}, *Gli>DmGluRA*^{RNAi} vs. *ine*^{1}, *push*^{1}, *Gli>PTEN*, P = 0.00033).

These results suggest that the peripheral glial Ras-PI3K pathway is not involved in increasing perineurial glial size specifically when *ine* and *push* are simultaneously mutated. It is also possible that Push is acting downstream of

peripheral glial PI3K and is therefore not inhibited by PI3K inhibition. A less likely scenario is that the Ras-PI3K pathway is not involved or is only partially involved in peripheral glial DmGluRA-mediated perineurial glial growth and that DmGluRA also activates other signals that compensate for any inhibition of this pathway.

8.7: Ras activation of PI3K is necessary for *ine[1], push[1]* perineurial glial overgrowth

While Ras-PI3K inhibition does not reduce perineurial glial growth from the peripheral glia with regards to *ine[1], push[1]* mutants, Ras-PI3K signaling does appear to be essential in other tissues to facilitate perineurial glial growth within *ine[1], push[1]* mutants. This can be witnessed when replacing endogenous *Drosophila* PI3K with *Cos-PI3K^{RBD}* which is a PI3K that possesses mutations in its Ras binding domain (RBD). The mutations T231D, K250A, R253A, and K257A in the PI3K RBD allow Cos-PI3K^{RBD} to be activated through all other means except for direct activation via Ras (Orme, et al., 2006). In this case, Cos-PI3K^{RBD} replaces endogenous PI3K within the entire organism and is not tissue specific. Using the genotype *ine[1], push[1], Cos-PI3K^{RBD}*, I observed a perineurial glial size similar to that of Wild Type and thus greatly reduced from *ine[1], push[1]* (Figure 27).

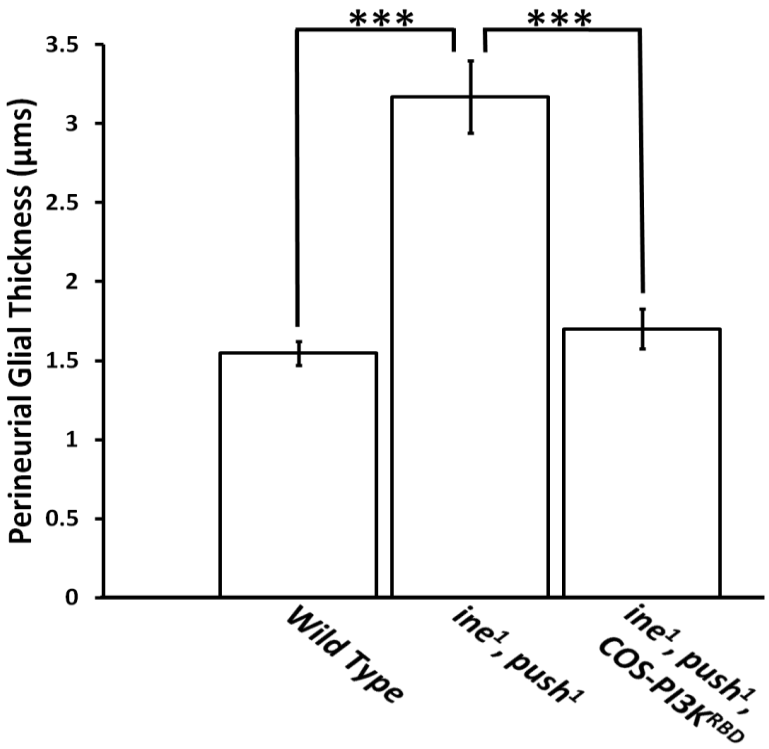

Figure 27: Ras activation of PI3K is necessary for *ine[1], push[1]* perineurial glial growth. Ras activation of PI3K is critical to induce perineurial glial growth in *ine[1], push[1]* mutants although it is not known in which tissues this occurs. It appears that this is occurring in a cell type other than the peripheral glia due to the results observed in Figure 9. Measurements were obtained by subtracting the radius of the interior axon bundle from the radius of the total nerve. Bars and error bars are representative of averages and standard errors, respectively. Number of larvae assayed for each genotype = 4. Number of nerves measured for each genotype: Wild Type, N = 33; *ine[1], push[1]*, N = 16; *ine[1], push[1], Cos-PI3K[RBD]*, N = 37. (Wild Type vs. *ine[1], push[1]*, $P < 0.00001$; *ine[1], push[1]* vs. *ine[1], push[1], Cos-PI3K[RBD]*, $P < 0.00001$).

This demonstrates that Ras-PI3K signaling is necessary to produce the perineurial glial size observed in *ine[1], push[1]* mutants. One possibility is that the essential Ras-PI3K signaling is occurring in the perineurial glia. If this were the case, Ras-PI3K signaling inhibition specifically within the perineurial glia should prevent an overgrowth phenotype in *ine[1], push[1]* mutants.

8.8: Expression of the "leaky" Ca^{2+} channel *NMDAR1 (Lurcher)* increases perineurial glial size

Another group of molecules that may be involved in the pathway affected by *ine*[1]*, push*[1] mutations independent of DmGluRA are the ionotropic glutamate receptors which may respond to an excess of neurotransmitter release. To establish if ionotropic glutamate receptors are capable of influencing perineurial glial size, I expressed a mutated version of the NMDAR1 ionotropic glutamate receptor/Ca^{2+} channel known as *NMDAR1 (Lurcher)*. This transgene possesses what is known as a Lurcher (Lc) mutation which is a transition point mutation from guanine to adenine, causing an alanine to become a threonine (Zuo et al., 1997). This is a gain of function mutation which causes the channel to become "leaky" and allows for an influx of Ca^{2+} into the cell. Larvae expressing *Gli>NMDAR1 (Lc)* possessed a significant increase in perineurial glial growth (Figure 28).

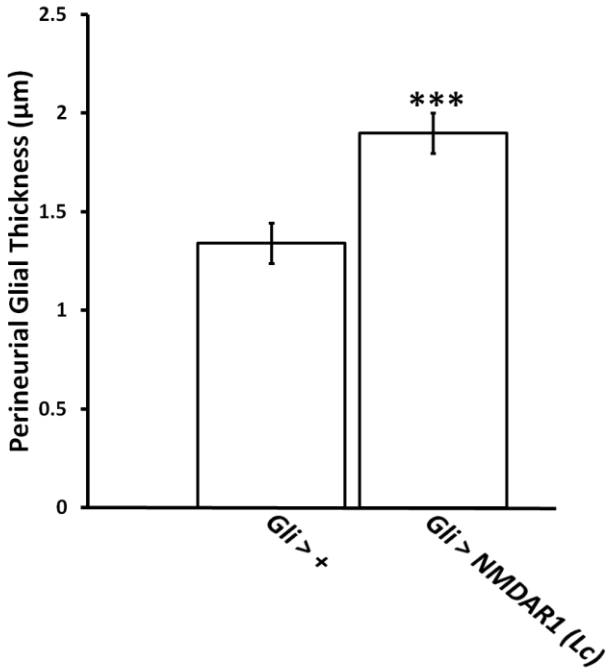

Figure 28: *Gli>NMDAR1 (Lc)* increases perineurial glial growth. Expression of a "leaky" ionotropic glutamate receptor, *NMDAR1 (Lc)*, yields a significant perineurial glial size increase. This is possibly due to an increase in the amount of Ca^{2+} entering into the peripheral glia and activating downstream effector proteins which influence perineurial glia size. Measurements were obtained by subtracting the radius of the interior axon bundle from the radius of the total nerve. Bars and error bars are representative of averages and standard errors, respectively. Number of larvae assayed for each genotype = 4. Number of nerves measured for each genotype: *Gli*>+, N = 25; *Gli>NMDAR1 (Lc)*, N = 32. (P = 0.00038).

8.9: Peripheral glial DmGluRA may activate the Ca^{2+}/calmodulin-dependent kinase II

The fact that increased Ca^{2+} influx increases perineurial glial size raises the possibility that peripheral glial DmGluRA may be signaling through Ca^{2+} intermediates to affect glial size. DmGluRA shares homology with mammalian Group II mGluRs (Parmentier et al., 1996; Bogdanik et al., 2004). Although this

class of mGluRs is associated with adenylate cyclase signaling rather than activating Ca^{2+} signaling intermediates, the fact that DmGluRA is the solely functioning Drosophila metabotropic glutamate receptor makes it feasible that DmGluRA performs the tasks of all mammalian mGluRs (Pan et al., 2008; Lin et al., 2011). If this were the case, DmGluRA may be capable of activating Ca^{2+} signaling intermediates within the peripheral glia and subsequently eliciting growth of the perineurial glia. In agreement with this thinking, it has been shown that DmGluRA activates the Ca^{2+}/calmodulin-dependent kinase II (CAMKII) within Drosophila motor neurons (Lin et al., 2011). I wished to see if CAMKII activity affected perineurial glial size by expressing a constitutively active form of CAMKII known as *CAMKII*^{T287D}. The point mutation in *CAMKII*^{T287D} is a phosphomimetic substitution at the autophosphorylation site which renders the kinase Ca^{2+}/calmodulin-independent and therefore constitutively active (Park et al., 2002). I found that *Gli>CAMKII*^{T287D} larvae did possess thickened perineurial glia (Figure 29). However, larvae expressing *Gli>CAMKII*^{T287A}, the nonphosphorylatable form of CAMKII, did not have thickened perineurial glia (Figure 29). CAMKII is also known to activate PI3K in human monocytic cells (Ma et al., 2007), in ovarian cancer cells (Ma et al., 2009), and in Drosophila motor neurons via focal adhesion kinase (FAK) (Lin et al., 2011). Although peripheral glial Ras-PI3K signaling does not appear to be downstream of DmGluRA in regards to affecting perineurial glial size in *ine*^{1}*, push*^{1} mutants (Figure 26), I still wished to see if inhibiting the Ras-PI3K pathway in conjunction with CAMKII

constitutive activity would decrease perineurial glial size. To do this, I expressed *gli>CAMKII*^{T287D}*, Ras*^{N17} and *gli>CAMKII*^{T287D}*, PTEN* (Figure 29).

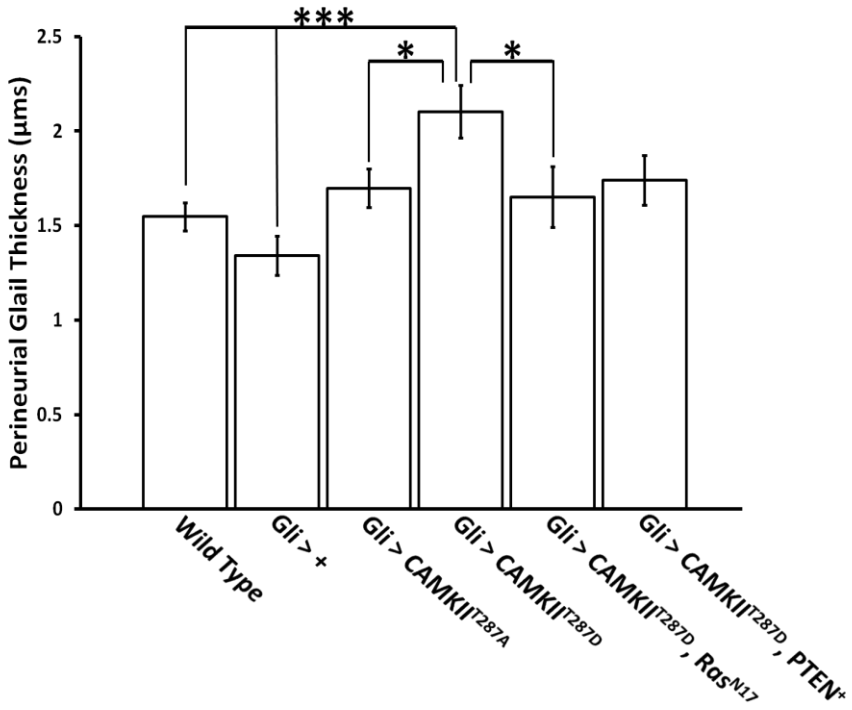

Figure 29: Perineurial glial growth is significantly increased in *Gli>CAMKII*^{T287D} flies. This suggests that CAMKII may increase perineurial glial growth via a pathway that is partially or completely independent from the Ras-PI3K pathway. Measurements were obtained by subtracting the radius of the interior axon bundle from the radius of the total nerve. Bars and error bars are representative of averages and standard errors, respectively. Number of larvae assayed for each genotype = 4. Number of nerves measured for each genotype: Wild Type, N = 33; *Gli*>+, N = 25; *Gli>CAMKII*^{T287A}, N = 39; *Gli>CAMKII*^{T287D}, N = 32; *Gli>CAMKII*^{T287D}*, PTEN*, N = 41; *Gli>CAMKII*^{T287D}*, Ras*^{N17}, N = 22. (*Wild Type* vs. *Gli>CAMKII*^{T287D}, P = 0.00079; *Gli*>+ vs. *Gli>CAMKII*^{T287D}, P = 0.00011; *Gli>CAMKII*^{T287A} vs. *Gli>CAMKII*^{T287D}, P = 0.019; *Gli>CAMKII*^{T287D} vs. *Gli>CAMKII*^{T287D}*, Ras*^{N17}, P = 0.040).

Gli>CAMKII^{T287D}*, Ras*^{N17} significantly (P = 0.040) decreased perineurial glial size from that of *Gli>CAMKII*^{T287D} while *Gli>CAMKII*^{T287D}*, PTEN*$^{+}$ did not (Figure 29). It should also be noted that *Gli>CAMKII*^{T287D}*, Ras*^{N17} and

Gli>CAMKII^{T287D}*, PTEN*$^{+}$ are not significantly different from the Wild Type and *Gli*>+ controls (Figure 29). While these findings do not exhibit a strong independence from peripheral glial Ras-PI3K signaling as in the case of *ine*^{1}*, push*^{1} (Figure 26), this may be because the growth effect seen in *ine*^{1}*, push*^{1} is much greater than that of *Gli>CAMKII*^{T287D}. These findings present an interesting possibility for a signaling pathway within the peripheral glia in regards to increasing perineurial glial size. Inhibition of peripheral glial DmGluRA in an *ine*^{1}*, push*^{1} background decreases perineurial glial size from that of *ine*^{1}*, push*^{1} (Figure 26) while peripheral glial Ras and PI3K inhibition in an *ine*^{1}*, push*^{1} background does not decrease perineurial glial size in comparison to *ine*^{1}*, push*^{1} (Figure 26). Also, peripheral glial expression of a constitutively active CAMKII increases perineurial glial size, but inhibition of peripheral glial Ras-PI3K signaling does not convincingly decrease perineurial glial growth in comparison to *Gli>CAMKII*^{T287D} (Figure 29). This raises the possibility that DmGluRA upregulates Ca^{2+} signaling via CAMKII within the peripheral glia to augment the perineurial glia using a pathway that is partially or fully independent from that of Ras-PI3K.

8.10: Peripheral glial DmGluRA may activate Focal Adhesion Kinase (FAK)

I also expressed *FAK*$^{+}$ (*UAS-FAK*) within the peripheral glia using *Gli>FAK*$^{+}$ as this is a direct target of CAMKII. While *FAK*$^{+}$ expression within the peripheral glia significantly increases perineurial glial size (Figure 30), I had previously examined if *FAK* inhibition would elicit perineurial glial growth. I employed the mutant line *FAK*^{CG1}, a chromosomal null mutation which removes

the first 1263 base pairs (bp) of the *FAK* coding sequence and thus the first 421 amino acids of the FAK protein (Grabbe et al., 2004). I did not expect to see an increase in perineurial glial growth in the FAK^{CG1} mutant as it seems FAK would be needed in the peripheral glia to facilitate this growth. However, I did observe a significant increase in perineurial glial growth when *FAK* was no longer expressed (Figure 30). Although I witnessed a significant perineurial glial size increase in FAK^{CG1} mutants, which do not have a mutation in *ine*, ine^{1}, FAK^{CG1} mutants may possess even larger perineurial glia. I also tested FAK^{CG1}; *D42>*FAK^{+} and determined that FAK^{+} expression solely within the motor neuron in a FAK^{CG1} background significantly reduces perineurial glial size from that of FAK^{CG1} but not back to that of wildtype (Figure 30). I therefore wished to assay if FAK^{+} expression solely within the peripheral glia in a FAK^{CG1} background would also decrease perineurial glial thickness in comparison to FAK^{CG1}. Using FAK^{CG1}, *MZ709>*FAK^{+}, I also determined that peripheral glial *FAK* expression in a FAK^{CG1} background significantly reduced perineurial glial size in comparison to FAK^{CG1} and also significantly reduced perineurial glial size compared to FAK^{CG1}; *D42>*FAK^{+} (Figure 30). FAK^{CG1}, *MZ709>*FAK^{+} also no longer possessed a significantly increased perineurial glia in comparison to the peripheral glial control *Gli>+* (Figure 30).

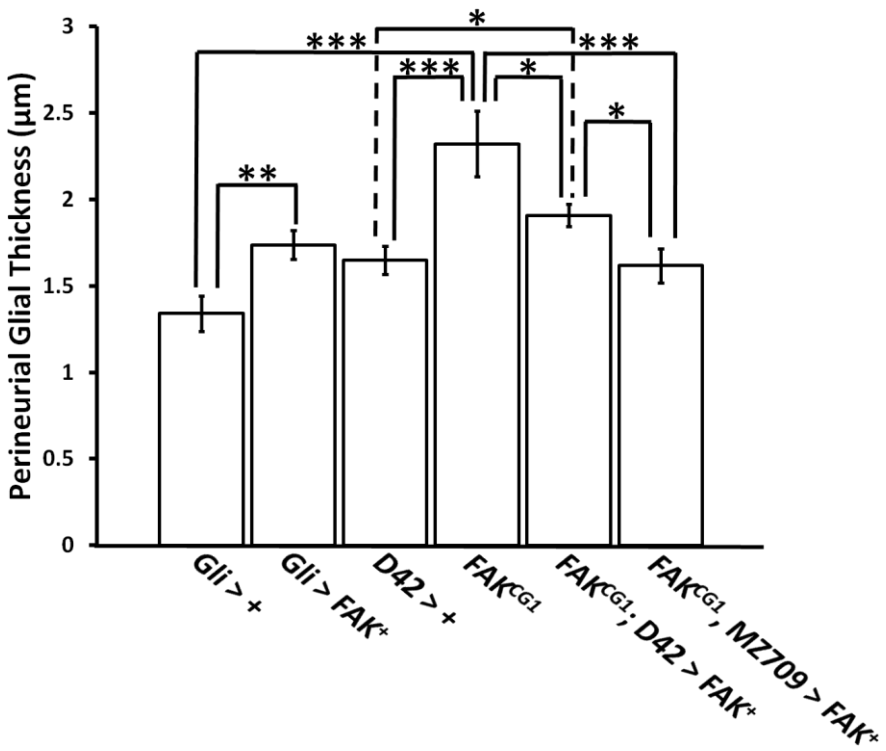

Figure 30: Motor neuronal and peripheral glial expression of *FAK*$^{+}$ within a *FAK*^{CG1} background reduces perineurial glial growth. Measurements were obtained by subtracting the radius of the interior axon bundle from the radius of the total nerve. Bars and error bars are representative of averages and standard errors, respectively. Number of larvae assayed for each genotype = 4. Number of nerves measured for each genotype: *Gli*>+, N = 25; *Gli>FAK*, N = 25; *D42*>+, N = 48; *FAK*^{CG1}, N = 24; *FAK*^{CG1}*; D42>FAK*, N = 32; *FAK*^{CG1}*, MZ709>FAK*, N = 33. (*Gli*>+ vs. *Gli>FAK*, p = 0.0040; *Gli*>+ vs. *FAK*^{CG1}, P = 0.000029; *D42*>+ vs. *FAK*^{CG1}, P = 0.00029; *D42*>+ vs. *FAK*^{CG1}*; D42>FAK*, P = 0.026; *FAK*^{CG1} vs. *FAK*^{CG1}*; D42>FAK*, P = 0.026; *FAK*^{CG1} vs. *FAK*^{CG1}*, MZ709>FAK*, P = 0.00079; *FAK*^{CG1}*; D42>FAK* vs. *FAK*^{CG1}*, MZ709>FAK*, P = 0.018).

This demonstrates that FAK is necessary in both the motor neuron and the peripheral glia to maintain proper perineurial glial size. The results for both *FAK*^{CG1} and the rescue genotypes appear to be contradictory to *Gli>FAK*$^{+}$ expression causing perineurial glial growth (Figure 30). However, these results may be due to FAK interacting with different signaling molecules in each

individual case or perhaps dependent upon the exact level of FAK present within the peripheral glia. Further experiments are necessary to discern what role FAK truly plays in perineurial glial size determination.

8.11: What DmGluRA-associated G proteins are involved in *ine*^{1}, *push*^{1} signaling?

Wanting to know what downstream effectors DmGluRA might activate and knowing that DmGluRA is a GPCR, I manipulated the small G proteins associated with GPCRs to identify which of these proteins may affect perineurial glial growth. First, in the peripheral glia I expressed both $G\alpha_i$ and $G\alpha_o$ proteins that are locked in the GTP bound state and are therefore constitutively active using the stocks *Gli>Gα$_i$** and *Gli>Gα$_o$-GTP*. However, I did not witness any increase in perineurial glial size (Figure 31). These results suggest that DmGluRA may be signaling through its Gβγ proteins to augment the perineurial glia. If this were the case, the absence of a Gα protein would allow the Gβγ heterodimer to be free and capable of activating downstream effectors. Therefore, I observed peripheral nerves within flies possessing a null mutation in $G\alpha_i$ known as the *Gα$_i^{P8}$* mutation. This mutation deletes the base pairs from +29 to +6104 in relation to the transcription start site, removing the first two exons while still producing a transcript (Yu et al., 2003; Ogden et al., 2008). Other null mutations of the $G\alpha_i$ protein exist that delete the entire coding region, but they are lethal at the embryonic stage (Yu et al., 2003). Most of the *Gα$_i^{P8}$* homozygotic mutants possess locomotory defects and die as larvae (Yu et al., 2003), but this

sustainability is enough for dissection and observation of peripheral nerves. Larvae possessing the $G\alpha_i^{P8}$ mutation illustrate a significantly increased perineurial glial layer (Figure 31). This suggests that the signaling pathway responsible for perineurial glial growth travels through the remaining unrestricted Gβγ subunit.

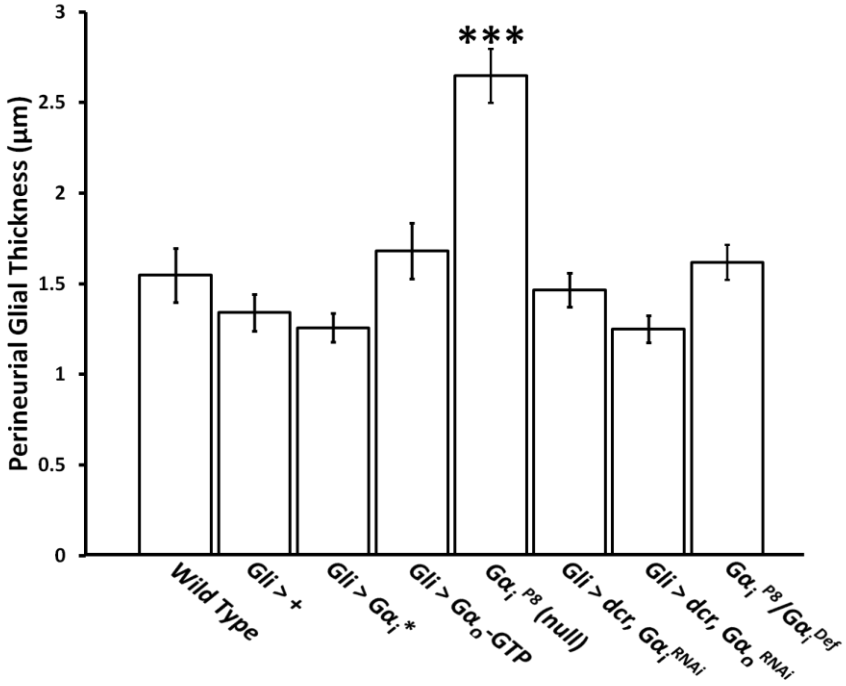

Figure 31: Deletion of $G\alpha_i$ significantly increases perineurial glial size. Both expression of constitutively active $G\alpha_i$ and $G\alpha_o$ as well as inhibition of $G\alpha_i$ and $G\alpha_o$ from the peripheral glia do not increase perineurial glial size, but chromosomal deletion of $G\alpha_i$ ($G\alpha_i^{P8}$) significantly augments the perineurial glia. Measurements were obtained by subtracting the radius of the interior axon bundle from the radius of the total nerve. Bars and error bars are representative of averages and standard errors, respectively. Number of larvae assayed for each genotype = 4. Number of nerves measured for each genotype: Wild Type, N = 33; *Gli*>+, N = 25; *Gli*>$G\alpha_i$*, N = 32; *Gli*>$G\alpha_o$-*GTP*, N = 32; $G\alpha_i^{P8}$ *(*null*)*, N = 30; *Gli>dcr,* $G\alpha_i^{RNAi}$, N = 36; *Gli>dcr,* $G\alpha_o^{RNAi}$, N = 39. (Wild Type vs. $G\alpha_i^{P8}$ (null) and *Gli*>+ vs. $G\alpha_i^{P8}$ *(null)*, P < 0.00001).

While this result suggests that perineurial glial growth is directed through the Gβγ heterodimer, it does not identify the specific cell types where this signaling takes place. To determine if Gβγ is eliciting perineurial glial growth from the peripheral glia, I attempted to knockdown Gα signaling using the genotypes *Gli>dcr, Gαi*^{RNAi} and *Gli>dcr, Gα*$_{o}^{RNAi}$. However, I did not witness any increase in perineurial glial size (Figure 31). Not being able to repeat the Gα$_{i}^{P8}$ results observed using *Gli-Gal4*, I wanted to verify that the perineurial glial overgrowth observed was indeed due to loss of *Gα$_i$* and not a consequence of the genetic background. To do this I assayed *Gα$_{i}^{P8}$/Gα$_{i}^{Def}$* larvae, where *Gα$_{i}^{Def}$* is another deletion of *Gα$_i$* that differs from *Gα$_{i}^{P8}$*. Unfortunately, *Gα$_{i}^{P8}$/Gα$_{i}^{Def}$* larvae possessed normal sized perineurial glia (Figure 31), suggesting that the overgrowth phenotype observed in *Gα$_{i}^{P8}$* larvae was not due to loss of *Gα$_i$*.

8.12: Peripheral glial Ras-PI3K signaling may target activation of matrix metallopeptidases

While it appears that peripheral glial Ras-PI3K signaling is not an integral part of *ine^1, push^1* perineurial glial growth (Figure 26), it remains that expressing constitutively active peripheral glial Ras or PI3K elicits growth of the perineurial glia (Lavery et al., 2007). Additionally, *FOXO$^+$* expression negates the growth phenotype observed in *Gli>PI3K-CAAX* larvae (Lavery et al., 2007). Therefore, to better understand how this nonautonomous signaling between peripheral and perineurial glia elicits the observed growth effect, I attempted to identify potential downstream effectors that FOXO may be inhibiting. Potential targets of FOXO-mediated inhibition may be the matrix metallopeptidases (MMPs). MMPs belong

to a family of secreted and transmembrane endopeptidases which proteolytically cleave and subsequently activate a wide variety of extracellular matrix proteins involved in, among other processes, proliferation, differentiation, and apoptosis (Vu & Werb et al., 2000). These proteins possess several evolutionarily conserved domains including a signal sequence which prompts cellular secretion, a domain with a cysteine residue directing enzymatic dormancy, and a catalytic zinc-binding domain (Llano et al., 2002). Within *Drosophila* there are 2 MMPs denoted as MMP1 and MMP2. MMP1 a secreted protein while MMP2 is membrane bound (Llano et al., 2002). Interestingly, while MMP1 is highly expressed during embryonic stages 12-13 and limited thereafter (Llano et al., 2000), MMP2 is expressed in all developmental and adult stages and is found within neurons and glia (Miller et al., 2008). This makes the MMPs, specifically MMP2, possible candidates for involvement in facilitating perineurial glial growth if left unregulated. I assayed the genotypes *Gli>PI3K-CAAX; dcr; MMP1*^{RNAi} and *Gli>PI3K-CAAX; dcr; MMP2*^{RNAi} but did not witness a significant decrease in perineurial glial growth in comparison to *Gli>PI3K-CAAX* (Figure 32).

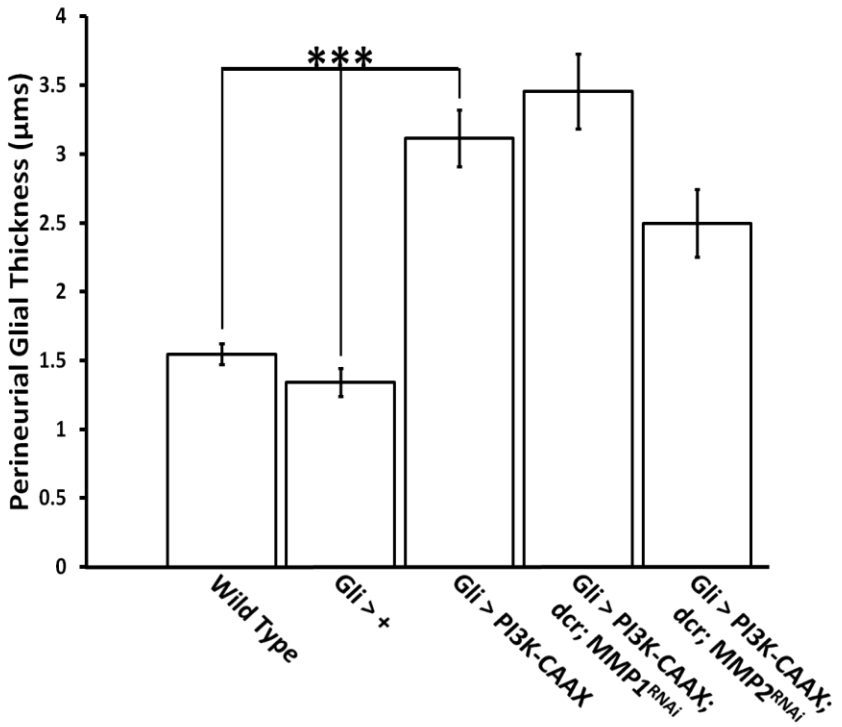

Figure 32: Inhibition of matrix metallopeptidases does not significantly decrease perineurial glial size induced by peripheral glial PI3K-CAAX expression. Simultaneous expression of a constitutively active PI3K and knockdown of MMP1 or MMP2 from the peripheral glia fails to significantly reduce size of the perineurial glia in comparison to expression of constitutively active PI3K alone. However, knockdown of MMP2 shows promise and may be significant with a slightly larger sample size. Measurements were obtained by subtracting the radius of the interior axon bundle from the radius of the total nerve. Bars and error bars are representative of averages and standard errors, respectively. Number of larvae assayed for each genotype = 4. Number of nerves measured for each genotype: Wild Type, N = 33; *Gli*>+, N = 25; *Gli>PI3K-CAAX*, N = 26; *Gli>PI3K-CAAX; dcr; MMP1*^{RNAi}, N = 32; *Gli>PI3K-CAAX; dcr; MMP2*^{RNAi}, P = 31. (Wild Type vs. *Gli>PI3K-CAAX*, P < 0.00001; *Gli*>+ vs. *Gli>PI3K-CAAX*, P < 0.00001).

Inhibition of *MMP2* in conjunction with *PI3K-CAAX* expression, while not significantly reduced from that of *Gli>PI3K-CAAX* alone, shows promise that MMP2 may be downstream of the peripheral glial Ras-PI3K-FOXO pathway. It is

possible that *MMP2* transcripts were not reduced enough to observe a stronger effect, but *MMP2* inhibition yields greater potential than the *MMP1*^{RNAi} construct. Knockdown of potential MMP2 targets may also be effective. Additionally, it is possible that metallopeptidases other than MMP2 are implicated in this growth process.

8.13: Conclusions & Future Work

This study further expands upon three primary discoveries made previously within the Stern lab. The first is that mutations which increase neuronal excitability also confer perineurial glial overgrowth (Yager et al., 2001). The second is that the neuronal DmGluRA-PI3K-FOXO pathway acts as a negative feedback loop to attenuate increased neurotransmitter release (Howlett et al., 2008), and the third is that peripheral glial PI3K activation similarly increases perineurial glial overgrowth (Lavery et al., 2007). Our data suggest that loss of Push, an E3 ubiquitin ligase, inhibits the motor neuronal DmGluRA-PI3K-FOXO pathway. This inhibition increases neurotransmitter release and subsequently increases perineurial glial size. The DmGluRA-PI3K-FOXO signaling pathway, when activated by glutamate binding to DmGluRA, acts as a homeostatic mechanism to decrease neurotransmitter release into the synaptic cleft. When loss of the neurotransmitter transporter Ine is coupled with loss of Push, inhibition of neuronal DmGluRA or PI3K, or overexpression of neuronal FOXO, neuronal excitability is increased and perineurial glial overgrowth occurs. This suggests that these manipulations increase the amount of glutamate

introduced into the synaptic cleft, which can no longer be cleared efficiently due to loss of Ine. Thus, the problem of too much synaptic glutamate is compounded and prolonged.

This excess glutamate in turn may activate DmGluRA and subsequently PI3K in neighboring peripheral glial cells. Activation of peripheral glial PI3K and its inhibition of FOXO is thought to release a growth factor or signaling molecule that influences the size of the adjacent perineurial glia. This is how nonautonomous signaling among the motor neurons, peripheral glia, and perineurial glia is thought to augment perineurial glial size. Identity of this growth factor or other signaling molecule between the peripheral and perineurial glia is yet unknown, and details concerning peripheral glial PI3K pathway activation also remain. While it is believed that *ine* mutations contribute to heightened excitability and the ensuing perineurial glial overgrowth via prolonged glutamate presence in the synapse, how Push may inhibit the neuronal DmGluRA-PI3K-FOXO pathway is currently unclear. Push, as a ubiquitin ligase, may target specific inhibitors of this pathway, and losing Push might confer a greater degree of inhibition on the neuronal DmGluRA-PI3K-FOXO pathway. Future work will focus primarily on identifying targets of neuronal Push and the nonautonomous signal which ultimately triggers growth of the perineurial glia.

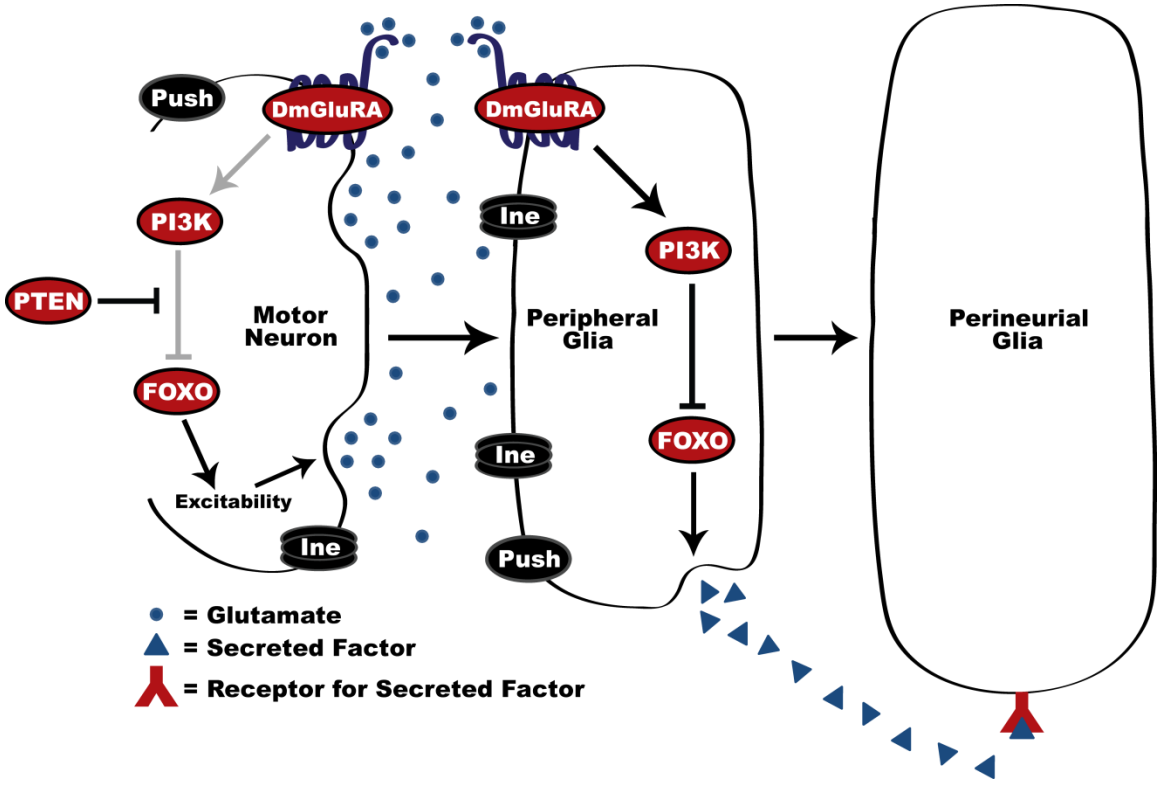

Figure 33: Hypothesized mechanism explaining how loss of neuronal excitability genes couples with inhibition of the neuronal DmGluRA-PI3K-FOXO pathway and activation of the peripheral glial DmGluRA-PI3K-FOXO pathway to cause perineurial glial overgrowth. The prolonged presence of excess glutamate within the synaptic cleft no longer activates presynaptic DmGluRA for neurotransmitter release attenuation due to some form of pathway inhibition. However, this excess glutamate may activate peripheral glial DmGluRA and subsequently cause release of a growth factor or other signaling molecule which stimulates growth of the perineurial glia. The darkened nature of Ine and Push in this scenario indicates their absence or inhibition. Transparent arrows indicate an interruption of the DmGluRA-PI3K signaling pathway.

9: References

Aberle, H., A.P. Haghighi, R.D. Fetter, B.D. McCabe, T.R. Magalhaes, and C.S. Goodman. 2002. wishful thinking encodes a BMP type II receptor that regulates synaptic growth in Drosophila. *Neuron*. 33:545-558.

Allison, R., J.H. Lumb, C. Fassier, J.W. Connell, D. Ten Martin, M.N. Seaman, J. Hazan, and E. Reid. 2013. An ESCRT-spastin interaction promotes fission of recycling tubules from the endosome. *J Cell Biol*. 202:527-543.

Aronson, D.E., L.M. Costantini, and E.L. Snapp. 2011. Superfolder GFP is fluorescent in oxidizing environments when targeted via the Sec translocon. *Traffic*. 12:543-548.

Auld, V. J., Fetter, R. D., Broadie, K., and Goodman, C. S. (1995). Gliotactin, a Novel Transmembrane Protein on Peripheral Gila, Is Required to Form the Blood-Nerve Barrier in Drosophila. Cell. 81:757-767.

Bakowska, J.C., H. Jupille, P. Fatheddin, R. Puertollano, and C. Blackstone. 2007. Troyer syndrome protein spartin is mono-ubiquitinated and functions in EGF receptor trafficking. *Mol Biol Cell*. 18:1683-1692.

Ballard, S.L., D.L. Miller, and B. Ganetzky. 2014. Retrograde neurotrophin signaling through Tollo regulates synaptic growth in Drosophila. *J Cell Biol*. 204:1157-1172.

Bernardoni, R., M. Kammerer, J-L. Vonesch, and A. Giangrande. 1999. Gliogenesis Depends on *glide/gcm* through Asymmetric Division of Neuroglioblasts. *Developmental Biology*. 216:265-275.

Berridge, M.J. 1998. Neuronal calcium signaling. Neuron *21*, 13–26.

Bian, X., Klemm, R. W., Liu, T. Y., Zhang, M., Sun, S., Sui, X., Liu, X., Rapoport T. A., and Hu, J. Structures of the atlastin GTPase provide insight into homotypic fusion of endoplasmic reticulum membranes. 2011. *Proc Natl Acad Sci U S A*. 108:3976-3981.

Bischof, J., R.K. Maeda, M. Hediger, F. Karch, and K. Basler. 2007. An optimized transgenesis system for Drosophila using germ-line-specific phiC31 integrases. *Proc Natl Acad Sci U S A*. 104:3312-3317.

Blackstone, C., C.J. O'Kane, and E. Reid. 2010. Hereditary spastic paraplegias: membrane traffic and the motor pathway. *Nat Rev Neurosci*. 1:31-42.

Bogdanik, L., R. Mohrmann, A. Ramaekers, J. Bockaert, Y. Grau, K. Broadie, and M.-L. Parmantier. 2004. The *Drosophila* Metabotropic Glutamate Receptor DmGluRA Regulates Activity-Dependent Synaptic Facilitation and Fine Synaptic Morphology. *The Journal of Neuroscience*. 24:9105-9116.

Bonni, A., Y. Sun, M. Nadal-Vicens, A. Bhatt, D.A. Frank, I. Rozovsky, N. Stahl, G.D. Yancopoulos, and M.E. Greenberg. 1997. Regulation of Gliogenesis in the Central Nervous System by the JAK-STAT Signaling Pathway. *Science*. 278:477-483.

Brew, K., D. Dinakarpandian, and H. Nagase. 2000. Tissue inhibitors of metalloproteinases: evolution, structure, and function. *Biochimica et Biophysica Acta*. 1477:267-283.

Campos, A. R., D.R. Rosen, S.N. Robinow, and K. White. 1987. Molecular analysis of the locus elav in *Drosophila* melanogaster: a gene whose embryonic expression is neural specific. *The EMBO Journal*. 6:425-431.

Carafoli, E., Santella, L., Branca, D., and Brini, M. 2001. Generation, control, and processing of cellular calcium signals. Crit. Rev. Biochem. Mol. Biol. *36*, 107–260.

Catterall, W.A. and A. P. Few. 2008. Calcium Channel Regulation and Presynaptic Plasticity. *Neuron*. 59:882–901.

Cens, T., M. Rousset, J.-P. Leyris, P. Fesquet, and P. Charnet. 2006. Voltage- and calcium-dependent inactivation in high voltage-gated Ca^{2+} channels. *Progress in Biophysics and Molecular Biology*. 90:104–117.

Chang, J., S. Lee, and C. Blackstone. 2013. Protrudin binds atlastins and endoplasmic reticulum-shaping proteins and regulates network formation. *Proc Natl Acad Sci U S A*. 110:14954-14959.

Chen, X., and B. Ganetzky. 2012. A neuropeptide signaling pathway regulates synaptic growth in Drosophila. *J Cell Biol*. 196:529-543.

Cichowski & Jacks. 2001. NF1 Tumor Suppressor Gene Function: Narrowing the GAP. *Cell*. 104:593-604.

Clapham, D. E. and E.J. Neer. 1993. New Roles for G-protein βγ-dimers in transmembrane signaling. *Nature*. 365:403-406.

Clapham, D.E. 2007. Calcium signaling. *Cell*. 131:1047–1058.

Cui, Y., R.M. Costa, G.G. Murphy, Y. Elgersma, Y. Zhu, D.H. Gutmann, L.F. Parada, L. Mody, and A.J. Silva. 2008. Neurofibromin Regulation of ERK Signaling Modulates GABA Release and Learning. *Cell*. 135:549-560.

Cully, M., H. You, A.J. Levine, and T.W. Mak. 2006. Beyond PTEN Mutations: the PI3K pathway as an integrator of multiple inputs during tumorigenesis. *Nature. Reviews*. 6:184-192.

Dermaut, B., K.K. Norga, A. Kania, P. Verstreken, H. Pan, Y. Zhou, P. Callaerts, and H.J. Bellen. 2005. Aberrant lysosomal carbohydrate storage accompanies endocytic defects and neurodegeneration in Drosophila benchwarmer. *J Cell Biol*. 170:127-139.

Di Sano, F., P. Bernardoni, and M. Piacentini. 2012. The reticulons: guardians of the structure and function of the endoplasmic reticulum. *Exp Cell Res*. 318:1201-1207.

Downward, J. 2004. PI 3-kinase, Akt and cell survival. *Seminars in Cell & Developmental Biology*. 15:177-182.

Duffy, J. B. 2002. GAL4 System in *Drosophila*: A Fly Geneticist's Swiss Army Knife. *Genesis*. 34:1-15.

Dunlap, K., J. I. Luebke, and T. J. Turner. 1995. Exocytotic Ca^{2+} channels in mammalian central neurons. *Trends in Neurosciences*. 18:89–98.

Edwards, T.L., V.E. Clowes, H.T. Tsang, J.W. Connell, C.M. Sanderson, J.P. Luzio, and E. Reid. 2009. Endogenous spartin (SPG20) is recruited to endosomes and lipid droplets and interacts with the ubiquitin E3 ligases AIP4 and AIP5. *Biochem J*. 423:31-39.

Edwards, J. S., L.S. Swales, and M. Bate. 1993. The Differentiation Between Neuroglia and Connective Tissue Sheath in Insect Ganglia Revisited: The Neural Lamella and Perineurial Sheath Cells are Absent in a Mesodermless Mutant of *Drosophila*. *The Journal of comparative Neurology*. 333:301-308.

Elbaz, Y., and M. Schuldiner. 2011. Staying in touch: the molecular era of organelle contact sites. *Trends Biochem Sci*. 36:616-623.

Emptage, N.J., C.A. Reid, and A. Fine. 2001. Calcium stores in hippocampal synaptic boutons mediate short-term plasticity, store-operated Ca^{2+} entry, and spontaneous transmitter release. *Neuron*. 29:197-208.

English, A.R., and G.K. Voeltz. 2013. Endoplasmic reticulum structure and interconnections with other organelles. *Cold Spring Harb Perspect Biol*. 5:a013227.

Evans, K., C. Keller, K. Pavur, K. Glasgow, B. Conn, and B. Lauring. 2006. Interaction of two hereditary spastic paraplegia gene products, spastin and atlastin, suggests a common pathway for axonal maintenance. *Proc Natl Acad Sci U S A*. 103:10666-10671.

Fan, R. S., R.O. Jácamo, X. Jiang, J. Sinnett-Smith, and E. Rozengurt. 2005. G Protein-coupled Receptor Activation Rapidly Stimulates Focal Adhesion Kinase Phosphorylation at Ser 843: Mediation by Ca+, Calmodulin, and Ca^{2+}/Calmodulin-Dependent Kinase II. *The Journal of Biological Chemistry*. 280:24212-24220.

Farmbrough, D., D. Pan, G.M. Rubin, and C.S. Goodman. 1996. The cell surface metalloproteinase/disintegrin Kuzbanian is required for axonal extension in Drosophila. *Proceedings of the National Academy of Sciences*. 93:13233-13238.

Fassier, C., J.A. Hutt, S. Scholpp, A. Lumsden, B. Giros, F. Nothias, S. Schneider-Maunoury, C. Houart, and J. Hazan. 2010. Zebrafish atlastin controls motility and spinal motor axon architecture via inhibition of the BMP pathway. *Nat Neurosci*. 13:1380-1387.

Faust, J.E., Desai, T., A. Verma, I. Ulengin, T.-L. Sun, T. J. Moss, M. A. Betancourt, H. W. Huang, T. Lee, and J. A. McNew. 2015. The Atlastin C-terminal Tail is an Amphipathic Helix that Perturbs Bilayer Structure during Endoplasmic Reticulum Homotypic Fusion. *J. Biol. Chem*. jbc.M114.601823.

Feig, L. A. and G.M. Cooper. 1988. Inhibition of NIH 3T3 Cell Proliferation by a Mutant *ras* Protein with Preferential Affinity for GDP. *Molecular and Cellular Biology*. 8:3235-3243.

Fernandez-Busnadiego, R., Y. Saheki, and P. De Camilli. 2015. Three-dimensional architecture of extended synaptotagmin-mediated endoplasmic reticulum-plasma membrane contact sites. *Proc Natl Acad Sci U S A*. 112:E2004-2013.

Fleischer, S. 2008. Personal recollections on the discovery of the ryanodine receptors of muscle. *Biochemical and Biophysical Research Communications*. 369:195–207.

Fox, G. L., Rebay, I., and Hynes, R. O. 1999. Expression of DFak56, a *Drosophila* homolog of vertebrate focal adhesion kinase, supports a role in cell migration in vivo. *Proceedings of the National Academy of Sciences*. 96:14978-14983.

Friedman, J.R., L.L. Lackner, M. West, J.R. DiBenedetto, J. Nunnari, and G.K. Voeltz. 2011. ER tubules mark sites of mitochondrial division. *Science*. 334:358-362.

Fuentes-Medel, Y., J. Ashley, R. Barria, R. Maloney, M. Freeman, and V. Budnik. 2012. Integration of a retrograde signal during synapse formation by glia-secreted TGF-beta ligand. *Curr Biol*. 22:1831-1838.

Ganetzky, B. and C.-F. Wu. 1983. Neurogenetic Analysis of Potassium Currents in *Drosophila*: Synergistic Effects on Neuromuscular Transmission in Double Mutants. *The Journal of Neurogenetics*. 1:17-28.

Giordano, F., Y. Saheki, O. Idevall-Hagren, S.F. Colombo, M. Pirruccello, I. Milosevic, E.O. Gracheva, S.N. Bagriantsev, N. Borgese, and P. De Camilli. 2013. PI(4,5)P(2)-dependent and Ca(2+)-regulated ER-PM interactions mediated by the extended synaptotagmins. *Cell*. 153:1494-1509.

Gomez-Sanchez, J. A., M.L. de Armentia, R. Lujan, N. Kessaris, W.D. Richardson, and H. Cabedo. 2009. Sustained Axon–Glial Signaling Induces Schwann Cell Hyperproliferation, Remak Bundle Myelination, and Tumorigenesis. *The Journal of Neuroscience*. 29:11304-11315.

Grabbe, C., C.G. Zervas, T. Hunter, N.H. Brown, and R.H. Palmer. 2004. Focal adhesion kinase is not required for integrin function or viability in *Drosophila*. *Development*. 131:5795-5805.

Gray, A., J. Van Der Kaay, and C.P. Downes. 1999. The pleckstrin homology domains of protein kinase B and GRP1 (general receptor for phosphoinositides-1) are sensitive and selective probes for the cellular detection of phosphatidylinositol 3,4-bisphosphate and/or phosphatidylinositol 3,4,5-trisphosphate *in vivo*. *The Biochemical Journal*. 344:929-936.

Griffith, L. C., L.M. Verselis, K.M. Aitken, C.P. Kyriacou, W. Danho, and R.J. Greesnpan. 1993. Inhibition of Calcium/Calmodulin-Dependent Protein Kinase in Drosophila Disrupts Behavioral Plasticity. *Neuron*. 10:501-509.

Grigoriev, I., Gouveia, S. M., van der Vaart, B., Demmers, J., Smtyh, J. T., Honnappa, S., Splinter, D., Steinmetz, M. O., Putney Jr., J. W., Hoogenraad, C. C., and A. Akhmanova. 2008. STIM1 Is a MT-Plus-End-Tracking Protein Involved in Remodeling of the ER. *Current Biology*. 18:177-182.

Gurkoff, G., K. Shahlaie, B. Lyeth, and R. Berman. 2013. Voltage-gated calcium channel antagonists and traumatic brain injury. *Pharmaceuticals (Basel)*. 6:788–812.

He W., Q. Shi, X. Hu, and R. Yan. 2007. The membrane topology of RTN3 and its effect on binding of RTN3 to BACE1. *J Biol Chem*. 282:29144-29151.

He, X., F. Yang, Z. Xie, B. and Lu. 2000. Intracellular Ca^{2+} and Ca^{2+}/calmodulin-dependent kinase II mediate acute potentiation of neurotransmitter release by neurotrophin-3. *J. Cell Biol*. 149:783–792.

Helle, S.C., G. Kanfer, K. Kolar, A. Lang, A.H. Michel, and B. Kornmann. 2013. Organization and function of membrane contact sites. *Biochim Biophys Acta*. 1833:2526-2541.

Howlett, E., C. C-J. Lin, W. Lavery, and M. Stern. 2008. A PI3-Kinase–Mediated Negative Feedback Regulates Neuronal Excitability. *PLoS Genetics*. 4:1-12.

Hu, J., W.A. Prinz, and T.A. Rapoport. 2011. Weaving the Web of ER Tubules. *Cell*. 147:1226-1231.

Hu, J., Y. Shibata, C. Voss, T. Shemesh, Z. Li, M. Coughlin, M.M. Kozlov, T.A. Rapoport, and W.A. Prinz. 2008. Membrane proteins of the endoplasmic reticulum induce high-curvature tubules. *Science*. 319:1247-1250.

Hu, J., Y. Shibata, P.P. Zhu, C. Voss, N. Rismanchi, W.A. Prinz, T.A. Rapoport, and C. Blackstone. 2009. A class of dynamin-like GTPases involved in the generation of the tubular ER network. *Cell*. 138:549-561.

Huang, Y., and M. Stern. 2002. In vivo properties of the Drosophila inebriated-encoded neurotransmitter transporter. *J Neurosci*. 22:1698-1708.

Jahn, T.R., K.J. Kohlhoff, M. Scott, G.G. Tartaglia, D.A. Lomas, C.M. Dobson, M. Vendruscolo, and D.C. Crowther. 2011. Detection of early locomotor abnormalities in a Drosophila model of Alzheimer's disease. *J Neurosci Methods*. 197:186-189.

Jan, L.Y., and Y.N. Jan. 1976. Properties of the larval neuromuscular junction in Drosophila melanogaster. *J Physiol*. 262:189-214.

Jaskiewicz & Filipowicz. 2008. Role of Dicer in Posttrancriptional RNA Silencing. *Current Topics in Microbiology and Immunology*. 320:77-97.

Jeong, S-W and S.R. Ikeda. 1999. Sequestration of G-Protein βγ Subunits by Different G-Protein a Subunits Blocks Voltage-Dependent Modulation of Ca^{2+} Channels in Rat Sympathetic Neurons. *The Journal of Neuroscience*. 19:4755-4761.

Johannessen, C. M., E.E. Reczek, M.F. James, H. Brems, E. Legius, and K. Cichowski. 2005. The NF1 tumor suppressor critically regulates TSC2 and mTOR. *Proceedings of the National Academy of Sciences*. 102:8573-8578.

Johnson, A.E., H. Shu, A.G. Hauswirth, A. Tong, and G.W. Davis. 2015. VCP-dependent muscle degeneration is linked to defects in a dynamic tubular lysosomal network in vivo. *Elife*. 4.

Jones, B. W. 2005. Transcriptional control of glial cell development in *Drosophila*. *Developmental Biology*. 278:265-273.

Jousset, H., M. Frieden, and N. Demaurex. 2007. STIM1 knockdown reveals that store-operated Ca^{2+} channels located close to SERCA pumps silently refill the endoplasmic reticulum. *Journal of Biological Chemistry*. 282:1-22.

Jozsef, L., K. Tashiro, A. Kuo, E.J. Park, A. Skoura, S. Albinsson, F. Rivera-Molina, K.D. Harrison, Y. Iwakiri, D. Toomre, and W.C. Sessa. 2014. Reticulon 4 is necessary for endoplasmic reticulum tubulation, STIM1-Orai1 coupling, and store-operated calcium entry. *J Biol Chem*. 289:9380-9395.

Jünger, M. A., F. Rintelen, H. Stocker, J.D. Wasserman, M. Végh, T. Radimerski, M.E. Greenberg, and E. Hafen. 2003. The *Drosophila* Forkhead transcription factor FOXO mediates the reduction in cell number associated with reduced insulin signaling. *Journal of Biology*. 2:20.1-20.17.

Karim, F. D. and G.M. Rubin. 1998. Ectopic expression of activated Ras1 induces hyperplastic growth and increased cell death in Drosophila imaginal tissues. *Development*. 125:1-9.

Kawasaki, F., B. Zou, X. Xu, and R.W. Ordway. 2004. Active zone localization of presynaptic calcium channels encoded by the cacophony locus of Drosophila. *J. Neurosci*. 24:282–285.

Kerr, K.S., Y. Fuentes-Medel, C. Brewer, R. Barria, J. Ashley, K.C. Abruzzi, A. Sheehan, O.E. Tasdemir-Yilmaz, M.R. Freeman, and V. Budnik. 2014. Glial wingless/Wnt regulates glutamate receptor clustering and synaptic physiology at the Drosophila neuromuscular junction. *J Neurosci*. 34:2910-2920.

Kohlhoff, K.J., T.R. Jahn, D.A. Lomas, C.M. Dobson, D.C. Crowther, and M. Vendruscolo. 2011. The iFly tracking system for an automated locomotor and behavioural analysis of Drosophila melanogaster. *Integrative biology : quantitative biosciences from nano to macro*. 3:755-760.

Lang, A., A.T. John Peter, and B. Kornmann. 2015. ER-mitochondria contact sites in yeast: beyond the myths of ERMES. *Curr Opin Cell Biol*. 35:7-12.

Lanner, J.T., D.K. Georgiou, A.D. Joshi, and S.L. Hamilton. 2010. Ryanodine receptors: structure, expression, molecular details, and function in calcium release. *Cold Spring Harb. Perspect. Biol*. 2:a003996.

Lavery, W., V. Hall, J.C. Yager, A. Rottgers, M.C. Wells, M. and Stern. 2007. Phosphatidylinositol 3-Kinase and Akt Nonautonomously Promote Perineurial Glial Growth in *Drosophila* Peripheral Nerves. *The Journal of Neuroscience*. 27:279-288.

Lee, Y., D. Paik, S. Bang, J. Kang, B. Chun, S. Lee, E. Bae, J. Chung, and J. Kim. 2008. Loss of spastic paraplegia gene atlastin induces age-dependent death of dopaminergic neurons in Drosophila. *Neurobiol Aging*. 29:84-94.

Lee, M., S.K. Paik, M.J. Lee, Y.J. Kim, S. Kim, M. Nahm, S.J. Oh, H.M. Kim, J. Yim, C.J. Lee, Y.C. Bae, and S. Lee. 2009. Drosophila Atlastin regulates the stability of muscle microtubules and is required for synapse development. *Dev Biol*. 330:250-262.

Lee, J., A. Ueda, and C.-F. Wu. 2014. Distinct roles of Drosophila cacophony and Dmca1D Ca^{2+} channels in synaptic homeostasis: genetic interactions with slowpoke Ca^{2+} -activated BK channels in presynaptic excitability and postsynaptic response. *Dev. Neurobiol*. 74:1–15.

Leiserson, W. M., Harkins, E. W., and Keshishian, H. 2000. Fray, a *Drosophila* Serine/Threonine Kinase Homologous to Mammalian PASK, Is Required for Axonal Ensheathment. *Neuron*. 28:793-806.

Letsou, A., Arora, K., Wrana, J. L., Simin, K., Twombly, V., Jamal, J., Staehling-Hampton, K., Hoffmann, F. M., Gelbart, W. M., Massagué, and M. B. O'Connor. Cell. 80:899-908.

Liang, Y., L.L. Yuan, D. Johnston, and R. Gray. 2002. Calcium signaling at single mossy fiber presynaptic terminals in the rat hippocampus. *Journal of neurophysiology*. 87:1132-1137.

Lin, C-J., J. Summerville, E. Howlett, and M. Stern. 2011. CaMKII and DFak as critical intermediates in metabotropic glutamate receptor-mediated activation of PI3K. *Genetics*. 188:601-613.

Liou, J., M.L. Kim, W.D. Heo, J.T. Jones, J.W. Myers, J.E. Ferrell, and T. Meyer. 2005. STIM is a Ca^{2+} sensor essential for Ca^{2+}-store-depletion-triggered Ca^{2+} influx. *Current Biology*. 15:1235-1241.

Llano, E., G. Adam, A.M. Pendás, V. Quesada, L.M. Sánchez, I. Santamaria, S. Noselli, and C. López-Otín. 2002. Structural and Enzymatic Characterization of *Drosophila* Dm2-MMP, a Membrane-bound Matrix Metalloproteinase with Tissue-specific Expression. *The Journal of Biological Chemistry*. 277:23321-23329.

Llano, I., J. Gonzalez, C. Caputo, F.A. Lai, L.M. Blayney, Y.P. Tan, and A. Marty. 2000. Presynaptic calcium stores underlie large-amplitude miniature IPSCs and spontaneous calcium transients. *Nat Neurosci*. 3:1256-1265.

Llano, E., A.M. Pendás, P. Aza-Blanc, T.B. Kornberg, and C. López-Otín. 2000. *Dm1-* MMP, a Matrix Metalloproteinase from *Drosophila* with a Potential Role in Extracellular Matrix Remodeling during Neural Development. *The Journal of Biological Chemistry*. 275:35978-35985.

Lo Giudice, T., F. Lombardi, F.M. Santorelli, T. Kawarai, and A. Orlacchio. 2014. Hereditary spastic paraplegia: clinical-genetic characteristics and evolving molecular mechanisms. *Exp Neurol*. 261:518-539.

Ma, W., S. Mishra, K. Gee, J.P. Mishra, D. Nanden, N.E. Reiner, J.B. Angel, and A. Kumar. 2007. Cyclosporin A and FK506 Inhibit IL-12p40 Production through the /Calmodulin-dependent Protein Kinase-activated Phosphoinositide 3-Kinase in Lipopolysaccharide-stimulated Human Monocytic Cells. *The Journal of Biological Chemistry*. 18:13351-13362.

Ma, S., Y. Yang, C. Wang, N. Hui, L. Gu, H. Zhong, Z. Cai, Q. Wang, Q. Zhang, N. Li, and X. Cao. 2009. Endogenous Human CaMKII Inhibitory Protein Suppresses Tumor Growth by Inducing Cell Cycle Arrest and Apoptosis through Down-regulation of the Phosphatidylinositide 3-Kinase/Akt/HDM2 Pathway. *The Journal of Biological Chemistry*. 284:24773-24782 .

Macleod, G.T., M. Hegstrom-Wojtowicz, M.P. Charlton, and H.L. Atwood. 2002. Fast calcium signals in Drosophila motor neuron terminals. *Journal of neurophysiology*. 88:2659-2663.

Manjarrés, I.M., A. Rodriguez-Garcia, M.T. Alonso, and J. Garcia-Sancho. 2010. The sarco/endoplasmic reticulum Ca^{2+} ATPase (SERCA) is the third element in capacitative calcium entry. *Cell Calcium*. 5:412-418.

Marsh, J. L. and Thompson, L. M. 2004. Can flies help humans treat neurodegenerative diseases? *BioEssays*. 26:485-496.

Martin, A.R. 1955. A further study of the statistical composition on the end-plate potential. *J Physiol*. 130:114-122.

Martin, G. A., Viskochil, D., Bollag, G., McCabe, P. C., Crosler, W. J., Haubruck, H., Conroy, L., Clark, R., O'Connell, P., Cawthon, R. M., Innis, M. A., and McCormick, F. 1990. The GAP-Related Domain of the Neurofibromatosis Type 1 Gene Product Interacts with ras p21. *Cell*. 63:843-849.

McCabe, B.D., G. Marques, A.P. Haghighi, R.D. Fetter, M.L. Crotty, T.E. Haerry, C.S. Goodman, and M.B. O'Connor. 2003. The BMP homolog Gbb provides a retrograde signal that regulates synaptic growth at the Drosophila neuromuscular junction. *Neuron*. 39:241-254.

McNew, J.A., H. Sondermann, T. Lee, M. Stern, and F. Brandizzi. 2013. GTP-dependent membrane fusion. *Annu Rev Cell Dev Biol*. 29:529-550.

Melzer, W., A. Herrmann-Frank, and H.C. Lüttgau. 1995. The role of Ca^{2+} ions in excitation-contraction coupling of skeletal muscle fibres. *Biochim. Biophys. Acta*. 1241:59–116.

Meyer, F. and Aberle, H. 2006. At the next stop turn right: the metalloprotease Tolloid-related 1 controls defasciculation of motor axons in *Drosophila*. *Development*. 133:4035-4044.

Michel, A.H., and B. Kornmann. 2012. The ERMES complex and ER-mitochondria connections. *Biochem Soc Trans*. 40:445-450.

Mikoshiba, K. 2007. IP3 receptor/Ca2+ channel: from discovery to new signaling concepts. *Journal of Neurochemistry*. 102:1426-1446.

Miller, C. M., Page-McCaw, A., and Broihier, H. T. 2008. Matrix metalloproteinases promote motor axon fasciculation the *Drosophila* embryo. *Development*. 135:95-109.

Miyazono, K., Y. Kamiya, and M. Morikawa. 2010. Bone morphogenetic protein receptors and signal transduction. *J Biochem*. 147:35-51.

Möller, C., J. Alfredsson, M. Engström, H. Wootz, Z. Xiang, J. Lennartsson, J-I. Jönsson, and G. Nilsson. 2005. Stem cell factor promotes mast cell survival via inactivation of FOXO3a-mediated transcriptional induction and MEK-regulated phosphorylation of the pro-apoptotic protein Bim. *Blood*. 106:1330-1336.

Montenegro G., A.P. Rebelo, J. Connell, R. Allison, C. Babalini, M. D'Aloia, P. Montieri, R. Schüle, H. Ishiura, J. Price, A. Strickland, M.A. Gonzalez, L. Baumbach-Reardon, T. Deconinck, J. Huang, G. Bernardi, J.M. Vance, M.T. Rogers, S. Tsuji, P. De Jonghe, M.A. Pericak-Vance, L. Schöls, A. Orlacchio, E. Reid, and S. Züchner. 2012. Mutations in the ER-shaping protein reticulon 2 cause the axon-degenerative disorder hereditary spastic paraplegia type 12. *Journal of Clinical Investigation*. 122:538-544.

Mothet, J.P., P. Fossier, F.M. Meunier, J. Stinnakre, L. Tauc, and G. Baux. 1998. Cyclic ADP-ribose and calcium-induced calcium release regulate neurotransmitter release at a cholinergic synapse of Aplysia. *J. Physiol. (Lond.)* 507 (Pt 2):405–414.

Moss, T.J., A. Daga, and J.A. McNew. 2011. Fusing a lasting relationship between ER tubules. *Trends Cell Biol*. 21:416-423.

Moss, T.J., C. Andreazza, A. Verma, A. Daga, and J.A. McNew. 2011. Membrane fusion by the GTPase atlastin requires a conserved C-terminal cytoplasmic tail and dimerization through the middle domain. *Proc Natl Acad Sci U S A*. 108:11133-11138.

Mouton, J., I. Marty, M. Villaz, A. Feltz, and Y. Maulet. 2001. Molecular interaction of dihydropyridine receptors with type-1 ryanodine receptors in rat brain. *Biochem. J*. 354:597–603.

Nahm, M., M.J. Lee, W. Parkinson, M. Lee, H. Kim, Y.J. Kim, S. Kim, Y.S. Cho, B.M. Min, Y.C. Bae, K. Broadie, and S. Lee. 2013. Spartin regulates synaptic growth and neuronal survival by inhibiting BMP-mediated microtubule stabilization. *Neuron*. 77:680-695.

Neuser, K., Husse, J., Stock, P. and Gerber, B. 2005. Appetitive olfactory learning in *Drosophila* larvae: effects of repetition, reward strength, age, gender, assay type and memory span. *Animal Behaviour*. 69:891-898.

Noreau, A., P.A. Dion, and G.A. Rouleau. 2014. Molecular aspects of hereditary spastic paraplegia. *Exp Cell Res*. 325:18-26.

O'Connor-Giles, K.M., L.L. Ho, and B. Ganetzky. 2008. Nervous wreck interacts with thickveins and the endocytic machinery to attenuate retrograde BMP signaling during synaptic growth. *Neuron*. 58:507-518.

Ogden, S. K., Fei, D. L., Schilling, N. S., Ahmed, Y. F., Hwa, J., and Robbins, D. J. 2008. G protein Gαi functions immediately downstream of Smoothened in Hedgehog signaling. *Nature*. 456:967-971.

Orme, M. H., S. Alrubaie, G.L. Bradley, C.D. Walker, and S.J. Leevers. 2006. Input from Ras is required for maximal PI(3)K signalling in *Drosophila*. *Nature Cell Biology*. 8:1298-1302.

Orso, G., D. Pendin, S. Liu, J. Tosetto, T.J. Moss, J.E. Faust, M. Micaroni, A. Egorova, A. Martinuzzi, J.A. McNew, and A. Daga. 2009. Homotypic fusion of ER membranes requires the dynamin-like GTPase Atlastin. *Nature*. 460:978-983.

O'Sullivan, N.C., T.R. Jahn, E. Reid, and C.J. O'Kane. 2012. Reticulon-like-1, the Drosophila orthologue of the Hereditary Spastic Paraplegia gene reticulon 2, is required for organization of endoplasmic reticulum and of distal motor axons. *Hum Mol Genet*. 21:3356-3365.

Ozdowski, E.F., S. Gayle, H. Bao, B. Zhang, and N.T. Sherwood. 2011. Loss of Drosophila melanogaster p21-activated kinase 3 suppresses defects in synapse structure and function caused by spastin mutations. *Genetics*. 189:123-135.

Park, D., M.J. Coleman, J.J.L. Hodge, V. Budnik, and L.C. Griffith. 2002. Regulation of Neuronal Excitability in Drosophila by Constitutively Active CaMKII. *Journal of Neurobiology*. 52:24-42.

Park, S.H., P.-P. Zhu, R. L. Parker, and C. Blackstone. 2010. Hereditary spastic paraplegia proteins REEP1, spastin, and atlastin-1 coordinate microtubule interactions with the tubular ER network. *Journal of Clinical Investigation*. 120:1097–1110.

Parkes, T. L., Elia, A. J., Dickinson, D., Hilliker, A. J., Phillips, J. P., and Boulianne, G. L. 1998. Extension of *Drosophila* lifespan by overexpression of human *SOD1* in motorneurons. *Nature Genetics*. 19:171-174.

Parrinello, S., Noon, L. A., Harrisingh, M. C., Digby, P. W., Rosenberg, L. H., Cremona, C. A., Echave, P., Flanagan, A. M., Parada, L. F., and Lloyd, A. C. 2008. NF1 loss disrupts Schwann cell–axonal interactions: a novel role for semaphorin 4F. *Genes & Development*. 22:3335-3348.

Pendin, D., J.A. McNew, and A. Daga. 2011. Balancing ER dynamics: shaping, bending, severing, and mending membranes. *Curr Opin Cell Biol*. 23:435-442.

Pendin, D., J. Tosetto, T.J. Moss, C. Andreazza, S. Moro, J.A. McNew, and A. Daga. GTP-dependent packing of a three-helix bundle is required for atlastin-mediated fusion. 2011. *Proceedings of the National Academy of Sciences*. 108:16283-16288.

Peng, I.-F., and C.-F. Wu. 2007. Drosophila cacophony Channels: A Major Mediator of Neuronal Ca2+ Currents and a Trigger for K^+ Channel Homeostatic Regulation. *J. Neurosci*. 27:1072–1081.

Pfrieger, F. W. and Barres, B. A. 1997. Synaptic Efficacy Enhanced by Glial Cells in Vitro. *Science*. 277:1684-1687.

Raiborg, C., E.M. Wenzel, N.M. Pedersen, H. Olsvik, K.O. Schink, S.W. Schultz, M. Vietri, V. Nisi, C. Bucci, A. Brech, T. Johansen, and H. Stenmark. 2015a. Repeated ER-endosome contacts promote endosome translocation and neurite outgrowth. *Nature*. 520:234-238.

Raiborg, C., E.M. Wenzel, and H. Stenmark. 2015b. ER-endosome contact sites: molecular compositions and functions. *EMBO J*. 34:1848-1858.

Reid, E. (2003). Science in motion: common molecular pathological themes emerge in the hereditary spastic paraplegias. *The Journal of Medical Genetics*. 40:81-86.

Reiske, H.R., S-C. Kao, L.A. Cary, J-L. Guan, J-F. Lai, and H-C. Chen. 1999. Requirement of Phosphatidylinositol 3-Kinase in Focal Adhesion Kinase-promoted Cell Migration. The Journal of Biological Chemistry. 274:12361-12366.

Reiter, L. T., Potocki, L., Chien, S., Gribskov, M., and Bier, E. 2001. A Systematic Analysis of Human Disease-Associated Gene Sequences In *Drosophila melanogaster. Genome Research*. 11:1114-1125.

Riccardi, V. M. 2007. The genetic predisposition to and histogenesis of neurofibromas and neurofibrosarcoma in neurofibromatosis Type 1. *Neurosurgical Focus*. 22(6): E3 1-11.

Richards, S., T. Hillman, M. and Stern. 1996. Mutations in the *Drosophila pushover* Gene Confer Increased Neuronal Excitability and Spontaneous Synaptic Vesicle Fusion. *Genetics*. 142:1215-1223.

Rismanchi N, C. Soderblom, J.Stadler, P.P. Zhu, and C.Blackstone. 2008. Atlastin GTPases are required for Golgi apparatus and ER morphogenesis. *Hum. Mol. Genet*. 17:1591-1604.

Robinow, S. and K. White. 1991. Characterization and spatial distribution of the ELAV protein during *Drosophila melanogaster* development. *Journal of Neurobiology*. 22:443-461.

Rowland, A.A., P.J. Chitwood, M.J. Phillips, and G.K. Voeltz. 2014. ER contact sites define the position and timing of endosome fission. *Cell*. 159:1027-1041.

Rowland, A.A., and G.K. Voeltz. 2012. Endoplasmic reticulum-mitochondria contacts: function of the junction. *Nat Rev Mol Cell Biol*. 13:607-625.

Sanderson, C.M., J.W. Connell, T.L. Edwards, N.A. Bright, S. Duley, A. Thompson, J.P. Luzio, and E. Reid. 2006. Spastin and atlastin, two proteins mutated in autosomal-dominant hereditary spastic paraplegia, are binding partners. *Hum. Mol. Genet*. 15:307-318.

Sanyal, S., C. Consoulas, H. Kuromi, A. Basole, L. Mukai, Y. Kidokoro, K.S. Krishnan, and M. Ramaswami. 2005. Analysis of conditional paralytic mutants in Drosophila sarco-endoplasmic reticulum calcium ATPase reveals novel mechanisms for regulating membrane excitability. *Genetics*. 169:737-750.

Sauvageot, C. M. and C.D. Stiles. 2002. Molecular mechanisms controlling cortical gliogenesis. *Current Opinion in Neurobiology*. 12:244-249.

Scarano, V., P. Mancini, C. Criscuolo, G. De Michele, C. Rinaldi, T. Tucci, A. Tessa, F.M. Santorelli, A. Perretti, L. Santoro, and A. Filla. 2005. The R495W mutation in SPG3A causes spastic paraplegia associated with axonal neuropathy. *J. Neurol*. 252:901-903.

Schauder, C.M., X. Wu, Y. Saheki, P. Narayanaswamy, F. Torta, M.R. Wenk, P. De Camilli, and K.M. Reinisch. 2014. Structure of a lipid-bound extended synaptotagmin indicates a role in lipid transfer. *Nature*. 510:552-555.

Schmidt, I., S. Thomas, P. Kain, B. Risse, E. Naffin, and C. Klambt. 2012. Kinesin heavy chain function in Drosophila glial cells controls neuronal activity. *J Neurosci*. 32:7466-7476.

Sepp, K.J., and V.J. Auld. 1999. Conversion of lacZ enhancer trap lines to GAL4 lines using targeted transposition in Drosophila melanogaster. *Genetics*. 151:1093-1101.

Serra, E., Rosenbaum, T., Winner, U., Aledo, R., Ars, E., Estivill, X., Lenard, H-G., and Lázaro, C. 2000. Schwann cells harbor the somatic *NF1* mutation in neurofibromas: evidence of two different Schwann cell subpopulations. *Human Molecular Genetics*. 20:3055-3064.

Shakiryanova, D., Klose, M. K., Zhou, Y., Gu, T., Deitcher, D. L., Atwood, H. L., Hewes, R. S., and Levitan, E. S. 2007. Presynaptic Ryanodine Receptor-Activated Calmodulin Kinase II Increases Vesicle Mobility and Potentiates Neuropeptide Release. *The Journal of Neuroscience*. 27:7799-7806.

Sherwood, N.T., Q. Sun, M. Xue, B. Zhang, and K. Zinn. 2004. Drosophila spastin regulates synaptic microtubule networks and is required for normal motor function. *PLoS Biol*. 2:e429.

Shibata, Y., J. Hu, M.M. Kozlov, and T.A. Rapoport. 2009. Mechanisms shaping the membranes of cellular organelles. *Annu Rev Cell Dev Biol*. 25:329-354.

Shibata, Y., G.K. Voeltz, and T.A. Rapoport. 2006. Rough sheets and smooth tubules. *Cell*. 126:435-439.

Shibata, Y., C. Voss, J.M. Rist, J. Hu, T.A. Rapoport, W.A. Prinz, and G.K. Voeltz. 2008. The reticulon and DP1/Yop1p proteins form immobile oligomers in the tubular endoplasmic reticulum. *J Biol Chem*. 283:18892–18904.

Smith, R.B., J.B. Machamer, N.C. Kim, T.S. Hays, and G. Marqués. 2012. Relay of retrograde synaptogenic signals through axonal transport of BMP receptors. *J of Cell Science*. 125:3752-3764.

Soboloff, J., B.S. Rothberg, M. Madesh, and D.L. Gill. 2012. STIM proteins: dynamic calcium signal transducers. *Nat Rev Mol Cell Biol*. 13:549-565.

Soehnge, H., Huang, X., Becker, M., Whitley, P., and Conover, D., and Stern, M. 1996. A neurotransmitter transporter encoded by the *Drosophila* inebriated gene. *Proceedings of the National Academy of Sciences*. 93:13262-13267.

Sonoda, Y., Watanabe, S., Matsumoto, Y., Aizu-Yokota, E., and Kasahara, T. 1999. FAK Is the Upstream Signal Protein of the Phosphatidylinositol 3-Kinase-Akt Survival Pathway in Hydrogen Peroxide-induced Apoptosis of a Human Glioblastoma Cell Line. *The Journal of Biological Chemistry*. 274:10566-10570.

Stefan, C.J., A.G. Manford, and S.D. Emr. 2013. ER-PM connections: sites of information transfer and inter-organelle communication. *Curr Opin Cell Biol*. 25:434-442.

Stern, M. and B. Ganetzky. 1992. Identification and Characterization of Inebriated, a Gene Affecting Neuronal Excitability in *Drosophila*. *Journal of Neurogenetics*. 8:157-172.

Stewart, B.A., H.L. Atwood, J.J. Renger, J. Wang, and C.F. Wu. 1994. Improved stability of Drosophila larval neuromuscular preparations in haemolymph-like physiological solutions. *Journal of comparative physiology. A, Sensory, neural, and behavioral physiology*. 175:179-191.

Stork, T., D. Engelen, A. Krudewig, M. Silies, R.J. Bainton, and C. Klämbt. 2008. Organization and Function of the Blood–Brain Barrier in *Drosophila*. *The Journal of Neuroscience*. 28:587-597.

Sweeney, S.T., and G.W. Davis. 2002. Unrestricted synaptic growth in spinster-a late endosomal protein implicated in TGF-beta-mediated synaptic growth regulation. *Neuron*. 36:403-416.

Tasaki, T., L.C.F. Mulder, A. Iwamatsu, M.J. Lee, I.V. Davydov, A. Varhavsky, M. Muesing, and Y.T. Kwon. 2005. A Family of Mammalian E3 Ubiquitin Ligases That Contain the UBR Box Motif and Recognize N-Degrons. *Molecular and Cellular Biology*. 25:7120-7136.

Taveggia, C., Zanazzi, G., Petrylak, A., Yano, H., Rosenbluth, J., Einheber, S., Xu, X., Esper, R. M., Loeb, J. A., Shrager, P., Chao, M. V., Falls, D. L., Role, L., and J. L. Salzer. 2005. Neurgegulin-1 Type III Determines the Ensheathment Fate of Axons. *Neuron*. 47:681-694.

Terasaki, M., T. Shemesh, N. Kasthuri, R.W. Klemm, R. Schalek, K.J. Hayworth, A.R. Hand, M. Yankova, G. Huber, J.W. Lichtman, T.A. Rapoport, and M.M. Kozlov. 2013. Stacked endoplasmic reticulum sheets are connected by helicoidal membrane motifs. *Cell*. 154:285-296.

Tombola, F., M.M. Pathak, and E.Y. Isacoff. 2006. How Does Voltage Open an Ion Channel? *Annual Review of Cell and Developmental Biology*. 22:23–52.

Tsang, H.T., T.L. Edwards, X. Wang, J.W. Connell, R.J. Davies, H.J. Durrington, C.J. O'Kane, J.P. Luzio, and E. Reid. 2009. The hereditary spastic paraplegia proteins NIPA1, spastin and spartin are inhibitors of mammalian BMP signalling. *Hum Mol Genet*. 18:3805-3821.

Tse, F.W., A. Tse, B. Hille, H. Horstmann, and W. Almers. 1997. Local Ca^{2+} Release from Internal Stores Controls Exocytosis in Pituitary Gonadotrophs. *Neuron*. 18:121–132.

Upadhyaya, A. and M. P. Sheetz. 2004. Tension in Tubulovesicular Networks of Golgi and Endoplasmic Reticulum Membranes. 86:2923-2928.

Vance, J.E. 2013. MAM (mitochondria-associated membranes) in mammalian cells: Lipids and beyond. *Biochim Biophys Acta*.

Várnai, P., L. Hunyady, and T. Balla. 2009. STIM and Orai: the long-awaited constituents of store-operated calcium entry. *Trends in Pharmacological Sciences*. 30:118-128.

Verkhratsky, A., and A. Shmigol. 1996. Calcium-induced calcium release in neurones. *Cell Calcium*. 19:1–14.

Voeltz, G.K., W.A. Prinz, Y. Shibata, J.M. Rist, and T.A. Rapoport. 2006. A class of membrane proteins shaping the tubular endoplasmic reticulum. *Cell*. 124:573-586.

Vu, T.H. and Z. Werb. 2000. Matrix metalloproteinases: effectors of development and normal physiology. *Genes & Development*. 14:2123-2133.

Wakefield, S., and G. Tear. 2006. The Drosophila reticulon, Rtnl-1, has multiple differentially expressed isoforms that are associated with a sub-compartment of the endoplasmic reticulum. *Cell Mol Life Sci*. 63:2027-2038.

Wang, X., W.R. Shaw, H.T. Tsang, E. Reid, and C.J. O'Kane. 2007. Drosophila spichthyin inhibits BMP signaling and regulates synaptic growth and axonal microtubules. *Nat Neurosci*. 10:177-185.

Warmke, J., R. Drysdale, and B. Ganetzky. 1991. A Distinct Potassium Channel Polypeptide Encoded by the *Drosophila* eag Locus. *Science*. 252:1560-1562.

Wegner, M. and C.C. Stolt. 2005. From stem cells to neurons and glia: a Soxist's view of neural development. *TRENDS in Neuroscience*. 28:583-588.

Westrate, L.M., J.E. Lee, W.A. Prinz, and G.K. Voeltz. 2015. Form follows function: the importance of endoplasmic reticulum shape. *Annu Rev Biochem*. 84:791-811.

Wong, C.O., K. Chen, Y.Q. Lin, Y. Chao, L. Duraine, Z. Lu, W.H. Yoon, J.M. Sullivan, G.T. Broadhead, C.J. Sumner, T.E. Lloyd, G.T. Macleod, H.J. Bellen, and K. Venkatachalam. 2014. A TRPV Channel in Drosophila Motor Neurons Regulates Presynaptic Resting Ca^{2+} Levels, Synapse Growth, and Synaptic Transmission. *Neuron*. 84:764-777.

Xie, X. and V.J. Auld. 2011. Integrins are necessary for the development and maintenance of the glial layers in the *Drosophila* peripheral nerve. *Development*. 138:3813-3822.

Yager, J., S. Richards, D.S. Hekmat-Scafe, D.D. Hurd, V. Sundaresan, D.R. Caprette, W.M. Saxton, J.R. Carlson, and M. Stern. 2001. Control of *Drosophila* perineurial glial growth by interacting neurotransmitter-mediated signaling pathways. *Proceedings of the National Academy of Sciences*. 98:10445-10450.

Yamakage, M., and A. Namiki. 2002. Calcium channels--basic aspects of their structure, function and gene encoding; anesthetic action on the channels--a review. *Can. J. Anaesth*. 49:151–164.

Yang, F-C., Ingram, D. A., Chen, S., Hingtgen, C. M., Ratner, N., Monk, K. R., Clegg, T., White, H., Mead, L., Wenning, M. J., Williams, D. A., Kapur, R., Atkinson, S.J., and Clapp, D.W. 2003. Neurofibromin-deficient Schwann cells secrete a potent migratory stimulus for Nf1+/– mast cells. *The Journal of Clinical Investigation*. 112:1851-1861.

Yang, Y.S., and S.M. Strittmatter. 2007. The reticulons: a family of proteins with diverse functions. *Genome Biol*. 8:234.

Yao, K-M and K. White. 1994. Neural Specificity of elav Expression: Defining a *Drosophila* Promoter for Directing Expression to the Nervous System. *Journal of Neurochemistry*. 63:41-51.

Yeh, E., K. Gustafson, and G.L. Boulianne. 1995. Green fluorescent protein as a vital marker and reporter of gene expression in Drosophila. *Proc Natl Acad Sci U S A*. 92:7036-7040.

Yu, F., Y. Cai, R. Kaushik, X. Yang, and W. Chia. 2003. Distinct Roles of Gαi and Gβ13F subunits of the heterotrimeric G protein complex in the mediation of *Drosophila* neuroblast asymmetric divisions. *The Journal of Cell Biology*. 162:623-633.

Zalk, R., S.E. Lehnart, and A.R. Marks. 2007. Modulation of the ryanodine receptor and intracellular calcium. *Annu. Rev. Biochem*. 76:367–385.

Zhu, Y., P. Ghosh, P. Charnay, D.K. Burns, and L.F. Parada. Neurofibromas in NF1: Schwann Cell Origin and Role of Tumor Environment. *Science*. 296:920-922.

Zuo, J., P.L. De Jager, K.A. Takahashi, W. Jiang, D.J. Linden, and N. Heintz. 1997. Neurodegeneration in Lurcher mice caused by mutation in δ2 glutamate receptor gene. *Letters to Nature*. 388:769-773.

Zurek, N., L. Sparks, and G. Voeltz. 2011. Reticulon short hairpin transmembrane domains are used to shape ER tubules. *Traffic*. 12:28-41.